

REVISION 2

Dating mantle peridotites using Re-Os isotopes: The complex message from whole rocks, base metal sulfides and platinum group minerals.

Ambre Luguet ^{1*} and D. Graham Pearson²

1: Steinman Institut für Geologie, Mineralogie und Paläontologie, Rheinische Friedrich-Wilhelms-Universität, Bonn, Germany. ambre.luguet@uni-bonn.de

2: Earth and Atmospheric Sciences, University of Alberta, Edmonton, Canada.

*: corresponding author: ambre.luguet@uni-bonn.de

Words: 23,418

Figures: 13

Keywords: Re-Os isotopic system, mantle peridotites, base metal sulfides, platinum group minerals.

Abstract

The Re-Os isotopic system is largely considered the geochronometer of choice to date partial melting of terrestrial peridotites and in constraining the evolution of Earth's dynamics from the mantle viewpoint. While whole-rock peridotite Re-Os isotopic signatures are the core of such investigations, the Re-Os dating of individual peridotite minerals – base metal sulfides (BMS) and platinum group minerals (PGM) - that are the main hosts for Re and Os in the mantle peridotites came into play two decades ago.

These micrometric-nanometric BMS and PGM display an extreme complexity and heterogeneity in their $^{187}\text{Os}/^{188}\text{Os}$ and $^{187}\text{Re}/^{188}\text{Os}$ signatures, which result from the origin of the BMS±PGM grains (residual versus metasomatic), the nature of the metasomatic agents, the transport/precipitation mechanisms, BMS±PGM mineralogy and subsequent Re/Os fractionation. Corresponding whole-rock host peridotites, typically plot within the $^{187}\text{Os}/^{188}\text{Os}$ and $^{187}\text{Re}/^{188}\text{Os}$ ranges defined by the BMS±PGM, clearly demonstrating that their Re-Os signatures represent the average of the different BMS±PGM populations. The difference between the $^{187}\text{Os}/^{188}\text{Os}$ ratios of the least radiogenic BMS±PGM and the respective host peridotite increases with the fertility of the peridotite reflecting the increasing contribution of metasomatic BMS±PGM to the whole-rock mass balance of Re and Os concentrations and Os isotope compositions. Corollaries to these observations are that (i) BMS may provide a record of much older partial melting event, pushing back in time the age of the lithospheric mantle stabilization, (ii) if only whole-rock peridotite Re-Os isotopic measurements are possible, then the best targets for constraining the timing of lithospheric stabilization are BMS-free/BMS-poor ultra-refractory spinel-bearing peridotites with very minimal metasomatic overprint, as their $^{187}\text{Os}/^{188}\text{Os}$ signatures may be geologically meaningful, (iii) while lherzolites are “fertile” in terms of their geochemical composition, they do not have a “primitive”, unmodified composition, certainly in terms of their highly siderophile elements (HSE) and Re-Os isotopic systematics, (iv) the combined

Re-Os isotopic investigations of BMS and whole-rock in BMS-rich mantle peridotites would provide a complementary view on the timing and nature of the petrological events responsible for the chemical and isotopic evolution and destruction of the lithospheric mantle.

In addition, the $^{187}\text{Os}/^{188}\text{Os}$ composition of the BMS±PGM (both residual and metasomatic) within any single peridotite may define several age clusters – in contrast to the single whole-rock value - and thus provide a more accurate picture of the complex petrogenetic history of the lithospheric mantle. When coupled with a detailed BMS±PGM petrographical study and whole-rock lithophile and HSE systematics, these BMS age clusters highlight the timing and nature of the petrological events contributing to the formation and chemical and isotopic evolution of the lithospheric mantle. These BMS±PGM age clusters may match regional or local crustal ages, suggesting that the formation and evolution of the lithospheric mantle and its overlying crust are linked, providing mirror records of their geological and chemical history. This is, however, not a rule of thumb as clear evidence of crust-mantle age decoupling also exist.

Although the BMS±PGM Re-Os model ages push back in time the stabilization of lithospheric mantle, the dichotomy between Archean cratonic and circum-cratonic peridotites; and post-Archean non cratonic peridotites and tectonites is preserved. This ability of BMS±PGM to preserve older ages than their host peridotite also underscores their survival for billions of years without being reset or reequilibrated despite the complex petrogenetic processes recorded by their host mantle peridotites. As such, they are the mantle equivalents of crustal zircons. Preservation of such old signatures in “young” oceanic peridotites ultimately rules out the use of the Re-Os signatures in both oceanic peridotites and their BMS to estimate the timescales of isotopic homogenization of the convecting mantle.

I. Introduction

Dating terrestrial mantle peridotites provides one of the most pivotal, yet basic, constraints that leads to a better understanding of the evolution of the Earth's mantle, and especially, the genetic and evolutionary relationships of the crust and mantle. Such data are increasingly used to constrain the evolution of the continental crust (Pearson et al., 2007; Hawkesworth et al., 2017) and bear upon the temporal accumulation of continental masses and the onset of plate tectonics. The most powerful contribution to these goals from the dating of mantle peridotites has been in documenting the stabilization of lithospheric roots as well as their evolution, "reworking" and possible destruction.

While a large range of lithophile-element based isotopic systems (e.g. Rb-Sr, U-Pb) are available to date crustal lithologies, mantle peridotites are best dated using the Re-Os isotopic system (e.g. Walker et al., 1989; Pearson et al., 1995a-b; 1999; 2007; Shirey and Walker, 1998; Chesley et al., 1999; Griffin et al., 2003; Carlson, 2005; Pearson and Wittig, 2008; 2014; Rudnick and Walker, 2009). The Re-Os isotopic system is based on the radioactive decay of ^{187}Re into ^{187}Os (half-life: 42.3 Byr, Smoliar et al., 1996), for which the geochemical affinities of the parent and daughter isotopes range from mildly lithophile (Re) to chalcophile and highly siderophile (Re, Os) (see Fleet et al., 1991; Borisov and Walker, 2000; Ertel et al., 2001; Ballhaus et al., 2006; Mallmann and O'Neill, 2007; Brenan, 2008; Bennett and Brenan, 2013; Brenan et al., 2016 and refs therein). The rationale behind the Re-Os isotopic system being the geochronometer of choice for mantle peridotites lies in the compatibility of osmium during partial melting while Re behaves incompatibly (e.g., Fonseca et al., 2007; Brenan, 2008). This difference in compatibility between Os and Re, which in fact exists across the full spectrum of the highly siderophile elements (HSE: Os, Ir, Ru, Rh, Pt, Pd, Re, Au), has been repeatedly demonstrated over the last three decades from the HSE systematics of both melt-depleted peridotites and partial melts (i.e. MORB, OIB) (e.g., Morgan, 1986; Roy-Barman and Allègre, 1994; Lorand et al., 1999; 2003a; Pearson et al., 2002; 2004; Escrig et al., 2005; Becker et al., 2006; Luguet

et al., 2007, 2015; Ackerman et al., 2009; 2013; Fischer-Gödde et al., 2011; Harvey et al., 2011; O'Driscoll et al., 2012; Day, 2013; Aulbach et al., 2014; Lissner et al., 2014).

The isotopic dating of mantle rocks was originally performed on whole-rock peridotites but evolved in the late 1990s towards dating peridotite-forming minerals including base metal sulfides (BMS) and platinum group minerals (PGM), which are the main Re-Os host phases (e.g. Hart and Ravizza, 1996; Pearson et al., 1998; Burton et al., 1999, Lorand et al., 1999; 2013). These studies have revealed that the isotopic signatures - in terms of $^{187}\text{Os}/^{188}\text{Os}$ as well as $^{187}\text{Re}/^{188}\text{Os}$ - at the mineral scale varied significantly, encompassing the whole-rock signatures of the host mantle peridotite. This has challenged our understanding of the Re-Os geo-chronometer, especially its robustness and geological meaning when approached from both the whole-rock peridotites and their Re-Os host minerals perspectives.

The aim of this article is to review the knowledge acquired over the last three decades from coupling whole-rock and mineral Re-Os isotopic signatures in mantle peridotites and to document how this has impacted our understanding of the Re-Os system in peridotites, especially its resistance/ease to resetting and overprinting as well as, more critically, our understanding of Earth's formation, evolution and geodynamics.

II. Re-Os isochrons and model ages

II.1. Re-Os Isochron: Principle and Pitfalls

Long lived isotopic chronometers such as the Re-Os isotopic system offer two possible ways to date mantle peridotites and their minerals, which are not equivalent. First, analyses of multiple whole-rock peridotites from a specific locality or of the analysis of the different minerals constituting one

single whole-rock peridotite may produce an isochron between the $^{187}\text{Os}/^{188}\text{Os}$ and the $^{187}\text{Re}/^{188}\text{Os}$ ratios, where both the age information and the reservoir source composition could be constrained. Obtaining a Re-Os isochron in mantle peridotite suites or between their minerals is however unusual and the few isochrons obtained rarely satisfy -if ever- the rigorous statistical criteria that define true isochrons (e.g. Gao et al., 2002). There are two dominant reasons for this. The first is that it seems unlikely that the Earth's mantle has been homogenized in terms of the distribution of HSE, due to their propensity to be sequestered in mineral "nuggets", sometimes shielded by enclosing silicate grains. This is evident in the significant Os isotopic heterogeneity recorded by a large age spectrum of whole-rock mantle peridotites (i.e., cratonic and off-craton xenoliths as well as abyssal, ophiolitic and orogenic peridotites) and MORBs (glasses) as well as at the mineral scale in both MORBs and peridotites (see Aulbach et al., 2016 and refs therein; Becker and Dale, 2016 and refs therein; Gannoun et al., 2016 and refs therein, see also Part VI.1) but also in diamond-hosted BMS recovered from cratonic peridotites (i.e., Pearson et al., 1998; Aulbach et al., 2004; 2018; Westerlund et al., 2006; Smit et al., 2010). As isotopic homogenization is a pre-requisite of statistically viable isochrons, then the system is at a disadvantage. The second reason why Re-Os isochrons are rarely preserved in peridotites is that many have acted as open systems to the ingress of melts and fluids since their formation by melt depletion. This metasomatic disturbance has a more obvious effect on the parent element (Re) due to its incompatible and partly lithophile nature, and its greater mobility than Os in mantle and crustal derived fluids (e.g., Xiong and Wood, 2002; Pearson et al., 2004; Luguet et al., 2007; Mallmann et al., 2007; Dale et al., 2007; Mungall and Brenan, 2014; Coggon et al., 2015). The addition of Re early in the evolutionary history of a peridotite will modify the $^{187}\text{Os}/^{188}\text{Os}$ ratio due to ingrowth. Alternatively, direct alteration of the $^{187}\text{Os}/^{188}\text{Os}$ isotopic signature of a peridotite may potentially occur if a significant amount of metasomatic Os-rich (i.e. few 100s ppb-ppm concentration level of Os) BMS precipitate from a melt/fluid with a very distinct $^{187}\text{Os}/^{188}\text{Os}$ signature compared to that of the peridotite (e.g., Xu et al., 2008; Alard et al., 2011; Harvey et al., 2011 and Part VI.2. and Figure 7 for discussion).

Furthermore, interaction of peridotites with large volume of melts or fluids of distinct isotopic composition may lead to the melt/fluid imprinting its $^{187}\text{Os}/^{188}\text{Os}$ signature onto peridotites, either due to BMS reequilibration or removal (see Alard et al., 2011). Whether Re addition or Os concentration modification (increase or decrease), these overprintings will obviously alter the $^{187}\text{Re}/^{188}\text{Os}$ ratio.

II.2. Re-Os model Ages

II.2.1. Principle

In the absence of isochron relationships between the $^{187}\text{Os}/^{188}\text{Os}$ and the $^{187}\text{Re}/^{188}\text{Os}$ ratios, Re-Os model ages, whose principle was initially outlined by Luck and Allègre (1984) and Walker et al. (1989), with a modification by Pearson et al. (1995a) to take into account post-formation disturbance, can be calculated. Subsequent detailed explanations appeared in Shirey and Walker (1998), Carlson (2005), Rudnick and Walker (2009) and are summarized here. Model ages are extrapolated ages of separation from idealized “models” of geologically significant reservoirs, such as the terrestrial upper mantle, often termed the “Primitive Upper Mantle” or PUM (derived from global estimates of the present mantle composition, see Meisel et al., 2001; Becker et al., 2006) or a CI-chondrite-like mantle, derived from the mean Re-Os characteristics for that meteorite class (see Horan et al., 2003; Fischer-Gödde et al., 2010; Day et al., 2016). The use of either of these reservoirs implies that the mantle peridotites being dated are in fact the melting residues from partial melting of a CI-chondrite-like mantle or a PUM-like mantle, but not from a metasomatised mantle or an already depleted mantle. At present, there is no widely accepted model of a “depleted mantle reservoir” for the Re-Os isotopic system, such as those that exist for Nd or Hf isotopes (e.g., Patchett and Tatsumoto, 1980; DePaolo, 1981; Bennett et al., 1993; Nowell et al., 1998; Chauvel and Blichert-Toft, 1999), probably because of the very significant isotopic heterogeneity that has been documented in rocks commonly used for such purposes e.g., MORBs and abyssal peridotites (see Day et al., 2017).

For the Re-Os isotopic system, two main model ages can be calculated. The T_{MA} model age is analogous to model ages used in other decay systems, reflecting the age of separation of a melt, or mantle residue from the convecting mantle (either PUM-like or chondrite-like in composition), where the resulting rock remains isolated from the effects of convective and diffusional homogenization. The T_{MA} model age is back-calculated using the measured $^{187}\text{Re}/^{188}\text{Os}$ of the sample, thus accounting for ^{187}Os ingrowth after extraction from the convecting mantle. The T_{RD} model age also reflects the time of isolation from the convecting mantle of a melt-depleted residue and contains the inherent assumption that the extent of partial melting was high enough to quantitatively extract all Re into the partial melt, leaving the peridotite residue Re-free (Walker et al., 1989). In this scenario, the measured $^{187}\text{Os}/^{188}\text{Os}$ is that extant at the time of partial melting. If the degree of melting was insufficient to extract all the Re or some Re was later added to the residual peridotite again, then the T_{RD} model age is a *minimum* model age. A variant on the T_{RD} model age is the $T_{RD \text{ eruption}}$ model age of Pearson et al. (1995a), which is used specifically for mantle xenoliths and is a combination of both the T_{MA} and T_{RD} concepts. The $T_{RD \text{ eruption}}$ model age back-corrects radiogenic ^{187}Os ingrowth from any measured Re in the peridotite, to the time of eruption of the mantle xenolith to the Earth's surface, assuming that all Re was added at the time of xenolith entrainment and eruption of the host lava. After making this correction to the time of eruption, a T_{RD} model age is calculated from that "initial" Os isotope ratio at the time of eruption. However, even in mantle xenoliths, the $T_{RD \text{ eruption}}$ model age is not applicable for the peridotite-building minerals that should have contained inherent Re, such as base metal sulfides.

The $T_{RD \text{ eruption}}$ model age is designed to back-calculate the model ages of peridotites having experienced a multi-stage (Re-depletion due to partial melting followed by Re-addition due to the host lava infiltration) open system behavior. The choice to use the $T_{RD \text{ eruption}}$ model age as opposed to the T_{MA} or T_{RD} model ages depends on having additional information such as whole-rock HSE systematics, whole-rock lithophile major and trace element signatures and possibly the chemical composition of the peridotite minerals (olivine, clinopyroxene) in order to understand the petrological history (i.e., partial

melting and overprintings) of the peridotites. Only in such integrated studies can the geological meaning of the model ages be adequately assessed. If $T_{RD \text{ eruption}}$ model ages are applied to a BMS-free refractory peridotite showing evidence of extensive partial melting and of metasomatic enrichment that has affected only Re (i.e., no associated metasomatic BMS precipitation), the $T_{RD \text{ eruption}}$ age may be geologically meaningful. Alternatively, $T_{RD \text{ eruption}}$ or T_{MA} model ages extrapolated from peridotites that have clearly experienced metasomatic BMS precipitation (independent of the timing of these additions) would have no geological meaning. It is evident that the model ages providing the tightest age cluster will most likely have the highest geological significance.

II.2.2. Re depletion T_{RD} versus mantle extraction T_{MA} model ages.

If mantle peridotites are pure residues of partial melting at relatively large melt fractions, sufficient to remove all Re (~ 25 to 30% melting, clearly depending on the initial S content and Re partition coefficient e.g., Aulbach et al., 2016), then the T_{MA} and T_{RD} model ages should be identical. Where only a minor amount of Re remains, the two values will still be relatively similar (Figure 1A; as shown between the T_{RD} and the T_{MA} for the harzburgitic residue calculation), but the T_{RD} Re depletion model age will systematically yield a younger age than the T_{MA} model age. The difference between the T_{MA} and T_{RD} age will increase if we consider a mantle residue after a relatively low degree of partial melting such as a lherzolite (relatively higher $^{187}\text{Re}/^{188}\text{Os}$; Figure 1A). It is worth noting that the concept of the T_{RD} model age was specifically developed for highly refractory cratonic peridotites (Walker et al., 1989) where the estimated degree of melt extraction is ~ 30 to 50% (e.g., Pearson and Wittig, 2008), thus leading to Re-free peridotitic residues.

For estimating the mantle separation ages of peridotites or minerals with inherent Re, the T_{MA} model age is the most suitable. Obviously, for the T_{MA} model ages to have a geological significance, the $^{187}\text{Re}/^{188}\text{Os}$ ratio should be primary, i.e., unmodified since separation from the assumed parent reservoir. However, when investigating mantle peridotites, many researchers exclusively use the

measured whole-rock $^{187}\text{Re}/^{188}\text{Os}$ ratio of their peridotite as a proxy for screening out residual versus metasomatised peridotites. It should, however, be strongly emphasized that sub-chondritic $^{187}\text{Re}/^{188}\text{Os}$ alone cannot be taken as being synonymous of mantle peridotites being pure residues from partial melting, but can result from the action of metasomatic overprinting on such melt residues (see Luguët et al., 2015). Using an overestimated $^{187}\text{Re}/^{188}\text{Os}$ for T_{MA} model age calculation would then result in artificially older ages or unrealistic ones (e.g. older than Solar System). A better assessment of the origin and likely accuracy of a $^{187}\text{Re}/^{188}\text{Os}$ ratio in terms of the single-stage evolution inherent in model age calculations is based on using the HSE signatures and more specifically the $\text{Pd}_\text{N}/\text{Re}_\text{N}$ ratio of the whole-rock peridotite (Pearson et al., 2002; 2004; Luguët et al., 2015). A suprachondritic $\text{Pd}_\text{N}/\text{Re}_\text{N}$, associated with progressive depletion from Pt to Pd and Re when compared to the PUM HSE signature, typically supports a residual origin, while a sub-chondritic $\text{Pd}_\text{N}/\text{Re}_\text{N}$ ratio is indicative of Re overprinting, eliminating the T_{MA} model ages approach as one likely to give a meaningful estimate of the time of melt depletion. In such scenarios, the T_{RD} model ages offer then the most conservative approach; but because they do not include ingrowth correction, they provide only *minimum* ages.

When mineral phases, such as base metal sulfides, are to be dated, the same high-level of care applies, including detailed petrographical investigations (see part IV) and when possible, analysis of their complete HSE systematics to try to understand the petrological origin of these Re-Os host phases. The nature and complexity of the mineral assemblage analyzed should also be considered, -as for example- residual chalcopyrite will likely yield a suprachondritic $^{187}\text{Re}/^{188}\text{Os}$ and radiogenic $^{187}\text{Os}/^{188}\text{Os}$. Also of note is that, in BMS grains with complex mineralogical assemblages, Re-Os isotopic analysis that does not capture all phases present (see Part V), such as chalcopyrite, or un-radiogenic alloys, will be subjected to large uncertainties.

II.2.3. Choice of reference reservoirs and significance of the model ages.

Model ages are traditionally back-calculated to either a CI-chondrite-like mantle evolution or a putative PUM evolution (see Shirey and Walker, 1998). Using the initial $^{187}\text{Os}/^{188}\text{Os}$ composition of the Solar System extrapolated from the ^{187}Re - ^{187}Os isochron of iron meteorites (0.0952 ± 0.0002 ; Smoliar et al., 1996; Day et al., 2016), the time-integrated $^{187}\text{Os}/^{188}\text{Os}$ evolution of both reference reservoirs can be extrapolated from the present day $^{187}\text{Os}/^{188}\text{Os}$ of CI-chondrites (0.1262, Day et al., 2016; compilation data from Horan et al., 2003 and Fischer-Gödde et al., 2010) and the present day $^{187}\text{Os}/^{188}\text{Os}$ of the terrestrial upper mantle. This latter has been estimated from worldwide peridotites from different tectonic settings (Meisel et al., 2001; Becker et al., 2006) or from abyssal peridotites (Day et al., 2017), both approaches yield indistinguishable present-day $^{187}\text{Os}/^{188}\text{Os}$ values for the PUM (0.1296 versus 0.1292, respectively). These PUM estimates may however be subject to potential uncertainty (namely being overestimated) in the inclusion of metasomatised mantle material but are probably the best current estimates for the present-day upper mantle $^{187}\text{Os}/^{188}\text{Os}$ isotopic composition.

The $^{187}\text{Os}/^{188}\text{Os}$ compositions of these CI-Chondrite-like mantle and the PUM-like mantle reservoirs naturally diverges with time due to their different Re/Os ratios (Figure 1B). Therefore, the use of one or the other reference reservoir induces difference in the model age estimates, which worsen dramatically for relatively young samples and imposes the largest single uncertainty in the model age approach (see discussion in supplementary material of Pearson et al., 2007) (Figure 1B). The model ages obtained using the PUM reference reservoir will systematically be older than those estimated using the CI-chondrite-like reference reservoir (Figure 1B) due to the more radiogenic $^{187}\text{Os}/^{188}\text{Os}$ isotope composition of the PUM at any given time. For example, for an Archean mantle residue with a $^{187}\text{Os}/^{188}\text{Os}$ composition of 0.108, the T_{RD} will differ by ~ 165 Myr (T_{RD} of 2.71 versus 2.88 Ga, respectively). If the peridotite did not experience Re addition after extensive partial melting (i.e., $^{187}\text{Re}/^{188}\text{Os} = 0.1222$), the T_{MA} model ages would deviate by 80 Myr (T_{MA} of 3.90 and 3.98 Ga). These age differences for both the T_{RD} and T_{MA} may be fairly similar to the age uncertainty induced from the $^{187}\text{Os}/^{188}\text{Os}$ measurement uncertainty. For a Proterozoic mantle peridotite ($^{187}\text{Os}/^{188}\text{Os}$

composition=0.1220), the T_{RD} model ages differ by more than 350 Myr (see Figure 1B; 638 Ma and 994 Ma respectively for a CI-chondrite like mantle and a PUM-like mantle) and the T_{MA} by up to 460 Myr (923 and 1383 Ma respectively). It is then obvious that calculating model ages for peridotites that have likely melted during the Phanerozoic will be a relatively futile exercise due to the much broader isotopic heterogeneity of the Phanerozoic mantle and the geodynamic implications based on such Re-Os model ages are fraught with danger. In contrast, the impact of the choice of reference reservoirs on the uncertainty on the Re-Os model ages will be minimum for highly refractory Archean harzburgites having experienced minimal metasomatism, making them the best targets to date with the highest confidence the original stabilization (major melt extraction) of the lithospheric mantle. This further confirms that the use of Re-Os model ages in ultra-refractory cratonic mantle peridotites to understand the timing of the stabilization of the first large continental masses and the early Earth evolution is a very coherent strategy. This is, however, not the case for mantle peridotites that have experienced substantial metasomatism, especially Re addition.

III. Mantle peridotites analyzed for Re-Os isotope systematics at the mineral scale and at the whole-rock scale

Mantle peridotites available at the surface of Earth have been emplaced either tectonically or during volcanic eruptions. The tectonically emplaced mantle peridotites (hereafter referred to as tectonites following Becker and Dale, 2016) occur as km-long slices within orogenic massifs (e.g. the Betico-Rif orogenic massifs), ophiolitic belts (e.g. Alpine ophiolites) or constitute part of the present-day seafloor (e.g., abyssal peridotites of Gakkel Ridge and South West Indian Ridge). Their geochemistry has been summarized by Bodinier and Godard (2014). Additionally, mantle tectonites may have been emplaced within Earth's crust through the stacking of nappes, thus occurring as meter-

sized outcrops of peridotites embedded within intermediate to high-grade metamorphic terranes. Overall, tectonites traditionally offer a 3D view of the lithospheric mantle and namely of the relationships between the different mantle lithologies (peridotites-lherzolites and harzburgites-, pyroxenites, gabbros and possibly basalts). In contrast, mantle peridotites sampled during volcanic eruptions (hereafter referred to as peridotite xenoliths) (see Pearson et al., 2003; Pearson and Wittig, 2014 for a review of their geochemistry) provide a more fragmental view of the lithospheric mantle root as they are mainly few decimeters to centimeters long nodules within their host lavas. They are the wall-rocks to melt conduits and hence have all been modified in some way. Peridotite xenoliths are more geographically widespread than tectonites, and most of them preserve the chemical signatures and P-T conditions of their source depth due to their rapid ascent to the surface. Such features were obscured in mantle tectonites due to their long-time storage within the crust and the consequent high likelihood of low-temperature re-equilibration and prolonged exhumation histories during which the tectonites were exposed to fluids and/or melts. Mantle peridotite xenoliths have been brought up to Earth's surface by intraplate volcanism via (i) kimberlitic-lamproitic magmas associated with Archean cratons, as well as by alkali basaltic magmas (ii) on the edge of or within cratonic blocks (afterwards referred as circum-cratonic peridotites) that experienced delamination, extension and ultimately destabilization/destruction (e.g. East China), (iii) within or associated with continental rift systems (e.g., Rio Grande Rift) and (iv) within oceanic islands (Hawaii; see Nixon, 1987 for a summary of occurrences). Alternatively, peridotite xenoliths may also be found in association with convergent margins, either directly related to the arc volcanism (Kamchatka) or to post-subduction collision.

The mantle peridotite suites that have been characterized for the Re-Os isotope systematics of their constituent base metal sulfides and platinum group minerals, possibly in association with their whole-rock Re-Os isotopic systematics, cover the whole-range of mantle peridotites described above. Specifically, the peridotite suites on which this review is based are:

- Orogenic peridotites from the French Pyrénées (Lorand et al., 2013) and the Ronda massif, Spain (Marchesi et al., 2010).
- Ophiolitic peridotites from the Ligurides (Alard et al., 2005).
- Abyssal peridotites from Mid Atlantic Ridge (Kane Fracture zone: Alard et al., 2005; ODP Leg 209: Harvey et al., 2006; Burton et al., 2012); South West Indian Ridge (Alard et al., 2005; Warren and Shirey, 2012) and Gakkel Ridge (Warren and Shirey, 2012).
- Fragments of peridotites tectonically emplaced within HP terranes such as those of the Seve nappe Complex, Sweden (Brueckner et al., 2004) and for which a sub-continental origin (alpine-type) has been proposed.
- Cratonic peridotite xenoliths from the Kaapvaal craton (Griffin et al., 2004; Wainwright et al., 2016); the Zimbabwe craton (Wainwright et al., 2015); North Atlantic Craton (van Acken et al., 2017) and Rae Craton (Bragagni et al., 2017).
- Circum-cratonic peridotite xenoliths from the cratonic blocks edges in East China (Xu et al., 2008; Wang et al., 2009) and in Spitzbergen (Griffin et al., 2012; Kim et al., 2016),
- Peridotite xenoliths from the continental rift systems of the French Massif Central (N.J. Pearson et al., 2002; Alard et al., 2002; 2011; Harvey et al., 2010), of the Rio Grande Rift, USA (Hart and Ravizza, 1996; Burton et al., 1999; Harvey et al., 2011), of the East Africa Rift (Burton et al., 2000; Wang et al., 2005), of the Baikal Lake Rift (Tariat volcanic field: Wang et al., 2006), of Central Spain (Calavatra volcanic field: González-Jimenez et al., 2014) and of the South Vietnam peninsula (Burton et al., 2002). The mantle xenoliths from the Hyblean Plateau (Sicily) (Sapienza et al., 2007) are found in uplifted sides of the Lentini Graben, which is parallel to the Gela-Catania thrust front and perpendicular to the Malta escarpment (e.g. Behnke et al., 2004).
- Peridotite xenoliths from the Oceanic island of Cape Verde (Coltorti et al., 2010).

- Peridotite xenoliths associated with the post-subduction collision of Eastern Australia (Powell and O'Reilly; 2007).

These peridotites range in composition from “fertile” lherzolites to highly refractory harzburgites (i.e., no primary Cpx, low whole-rock Al_2O_3 and CaO contents, high forsterite content in Olivine, Al-rich spinel, see Simon et al., 2008) and, in addition to the main silicates (olivine, orthopyroxene and clinopyroxene), contain garnet and/or, spinel and/or rarely, plagioclase. For example, garnet peridotites are found in the Seve Nappe Complex (Brueckner et al., 2004) and the Ronda orogenic massif (Marchesi et al., 2010) or at depths in cratonic roots (see Griffin et al., 2004, Wainwright et al., 2015, van Acken et al., 2017; Bragagni et al., 2017) while plagioclase-spinel peridotites represent the former oceanic basins of the Ligurian ophiolites (Alard et al., 2005). All other mantle peridotites from the localities cited above are spinel-bearing.

These peridotites represent residues of partial melting having apparently experienced moderate to extensive melt extraction within the spinel or garnet stability field. They additionally present evidence of interactions with melts (e.g., silicate, carbonatitic or kimberlitic) and/or fluids having percolated the mantle column. Such interactions leave evidence such as trails of fluid inclusions within modally-major silicates, modal metasomatic minerals (carbonates, amphiboles, phlogopite, apatite), glass/melt pockets, or more cryptic geochemical signals such as spoon-shaped trace element patterns in clinopyroxene, chemically zoned olivine and orthopyroxene crystals, Re-enriched highly siderophile element signatures; all are inconsistent with the refractory whole-rock major element signatures and chemical composition of the modally-major silicates (e.g. olivine, spinel).

Considering the complex and multi-stage petrogenetic history recorded by mantle peridotites worldwide, a long-standing question has been to assess the impact of these multiple events on the Re-Os isotopic systematics at both the whole-rock and the mineral scales and; if and how the whole-rock and/or minerals could survive/be reset by such extensive modifications.

IV. The Re-Os host minerals in mantle peridotites.

IV.1. Base Metal Sulfides (BMS)

Base metal sulfides - also known as Fe-Ni-Cu sulfides - have been identified since the late 1970s-early 1980s as a main host phase of HSE in mantle peridotites worldwide (e.g., Jagoutz et al., 1979; Mitchell and Keays, 1981; Morgan and Baedeker, 1983; Hart and Ravizza, 1996; Pattou et al., 1996; Pearson et al., 1998; Burton et al., 1999; 2002; Alard et al., 2000; Luguet et al., 2001). These BMS typically contain ppm-level concentrations of Re and Os, generally 1-4 orders of magnitude higher than their respective whole-rock peridotites and 3-6 orders of magnitude higher than the modally-major silicates and oxides making up the peridotites. In S-bearing fertile to mildly refractory peridotites, mass balance calculations indicate that BMS account for 90-100% of the Os budget and 65% of the Re budget, with the remaining 35% of the Re budget being controlled by silicates (namely olivine and pyroxenes) (see Burton et al., 1999, Harvey et al., 2011).

These BMS are typically accessory (i.e., modal abundance $\ll 0.1\%$) micrometric (10-500 μm) minerals occurring as interstitial components or inclusions within silicates or melt/glass pockets. Interstitial BMS appear to be modally predominant over BMS inclusions in peridotites from orogenic and abyssal massifs as well as in post-Archean non-cratonic xenoliths (Burton et al., 1999; Alard et al., 2000; 2011; Liu et al., 2010). In contrast, Griffin et al. (2004) suggested that most BMS in the cratonic peridotites from the Kaapvaal craton occur as inclusions. The mineral assemblages of BMS traditionally comprise four main sulfide minerals: the monosulfide solid solution (Mss: $\text{Fe}_{(1-x)}\text{S}$, $\text{Ni}_{(1-x)}\text{S}$), pyrrhotite (Po: $\text{Fe}_{(1-x)}\text{S}$, with $x=0-0.2$), pentlandite (Pn: $(\text{Fe,Ni})_9\text{S}_8$) and chalcopyrite (Cp: FeCuS_2) (Figure 2). Such an assemblage likely results from the “closed-system” sub-solidus re-equilibration and solid-state reaction of a high-temperature sulfide melt that first crystallized the mss and then an iron-rich heazlewoodite (Cu-Ni-rich) solid solution (see Craig and Kullerud, 1969; Kullerud et al., 1969; Fleet

and Pan, 1994; Peregoedova and Ohnenstetter, 2002). Apart from these “primary” sulfides, BMS in cratonic peridotites may also contain djerfischerite (Dj: $K_6Na(Fe^{2+}, Cu, Ni)_{25}S_{26}Cl$), which most likely precipitated during the percolation of kimberlitic melts and any alkali-rich fluids or melts (Sharygin et al., 2007). Secondary sulfides, alloys or oxides such as mackinawite (Mw: $(Fe, Ni)_{1+x}S$), pyrite (Py: FeS_2), violarite (Vi: $FeNi_2S_4$), vaesite (Vs: NiS_2), chalcocite (Cc: Cu_2S), digenite (Dg: Cu_9S_5), covellite (Cv: CuS), bornite (Bo: Cu_5FeS_4), native Cu, millerite (Mi: NiS), heazlewoodite (Hz: Ni_3S_2), awaruite (Aw: Ni_3Fe), magnetite (Fe_3O_4) signals a shift toward a metal richer or metal poorer assemblage reflecting changes of fO_2 and fS_2 and ultimately of redox conditions due to serpentinization and/or low-temperature supergene alteration of BMS and of their host peridotite (see Lorand, 1987; 1990; Abrajano and Pasteris, 1989; Szabo and Bodnar, 1995; Luguët et al., 2003; 2004; Lorand and Grégoire, 2006; Foustoukos et al., 2015) (see Figure 2). When extensive, supergene alteration may lead to pseudomorphic replacements of the BMS by iron oxyhydroxydes (Lorand, 1990; Luguët and Lorand, 1998; Lorand et al., 2003b) with a composition close to $FeO(OH)$, 5-6 H_2O (Luguët and Lorand, 1998).

On the basis of the sulfide mineralogical assemblages and the textural relationship between BMS and silicates or oxides constituting the main peridotite assemblage as well as the textural, mineralogical and geochemical (i.e., trace elements, HSE, S, Se) characteristics of the whole-rock peridotites, four BMS types have been distinguished. The features of these four BMS types have been described over the last four decades in the literature (e.g., Lorand, 1987; 1991; 2003a; Dromgole and Pasteris, 1987; Szabo and Bodnar, 1995; Alard et al., 2002; 2011; Luguët et al., 2003; 2004; Lorand et al., 2004; Lorand and Grégoire, 2006; Delpech et al., 2012; Ackerman et al., 2013; González-Jiménez et al., 2014; Wainwright et al., 2015; Bragagni et al., 2017) and recently reviewed in Lorand and Luguët (2016) and Luguët and Reisberg (2016) (Figure 3). Considering the complexity of the petrological history of mantle peridotites that have been stored in the lithosphere sometimes for billions of years, it is however sensible to consider that many more BMS types or intermediate types between

the ones summarized below, may occur -even if only found in a single peridotite locality- as they are the complex interplay between the nature of the peridotitic protolith (depending on extent and depth of partial melting) and the number, type (fluid versus melt), nature (e.g., silicate melt, carbonatitic melt, S-undersaturated melt) and extent and mechanisms of metasomatic overprinting (small volume or large volume of percolating agents; reequilibration, removal or addition of BMS).

Type 1 BMS are mainly present as inclusions within silicates (olivine and pyroxene grains) (Figure 3), whose primary mantle origin is documented by the presence of kink-bands and deformation features that reflect deformation processes, that are also tracked by the sub-grain boundary features within olivine. They consist of $Mss-Po+Pn$ and minor amount of Cp , with a bulk Fe-Ni-rich Cu-poor S-rich composition. Type 1 BMS are interpreted as residual, having survived partial melt extraction that depleted the bulk peridotite in magmaphile elements.

In contrast, Type 2 to Type 4 BMS are all metasomatic in origin and result from either interaction between melt and peridotite protolith or fluid/vapor and peridotite protolith.

Type 2 BMS precipitated from small-volume of S-saturated silicate, carbonatitic or kimberlitic melts percolating the mantle column. Along with Type 1 BMS, they are the most ubiquitous BMS population recognized in worldwide peridotites. They are included in, or in direct contact with metasomatic silicates (generally Cpx), residual silicates and carbonatite/silicate melt pockets (Figure 3). The sulfide paragenesis tends to contain a higher proportion of pentlandite and chalcopyrite than Type 1 BMS, and is interpreted as resulting from the fractional crystallization of an evolved Ni-Cu-rich sulfide melt.

Type 3 BMS has been exclusively identified in peridotite xenoliths associated with large volumes of mafic magmatism (e.g., the Kerguelen plateau) and/or rift-systems such as the French Massif Central, East Africa, or the Rio Grande, USA, which bear evidences (e.g. poikilitic, granular textures; strain-free minerals, HT equilibration) for melt-rock reaction involving large volumes of silicate melt, possibly S-undersaturated. Type 3 BMS have a similar sulfide paragenesis as Type 1

BMS, being dominated by Mss and Pn-Po. Like Type 2 BMS, they occur as inclusions or intergranular components in close association with metasomatic silicates and melt pockets. They most likely represent remobilized Type 1 BMS during melt-rock reaction at high melt/rock ratios. The remobilization is concomitant with removal of some of the original BMS as suggested by the rather low BMS modal abundances, and low whole-rock S, Se, HSE concentrations (see Lorand et al., 2003b; Lorand and Luguët, 2016).

Type 4 BMS were interpreted as resulting from sulfidation reactions between C-H-O-S-rich fluids or vapors and peridotites. Type 4 BMS have, until now, only been clearly described, in terms of their petrography, in peridotite xenoliths from Montferrier (French Massif Central) and Kerguelen Island. Type 4 BMS exclusively occur as intergranular components, sometimes associated with polycrystalline dolomite grains (Figure 3) and tend to have high dihedral angles. They display an average bulk Fe-Ni-rich S-rich sulfide assemblage dominated by Mss and Po-Pn.

A possible variant of either Type 3 or Type 4 BMS seems to occur in the Calavatra peridotite xenoliths (Spain; González-Jiménez et al., 2014), where however the infiltration of carbonatitic fluids and silicic fluids was interpreted as the petrological process responsible for the mobilization of Type 1 BMS. The absence of whole-rock HSE, S and Se data in this study however prevents us from constraining the differences or similarities between Calavatra and the Montferrier, Kerguelen (Type 4 BMS) and the Massif Central mantle xenoliths (possibly Type 3 BMS).

IV.2. Platinum Group Minerals (PGM)

Platinum group minerals have been identified in mantle peridotites using conventional reflected light microscopy and high resolution imaging techniques (e.g., field emission gun-scanning electron microscope) (e.g. Keays et al., 1981; Luguët et al., 2003; Lorand et al., 2008; 2010; Delpech et al., 2012; Ackerman et al., 2013; González-Jiménez et al., 2014, Wainwright et al., 2016) but also revealed by highly non-reproducible HSE whole-rock abundances as well as concentration spikes within LA-

ICPMS ablation profiles of BMS (e.g., Handler and Bennett, 1999; Griffin et al., 2002; Luguët et al., 2004; Lorand et al., 2008; Ackerman et al., 2009; Marchesi et al., 2010). These PGM likely account dominantly for the whole-rock HSE budget of ultra-refractory orogenic harzburgites, where BMS have been entirely extracted by partial melting (Luguët et al., 2007). Such mass balance was not yet directly performed in cratonic peridotites, which have experienced very large degrees of partial melting able. Still ultra-refractory BMS-free cratonic peridotites display atypical but symptomatic suprachondritic Os/Ir ratios, highlighting most likely the occurrence of PGM in the form of Os-rich disulfides (erlichmanite) or alloys (Luguët et al., 2015).

In mantle peridotites, platinum group minerals are even smaller mineral phases than the BMS - with size ranging from a few tens of nanometers to a maximum 10-20 micrometers - , usually occurring as rods, platelets and prismatic grains. PGM comprise HSE alloys (e.g., Os-Ru alloys, Pt-Ir alloys, Pt-Fe alloys), high-temperature HSE disulfides (i.e. erlichmanite-laurite $\text{OsS}_2\text{-RuS}_2$) and HSE-bearing As-Te-Bi-phases (e.g., sperillyte) (Griffin et al., 2002; Luguët et al., 2003; 2004; 2007; Lorand et al., 2008; 2010; Wang et al., 2009; Marchesi et al., 2010; Delpech et al., 2012; González-Jiménez et al., 2014; Wainwright et al., 2016; Bragagni et al., 2017).

The Os-Ru disulfides (erlichmanite-laurite serie) and Os-Ru alloys; and the Pt-Ir-Os alloys have been recognized in highly refractory mantle residues, which are BMS-poor to BMS-free (Luguët et al., 2003; 2007; 2015; Lorand et al., 2010). They are high-temperature phases ($\gg 1100^\circ\text{C}$: Andrews and Brenan, 2002; Fonseca et al., 2017), having exsolved at the expense of the progressively diminishing mass of BMS during partial melting (Figure 3). If the refractory harzburgites containing residual PGM are metasomatised or refertilized, as clearly shown for the Pyrenean harzburgites-lherzolites (Le Roux et al., 2007), these residual PGM may appear as inclusions within later-formed metasomatic BMS (Lorand et al., 2010; 2013), having been entrapped by the metasomatic silicate/sulfide melts. They may also dissolved in metasomatic mss as suggested by the Os-Ru enriched HSE compositions of the mss

phases from Udachnaya xenocrystic olivine and Kerguelen peridotite xenoliths (Griffin et al., 2002; Delpech et al. 2012). This interpretation is supported by the high solubilities of Os and Ru (and Ir) in this sulfide mineral as well as in sulfide mattes (e.g. Li et al., 1996; Ballhaus et al., 2006; Fonseca et al., 2011).

The systematic association of the Pt-Fe-(Ir) alloys and Pt-Pd tellurides, telluro-bismuthides, telluro-arsenides (Pd-Te-As PGM) and arsenides (PtAs₂) with the pentlandite and chalcopyrite of the metasomatic Type 2 BMS (see Luguet et al., 2004; Lorand et al., 2010; Alard et al., 2011; Delpech et al., 2012; Wainwright et al., 2016) as well as the relatively low temperature stability limit of the Pt-Pd-Te-Bi PGM (875°C: Mackovicky, 2002 and 920°C: Helmy et al., 2007) suggest that Pt-Fe and Pt-Pd-Te-Bi PGM most likely exsolved during this sub-solidus re-equilibration leading to the Pn-Cpy assemblages (Figure 3), as Pt does not enter the octahedral site of these sulfide minerals (Luguet et al., 2004; Lorand et al., 2008; 2010; Wainwright et al., 2016). Finally, the reaction between these Pd-Pt-tellurides with As-bearing vapor may lead to the formation of PtAs₂ and Pd-Te-As nuggets (Delpech et al. 2012) found as inclusion within Type 4 BMS in peridotite xenoliths from Montferrier, Kerguelen (Alard et al. 2011; Delpech et al. 2012) (Figure 3).

IV.3. Re and Os systematics in the BMS±PGM Types

These often complex multi-sulfide mineral associations making up BMS, which are also possibly hosting PGM inclusions, may display a large range of Re/Os ratios and hence significantly different time-integrated ¹⁸⁷Os/¹⁸⁸Os isotope ratios. These Re/Os variations result from the contrasting geochemical affinities of Re and Os in the different sulfide minerals and PGM, the relative proportions of sulfide minerals and PGM within these different BMS populations (e.g., Ni-Cu-rich S-rich composition for BMS Type 2 versus Fe-Ni-rich S-rich for Types 1, 3 and 4; Os-rich sulfides or alloys in Type 1 BMS versus Os-poor Fe-Pt-Pd alloys, tellurides, arsenides, bismuthides in Type 2 and Type

4 BMS, see Figure 3) and the well-known differing overall behavior of Re versus Os during partial melting and melt/rock, fluid/rock or vapor/rock interactions (e.g., Barnes et al., 1985; Wood, 1987; Li et al., 1996; Lorand et al., 1999; Xiong and Wood, 2000; 2002; Pearson et al., 2004; Ballhaus et al., 2006; Dale et al., 2007; Fonseca et al., 2011; 2017; Mungall and Brenan, 2014; Coggon et al., 2015; Liu and Brenan, 2015).

Overall, reliable characterization of the full HSE systematics for the different BMS±PGM types are only available from two detailed petrographical and geochemical investigations (Alard et al., 2005; 2011) both conducted via LA-MC-ICPMS and having analyzed Type 1, 2 and 4 BMS±PGM types in tectonites (abyssal and ophiolitic peridotites) and non-cratonic peridotites xenoliths. Many studies on Re-Os isotopic analyses in BMS from mantle peridotites analyzed the Re and Os concentrations or even obtained the full HSE patterns of BMS±PGM grains for which they determined for the $^{187}\text{Os}/^{188}\text{Os}$ composition (e.g., Wang et al., 2009), but lack the petrographical information on BMS and whole-rock peridotite necessary to clear identify the origin of the BMS±PGM grains they analysed. On the other hand, many detailed petrographical investigations of the BMS in mantle peridotites did not include Re during their in-situ HSE analyses (e.g., Lorand and Alard, 2001; Delpech et al., 2012), preventing any implications to be made concerning their Re/Os ratios for the ^{187}Os isotopic evolution. This is especially critical in the case of the BMS from some Massif Central peridotite xenoliths (Lorand and Alard, 2001) as these BMS most likely represent Type 3 BMS±PGM (Lorand et al., 2003b). Still, HSE systematics of BMS±PGM grains obtained by laser-ablation MC-ICPMS or after the BMS±PGM extraction from the peridotite thin section and wet chemistry processing, only provide a biased view of the BMS±PGM compositions (see part V) as part of the grain has been removed by the preparation of the thin section. These analyses provide however the HSE signatures of the complex mixture of different sulfide minerals making up a BMS grains but not that of a single sulfide mineral.

Type 1, Type 2 and Type 4 BMS±PGM are characterized by distinct HSE systematics (Figures 3 and 4). Type 1 BMS±PGM chondrite-normalized HSE patterns are characterized by the highest

compatible HSE (Os, Ir, Ru) proportions (>10 - $1000 \times$ CI-chondrites) in comparison to the incompatible HSE (Pt, Pd and Re) (0.02 - $60 \times$ CI-Chondrites) (Figure 3) and are characterized by sub-chondritic to supra-chondritic Re_N/Os_N ratios (0.002 - 4.4 ; N =CI-chondrites normalized after Horan et al., 2003 and Fischer-Gödde et al., 2010, see Luguet and Reisberg, 2016) and Pd_N/Ir_N (0.003 - 7.2) ratios (Figure 4). Most importantly, despite their variability, the Re_N/Os_N and Pd_N/Ir_N are predominantly sub-chondritic (respective averages: 0.8 ± 1.0 (1sd) and 0.6 ± 1.4 (1sd)). Type 2 BMS±PGM show lower compatible HSE contents (1 - $10 \times$ CI-Chondrites) associated with Re_N/Os_N ratios varying from sub-chondritic to supra-chondritic (0.5 - 4.1), but being mostly suprachondritic (average 2.1 ± 1.1 (1sd)) and Pd_N/Ir_N ratios being exclusively suprachondritic (1.7 - 37.6). Type 4 BMS±PGM have the lowest compatible HSE contents (0.03 - $3 \times$ CI-chondrites) but similar Pd and Re contents as Type 1 and Type 2 BMS±PGM grains (Figure 3). This translates into Type 4 BMS±PGM having suprachondritic Re_N/Os_N (3.1 - 621) and Pd_N/Ir_N (3.4 - 1143) (Figure 4). Additionally, these Type 4 BMS±PGM display pronounced and systematic supra-chondritic Os/Ir ratios (1.8 - 54.5) (Figure 3), most likely symptomatic of their vapor/fluid related origin (see Part IV.1. and part VI.2.).

V. Methodological Strategies for determining Re-Os isotopic signatures at the mineral scale

(Figure 5)

V.1. Two decades of methodological developments and improvements.

Pioneering investigations focusing on the Re-Os isotopic signatures of minerals started in the mid-late 1990s early 2000s, specifically with studies on individual diamond-hosted sulfides (Pearson et al., 1998; 1999, ranging down to 10 micrograms or less in total weight) and with studies on modally major to accessory peridotite-building minerals (e.g. olivine, orthopyroxene, clinopyroxene, spinel, BMS), these latter being conducted at first on mineral fractions/separates (hand-picked from granular fractions) reaching up to a few tens to a few hundreds of milligrams (Hart and Ravizza, 1996; Burton et

al., 1999; 2000; 2002). All these investigations adopted isotopic dilution wet chemistry approaches after extraction or separation of the minerals of interest. For single diamond-hosted BMS grains (Pearson et al., 1998, 1999), the digestion of the BMS and Os separation by microdistillation were performed simultaneously, whereas the Re was subsequently separated via anion chromatographic exchange using micro-columns and a miniaturized chemistry. This chemistry procedure allows very low Os and Re blanks to be obtained. Analyses were carried out by negative thermal ionization mass spectrometry (N-TIMS) for the Os and Re concentrations and Os isotopic ratios. For the “bulk” mineral phases analyses (Hart and Ravizza, 1996; Burton et al., 1999; 2000; 2002), mineral fractions were digested using either a combination of nickel sulfide fire assay and sodium carbonate/tetraborate fluxing (Hart and Ravizza, 1996) or an HF+HBr mixture (Burton et al., 1999; 2002). The separation of Os from Re was conducted via distillation/chelex bead chemistry (Hart and Ravizza, 1996) while solvent extraction was employed by Burton et al. (1999; 2000; 2002). Os and Re analyses were also conducted via N-TIMS.

Subsequent studies, investigating the Re-Os isotopic signatures of silicates, oxides and/or BMS in mantle peridotites and using the wet chemistry approach (Harvey et al., 2010; 2011; Warren and Shirey, 2012; Wainwright et al., 2015; 2016; Kim et al., 2016; Bragagni et al., 2017; van Acken et al., 2017), combined the Pearson et al. (1998) method for the BMS determination - as it allows single BMS grain analysis - with the “bulk” mineral fraction approach of Hart and Ravizza (1996) and Burton et al. (1999; 2000; 2002) for the silicates and oxides since their extremely low Os and Re concentrations do not permit single silicate or oxide grains to be analyzed. Additionally, Luguet et al. (2007), who studied BMS-free but PGM-bearing ultra-refractory mantle peridotites, analyzed the fine grain boundary fraction (from <25 μ m sieved crushates), as a possible repository of residual PGM particles. Luguet et al. (2007) along with all the studies having focused on Re-Os analyses of single BMS grains via wet chemistry approach adapted some aspects of the original procedures of Pearson et al. (1998), Hart and Ravizza (1996) and Burton et al. (1999) to the challenge of analyzing Re-Os isotopic signatures and

their respective concentrations within single BMS, PGM and silicates/oxides in mantle peridotites. Specifically, single BMS grains are either hand-picked from granulites/sieved crushates of mantle peridotites (Harvey et al., 2010; 2011; Kim et al. 2016) or alternatively are directly sampled from the peridotite thin sections using a diamond scribe (Warren and Shirey, 2012) or a combination of laser beam and diamond scribe (Wainwright et al. 2015; 2016; Bragagni et al. 2017; van Acken et al. 2017) to excavate a cavity around the BMS that facilitates them being lifted out of the thin section as an unbroken BMS grain. Additionally, in Wainwright et al. (2016), where BMS and their PGM inclusions were analyzed for $^{187}\text{Os}/^{188}\text{Os}$ isotopic compositions, the nanometric PGM grains were extracted using the focused ion beam (FIB) technique. On the other hand, the digestion step employed for oxides and silicates by Harvey et al. (2010; 2011) remains similar to that of Burton et al (1999; 2002) whereas Luguet et al. (2007) used high-temperature high-pressure Carius tube digestions for investigating the silicates, oxides and fine-grain boundary fractions in highly refractory BMS-free to BMS-poor mantle harzburgites. High temperature (220°C) and high-pressure digestions using an HP-asher (Anton Paar) was also recently used to digest BMS and their nanometric PGM inclusions in one Bultfontein cratonic peridotite (Wainwright et al., 2016). These HT-HP digestions were shown to ensure a more efficient digestion of PGM grains (i.e. Pt-Ir-Fe alloys, OsS_2 - RuS_2 or Pt-Fe alloys) (Meisel and Moser, 2004).

In parallel to the onset and evolution of the analytical approach for Re-Os isotopic analyses in single BMS grains via extraction, digestion and wet chemistry; the analysis of BMS grains directly on thin sections via laser-ablation (LA) multi collector inductively coupled plasma mass spectrometry (MC-ICPMS) was developed (Pearson N.J. et al., 2002; Alard et al., 2002; 2005; 2011; Bruckner et al., 2004; Griffin et al., 2004; 2012; Powell and O'Reilly, 2007; Sapienza et al., 2007; Wang et al., 2009; Marchesi et al., 2010; González-Jiménez et al. 2013; 2014). The original investigations from the early 2000s as well as all subsequent ones were conducted using a nm-laser ablation system. This approach

allows single BMS grains in peridotites and, if size allows, even single sulfide minerals -making up multi-sulfide BMS assemblages- to be investigated.

Overall, 24 studies have been conducted on Re-Os isotopic systematics in BMS from mantle peridotites, among which 60% were performed using LA-MC-ICPMS at the GEMOC (Macquarie University, Australia), producing 85% of the currently available data. Studies using the wet chemistry approach were conducted in 6 different laboratories (i.e., Woods Hole Oceanography Institution-USA, Carnegie Institution of Washington-USA, Institut de Physique du Globe de Paris-France, Open University-UK, University of Durham-UK, University of Bonn-Germany).

V.2. Pros and cons of the sampling/extraction approach

Considering the complex crystallization and sub-solidus re-equilibration history that affects mineralogical assemblages of BMS, together with the consequence of these effects on the partitioning and fractionation between the parent and daughter elements of the Re-Os isotopic system, only the complete analysis of any given BMS grain will provide a representative view of the $^{187}\text{Os}/^{188}\text{Os}$ composition of the sulfide melt they derive from and potentially a better characterization of the source reservoir of these sulfide melts. This issue has been recently highlighted by Kemppinen et al. (2018) regarding the possible non-recovery of Re-rich molybdenite associated with diamond-hosted sulfide inclusions, as the molybdenite most likely constitutes the outermost rim of the sulfide inclusion or fills decompression fractures inside the diamonds. Not recovering and thus not analyzing the Re-rich molybdenite may impose substantial consequences on the $^{187}\text{Os}/^{188}\text{Os}$ composition of the BMS, leading to erroneous ages for the sulfide inclusions and improper characterization of the source reservoir of the diamonds and sulfides. This emphasizes the great care needed to recover as much material as possible during any sulfide analysis.

According to Kim et al. (2016), hand-picking of BMS grains from crushate allows for the complete BMS grain to be extracted and analyzed. This is an optimistic view as it is necessary to know the size and shape of the BMS prior to and after the crushing step, and there is the possibility that delicate exterior exsolutions (i.e., chalcopyrite) have been abraded by the crushing process (see Kemppinen et al., 2018). Furthermore, the possibility that BMS break apart during the crushing step of the peridotite cannot be ruled out. Nonetheless, among all the extraction procedures currently used for BMS, mineral hand-picking is the one most likely to sample the full BMS grains, as demonstrated by (i) the preservation of Re-Os isochron among hand-picked BMS from the central Slave craton pyroxenites (Aulbach et al., 2009b) and whose isochron age (1.84 ± 0.14 Ga) matches perfectly that obtained from the Re-Os isochron defined by eclogitic sulfide inclusions in diamonds from the same kimberlite pipes (Diavik; Aulbach et al., 2009a) and (ii) the consistent finding of similar ages in sulfide Re-Os isochrons within the cores and rims of Siberian diamonds (Wiggers de Vries et al., 2013). The main drawback of hand-picking BMS from crushates is the lack of any mineralogical and textural relationship information (with respect to other mineral phases) and the limited ability to characterize the BMS chemical compositions. At best, the Fe, Ni, Cu contents of the hand-picked sulfides could be determined via electron microprobe (Harvey et al., 2011) or by standard addition and external calibration of the washout of the column chemistry (e.g., Richardson et al., 2001; Laiginhas et al., 2009; Warren and Shirey, 2012) but does not allow, for example, to distinguish between small but variable modal proportions of individual Cu-sulfides/native Cu (with variable Cu/S ratio) and a much larger modal proportion of Cu-bearing pentlandite. Such fine-scale information is critical to understand the origin of the BMS populations and interpret the $^{187}\text{Os}/^{188}\text{Os}$ signatures of the BMS.

Textural, mineralogical as well as chemical characterization are possible for BMS being analyzed from thin section either via LA-MC-ICPMS or via extraction, digestion and wet-chemistry procedures. Unfortunately, analyzing BMS from a thin section implies that the BMS grains of interest provides only a partial picture of the whole original BMS due to the sectioning and/or polishing

necessary to the thin section preparation. The picture becomes more blurred when in-situ LA-MC-ICPMS analyses are considered as only a limited volume of the BMS grains is sampled, imposing even more bias on the representativeness of the Re-Os isotopic signature being conducted by LA-MC-ICPMS. However, the ability to analyze a number of individual sulfides and related phases making up single BMS grain via either in-situ LA-MC-ICPMS analyses or the mechanical extraction of the mineral from the thin section combined with wet-chemical procedures (Wainwright et al., 2016; Bragagni et al., 2017) opens up the potential (i) for intra-BMS isochrons to be obtained in the same way that Nowell et al (2008) exploited the complexity of PGM grains to obtain single “grain” Pt-Os isochrons or alternatively (ii) for nanometric to micrometric $^{187}\text{Os}/^{188}\text{Os}$ heterogeneity (Wainwright et al., 2016) and/or the absence of isotopic homogenization/re-equilibration to be better understood (Bragagni et al., 2017).

Further biases are imposed by these different analytical approaches (see Figure 5). As the LA-MC-ICPMS approach exclusively involves the use of nm-laser ablation system for investigating the Re-Os isotopic signatures of peridotite-hosted BMS, the size of BMS grains being analyzed is limited by the size of the laser beam to minimum dimensions of 60-80 μm (e.g., Pearson N.J., et al., 2002; Powell and O'Reilly, 2007; Marchesi et al., 2010). This guarantees sufficient signal to be obtained for a precise $^{187}\text{Os}/^{188}\text{Os}$ analysis. However, in mantle peridotites, BMS this large (>60-80 μm) tend to be metasomatic in origin while the residual BMS - due to the consumption of the primary sulfide minerals during partial melting - will tend to be of a much smaller size (see Luguet et al., 2003; Lorand and Grégoire, 2006; Wainwright et al., 2015), implying that the peridotites typically targeted via LA-MC-ICPMS for Re-Os isotopic investigations of their BMS grains will be predominantly metasomatised lherzolites and harzburgites with large BMS rather than refractory harzburgites with rare BMS of much smaller size ($\ll 50 \mu\text{m}$) that have likely the closest compositions to residues of partial melting. Still, as BMS in highly metasomatised and barely-metasomatised peridotites are a mixture (in different proportions) of metasomatic and residual BMS, the full spectrum of their $^{187}\text{Os}/^{188}\text{Os}$ signatures will

likely unravel the whole petrological history of the lithospheric mantle root from its stabilization (melt extraction) to its multi-stage evolution via metasomatism, refertilization and, in some cases, destruction.

In contrast, the direct micro-sampling of BMS or PGM from thin section using (i) a diamond scribe and/or laser ablation or (ii) focused ion beam milling allows for high spatial resolution in terms of extraction and analyses of BMS grains down to 10 μm in size as well as the excavation of nanometric PGM particles (Warren and Shirey, 2012; Wainwright et al., 2015; 2016; Bragagni et al., 2017, van Acken et al., 2017). As such, this approach facilitates the analysis of Re-Os isotopic signatures in BMS down to 10-20 μm in size and in nanometric PGM from BMS-poor ultra-refractory harzburgites to metasomatized harzburgites and lherzolites richer in BMS, and allows the exploration of new dimensions not accessible by the LA-MC-ICPMS approach.

V.3. Pros and cons of the analytical approaches (LA-MC-ICPMS versus wet chemistry+NTIMS and ICPMS)

One of the analytical strengths of the wet chemistry approach relies on the chemical separation of Os from Re, preventing the isobaric interference of ^{187}Re on ^{187}Os during measurement of the $^{187}\text{Os}/^{188}\text{Os}$ ratios. In contrast, during LA-MC-ICPMS analyses, these isobaric interferences may significantly affect the accuracy of the $^{187}\text{Os}/^{188}\text{Os}$ measurement of BMS having $^{187}\text{Re}/^{188}\text{Os}$ ratios $> \sim 1.6$ (Pearson N.J., et al., 2002). Nowell et al. (2008) suggested that accurate correction of the ^{187}Re interference on ^{187}Os could only be guaranteed in BMS grains having a maximum $^{187}\text{Re}/^{188}\text{Os}$ of ~ 0.6 , based on the complex laser-induced fractionation of Re from Os. Interestingly, subsequent LA-MC-ICPMS investigations of the $^{187}\text{Os}/^{188}\text{Os}$ signatures of BMS from mantle peridotites either complied to the Nowell et al. (2008) maximum $^{187}\text{Re}/^{188}\text{Os}$ values (0.5: see Marchesi et al., 2010) or used the original $^{187}\text{Re}/^{188}\text{Os}$ ratio (1.6) defined by Pearson N.J. et al. (2002) (see Alard et al., 2011) as the “accuracy cut-off”. This severe isobaric overlap issue imposes an additional strong bias on which BMS

grains can be accurately analyzed by LA-MC-ICPMS (see Alard et al., 2011). As such, Marchesi et al. (2010) stated that “Over 1000 sulfide grains were entirely sampled, [...] 88 had sufficiently high Os concentrations to give usefully precise isotopic results; 80 of these grains had $^{187}\text{Re}/^{188}\text{Os} < 0.5$ have been considered in the dataset”. The bias imposed on the $^{187}\text{Re}/^{188}\text{Os}$ ratios of the BMS analyzed by LA-MC-ICPMS is far from trivial considering the range of $^{187}\text{Re}/^{188}\text{Os}$ composition (0.01~ 68,000) reported in BMS from mantle peridotites processed via wet-chemistry and N-TIMS/ICPMS (Harvey et al., 2006; 2010; 2011; Warren and Shirey, 2012; Kim et al., 2016). BMS having $^{187}\text{Re}/^{188}\text{Os} < 0.5$ (the accuracy cut-off from Marchesi et al., 2010) represent 9%, 33%, 55% and 74% of the BMS processed respectively by Harvey et al. (2011), Warren and Shirey (2012), Harvey et al., (2006; 2011) and Kim et al. (2016).

Another significant difference between the LA-MC-ICPMS approach and the extraction, wet chemistry plus N-TIMS/ICPMS method lies in the analytical technique used to measure the $^{187}\text{Os}/^{188}\text{Os}$ ratios. It is well known that N-TIMS allows highly precise $^{187}\text{Os}/^{188}\text{Os}$ determination even for low-Os samples (see Pearson et al., 1998; Nowell et al., 2008). In-run (2 σ) precision of 0.006 to 0.03 % are obtained for N-TIMS measurements of 1-1000 pg Os load of the DROsS standard solutions conducted during the Re-Os isotopes analyses of BMS from peridotites (Wainwright et al. 2015, 2016; Bragagni et al. 2017; van Acken et al. 2017), while the in-run precision on the $^{187}\text{Os}/^{188}\text{Os}$ ratios measured by LA-MC-ICPMS (bigger than 50 μm) is 10-50 times (0.1-0.3 %) and 66-330 times (up to 1-2%) higher for BMS containing respectively 40 ppm Os and <5-10 ppm Os (see Wang et al., 2009).

One advantage of LA-MC-ICPMS is that along with the determination of $^{187}\text{Os}/^{188}\text{Os}$ and $^{187}\text{Re}/^{188}\text{Os}$ ratios, “semi-quantitative” Os and Pt concentrations of the BMS can also be estimated simultaneously by comparing the relative signal intensities of Os and Pt between the BMS grains and a sulfide standard such as PGE-A (see Griffin et al., 2012). The other HSE contents (Ir, Pd, Ru) can additionally be determined via LA-ICPMS on a different volume of the same BMS grains. Analysis of HSE concentrations, including Os and Re, based on isotope dilution and a wet-chemistry approach,

implies that the extracted BMS or PGM should be accurately and precisely weighed (achieved via multiple weighings) to determine the appropriate quantity of spike to be used during the digestion. However, these extracted BMS grains are extremely difficult to manipulate due to their small size (few μg) and thus this may lead to the loss of the BMS itself. Another issue to take into consideration is that to spike appropriately, it is necessary to estimate the Os content of the BMS grains to be analyzed, to avoid under or over spiking. This can be error prone. If weighing and/or spiking is successful, the wet-chemistry procedure may be extended to collect and determine Ir, Ru, Pt, Pd in addition of Re and Os on the same single BMS or PGM grain (see Luguet et al., 2008), or to determine Fe-Ni-Cu-Co concentrations along with those of Re and Os (e.g., Richardson et al., 2001; Laiginhas et al., 2009). Warren and Shirey (2012) and Burton et al. (2012) also analyzed simultaneously the Pb isotopic signatures.

Finally, on a more practical aspect, the LA-MC-ICPMS approach eliminates the difficulty of extraction of the BMS grains from the thin section and the risk of losing BMS while transferring them to the digestion vials or weighing them for the isotope dilution and wet-chemistry approach. LA-MC-ICPMS is a relatively fast approach permitting tens of BMS grains to be analyzed/screened in one day, while the procedure combining extraction, digestion, wet chemistry and N-TIMS+ICPMS measurements necessitates at least 6 days for 8-10 BMS grains to be analyzed and requires a very patient and dexterous operator as the work is time-consuming and painstaking. Ultimately, the LA-MC-ICPMS approach presents the advantage of being able to acquire relatively sizeable database theoretically permitting reliable statistical tests necessary to interpret the data themselves, but for the highest precision geochronology, the extraction-digestion-wet chemistry-NTIMS+ICPMS approach is best, especially for $<60 \mu\text{m}$ BMS or nanometer-size PGM from cpx-poor lherzolites and ultra-refractory harzburgites as well as BMS inclusions within diamonds.

VI. Mineral scale Re-Os isotopic signatures in mantle peridotites.

VI.1. Re-Os isotopic signatures of modally-major silicates and oxides.

Eleven studies have so far investigated the $^{187}\text{Os}/^{188}\text{Os}$ signatures along with the Os and/or Re contents of modally major minerals in mantle peridotites. These suites comprise BMS-bearing spinel lherzolites and harzburgites associated with continental rifts (Kilbourne Hole; Hart and Ravizza, 1996; Burton et al., 1999; Harvey et al., 2011; East Africa: Burton et al., 2000; Vietnam: Burton et al., 2002; Massif Central: Harvey et al., 2010), circum-cratonic garnet peridotites (Gibeon, Namibia: Aulbach et al., 2014) and cratonic spinel±garnet peridotites (e.g., Udachnaya, Siberia: Pearson et al., 1995a; Argyle, Australia: Luguet et al., 2009; West Greenland: Wittig et al., 2010; Udachnaya and Obnazhennaya, Siberia: Pernet-Fisher et al., 2015).

These studies highlighted several key aspects of the Re and Os concentrations as well as $^{187}\text{Os}/^{188}\text{Os}$ signatures mass balance (see Figure 6). The silicates and spinel of peridotites from continental rifts are systematically Os-poorer (from 5% to 480 times) than their corresponding whole-rock, with Os contents increasing from olivine to orthopyroxene, clinopyroxene and spinel (Burton et al., 1999; 2002; Harvey et al., 2010; 2011). Additionally, olivine has generally Re concentrations that are 3 to 50 times lower than the whole-rock peridotites, if two Kilbourne Hole peridotites (KH03-15 and KH03-16 from Harvey et al., 2011) are excluded. Analyses of olivine in cratonic peridotites confirm these trends for both Os and Re concentrations (Pearson et al., 1995a, Wittig et al., 2010; Pernet-Fisher et al., 2015) except for Greenland peridotites 474574 and 474576 (Wittig et al., 2010). In contrast, in two circum-cratonic peridotites from Gibeon (Aulbach et al., 2014), the Os and Re concentrations of the Ol fractions range from 5% lower to 30% higher than the respective whole-rock peridotite. These peridotites also differ in the fact that the Os contents of Ol and Opx are either similar or olivine is richer in Os (by ca. 25%) compared to the Opx fraction. Orthopyroxene, clinopyroxene and spinel, independent of the tectonic setting of the host peridotites (rift-related xenoliths, circum-cratonic xenoliths), do not show any strong systematic preferences and have either lower or higher Re

contents than the whole-rock peridotites. Interestingly, in the Argyle cratonic peridotite 6504257, the coarse primary chromite has Re contents 10 to 20 times higher than whole-rock peridotites while the isometric spinel symplectites show the opposite effect. Still both these cratonic chromite and spinel concentrates show variable Os contents extending to exceptionally high Os concentrations, up to 10 times that of the whole-rock peridotite (Luguet et al., 2009).

In continental-rift related peridotites and circum-cratonic peridotites, these findings translate into silicates and spinel having higher $^{187}\text{Re}/^{188}\text{Os}$; and $^{187}\text{Os}/^{188}\text{Os}$ ratios that vary from less radiogenic to more radiogenic than their corresponding whole-rock peridotites (Figure 6). On a $^{187}\text{Os}/^{188}\text{Os}$ versus $^{187}\text{Re}/^{188}\text{Os}$ plot, the silicates, spinel and whole-rock peridotites either appear to be in isotopic equilibrium, despite showing a large range of $^{187}\text{Re}/^{188}\text{Os}$ ratios (Figure 6A-B), or display a very loose positive trend, or are simply too scattered to display any trend. Interestingly in the cratonic peridotites, olivines yield $^{187}\text{Os}/^{188}\text{Os}$ compositions slightly to significantly less radiogenic than their corresponding whole-rock peridotites while having $^{187}\text{Re}/^{188}\text{Os}$ either higher (Pernet-Fisher et al., 2015) or lower (Pearson et al., 1995a) than the whole-rock peridotite.

The findings that silicates and spinel have more pronounced $^{187}\text{Re}/^{188}\text{Os}$ ratios highlight the partly lithophile character of rhenium, which was confirmed experimentally by Mallmann and O'Neill (2007) and Brenan (2008).

VI.2. Re-Os isotopic signatures of base metal sulfides.

Base metal sulfides have been analyzed for their $^{187}\text{Os}/^{188}\text{Os}$ compositions as separate fractions comprising a few grains each (Hart and Ravizza, 1996; Burton et al., 1999; 2000; 2002) within the same peridotites analyzed for $^{187}\text{Os}/^{188}\text{Os}$ ratios of silicates and spinels. These four studies demonstrated that separated BMS fractions (so-called “bulk” BMS fractions) had similar $^{187}\text{Os}/^{188}\text{Os}$ and/or $^{187}\text{Re}/^{188}\text{Os}$ to the whole-rock peridotites, highlighting that they controlled the whole-rock

$^{187}\text{Os}/^{188}\text{Os}$ and $^{187}\text{Re}/^{188}\text{Os}$ signatures. Burton et al. (1999) further showed that differences in $^{187}\text{Os}/^{188}\text{Os}$ signatures existed between the enclosed and the interstitial BMS, with the bulk enclosed BMS fraction being less radiogenic than the interstitial bulk BMS fraction (Figure 6A).

Subsequent studies investigated individual BMS signatures within mantle peridotites. While these studies confirmed the variable $^{187}\text{Re}/^{188}\text{Os}$ and $^{187}\text{Os}/^{188}\text{Os}$ compositions, they also added a level of complexity demonstrating that the $^{187}\text{Os}/^{188}\text{Os}$ variability exists between co-existing single BMS grains of Type 1 and/or Type 2, not only between enclosed versus interstitial BMS, as originally highlighted by Burton et al. (1999) (Figure 7A). Generally, it is observed that $^{187}\text{Os}/^{188}\text{Os}$ ratios of BMS extend from unradiogenic to radiogenic while their $^{187}\text{Re}/^{188}\text{Os}$ ratios range from lower than to higher than primitive upper mantle values (see Figure 6B and Figure 7).

In a $^{187}\text{Os}/^{188}\text{Os}$ versus $^{187}\text{Re}/^{188}\text{Os}$ plot, the BMS within a given peridotite show either (i) a relative large scatter (e.g., sample FRB 1500, Griffin et al., 2004) and no trend, (ii) fairly constant $^{187}\text{Os}/^{188}\text{Os}$ for a large range of $^{187}\text{Re}/^{188}\text{Os}$ (see orogenic peridotites DR93.10 and RPD07-6B from Ronda massif, Marchesi et al., 2010), (iii) a positive broad trend (see Figure 7A-B) or (iv) a negative trend (Figure 8). These positive or negative trends are not necessarily linear as seen for example for the BMS of the abyssal peridotite KN3-4 (Figure 7A) and the non-cratonic peridotite xenoliths MBr20 and GP12 (Figure 8). Positive trends are the most ubiquitous and are found in all types of mantle peridotites (tectonites, cratonic and non-cratonic xenoliths), while the negative trends, when observed, are confined to the non-cratonic peridotite xenoliths as well as the circum-cratonic peridotite xenoliths, both typically erupted by alkali basalts.

The positive $^{187}\text{Os}/^{188}\text{Os}$ versus $^{187}\text{Re}/^{188}\text{Os}$ trends defined by BMS from a given peridotite could be interpreted in terms of isochrons or rather errorchrons considering the scattered nature of the correlations (e.g. Bruckner et al., 2004; Wang et al., 2009; Kim et al., 2016). However, studies on the $^{187}\text{Os}/^{188}\text{Os}$ signatures of BMS, which were combined with extensive petrographical (habit, textural relationships, mineralogy, chemical composition) studies of the BMS (Luguet et al., 2001; 2003; 2004;

Alard et al., 2002; 2005; 2011) clearly showed that positive trends are defined by BMS from different petrological origins (Figure 7A). Specifically, the positive trends are defined by a mixture of residual Type 1 BMS, that survived the initial partial melting event, and a metasomatic Type 2 BMS, which precipitated during infiltration of small volume of silicate melts within the peridotites (see part IV). Generally, the Type 1 BMS yield $^{187}\text{Re}/^{188}\text{Os}$ lower than that of the PUM and have unradiogenic $^{187}\text{Os}/^{188}\text{Os}$ signatures, but “exceptions” to this exist. The metasomatic Type 2 BMS have generally higher $^{187}\text{Re}/^{188}\text{Os}$, above the PUM values and more radiogenic $^{187}\text{Os}/^{188}\text{Os}$ than Type 1 BMS but these $^{187}\text{Os}/^{188}\text{Os}$ signatures are not always radiogenic (see Figure 7A for BMS of the abyssal peridotite KN3-4: Alard et al. 2005). The development of errorchrons among the BMS populations suggest that the partial melting event that left the Type 1 BMS in the mantle residue, as well as the metasomatic event that formed the Type 2 BMS are both ancient enough to have enabled ^{187}Os ingrowth within both BMS populations (see Figure 7A). Nonetheless, the scatter in $^{187}\text{Os}/^{188}\text{Os}$ and $^{187}\text{Re}/^{188}\text{Os}$ ratios among the Type 2 BMS results in a non-linear positive trend (Figure 7A) either reflecting the occurrence of more than one generation of Type 2 BMS (multiple infiltrations of silicate melts) or a possible sampling artefact since neither the LA-MC-ICPMS nor the BMS extraction from thin section followed by wet chemistry and NTIMS+ICPMS allows the analysis of a whole single BMS (see part V.2.). Alternatively, if the Type 2 BMS grains show close to or isotopic equilibrium, this can be taken as an evidence for a relative recent overprinting especially if the BMS exhibit rather elevated $^{187}\text{Re}/^{188}\text{Os}$ ratios (see Marchesi et al., 2010).

In situations where BMS populations are clearly identified from textural, morphological and mineralogical criteria, positive trends defined within BMS populations may still be taken, at face value, as isochrons. For instance, Harvey et al. (2006) established, in the Mid Atlantic ridge abyssal peridotite 2R1 31-37, that five Type 1 BMS defined an isochron yielding an age of 2.06 ± 0.26 Ga (MSWD 3.3) for an initial $^{187}\text{Os}/^{188}\text{Os}$ composition of 0.11396 ± 0.00030 . Assuming a present-day mantle $^{187}\text{Os}/^{188}\text{Os}$ composition of 0.1292 as estimated from global abyssal peridotites (Day et al., 2017) and an initial

$^{187}\text{Os}/^{188}\text{Os}$ for the solar system of 0.0952 (see Smoliar et al., 1996; Day et al., 2016), the initial composition of this isochron is within error of the terrestrial mantle composition at 2.06 Ga, providing strong support to the interpretation that these BMS are residual (Type 1 BMS) and that their Re-Os isochron defines the age of partial melting of this specific mantle portion.

Negative $^{187}\text{Os}/^{188}\text{Os}$ versus $^{187}\text{Re}/^{188}\text{Os}$ trends defined by BMS in peridotites imply that BMS with low $^{187}\text{Re}/^{188}\text{Os}$ have the most radiogenic $^{187}\text{Os}/^{188}\text{Os}$ and that the BMS with the highest $^{187}\text{Re}/^{188}\text{Os}$ have the lowest, generally unradiogenic $^{187}\text{Os}/^{188}\text{Os}$ (Figure 8A). This highlights a decoupling between the parent/daughter ratio and the resulting $^{187}\text{Os}/^{188}\text{Os}$ composition of the BMS and indicates that overprinting occurred, due to a fluid or melt derived from a radiogenic $^{187}\text{Os}/^{188}\text{Os}$ (long term high Re/Os) source, via metasomatic addition of Os rather than solely Re addition followed by ^{187}Os ingrowth. Of course, once this metasomatic overprint happened, radiogenic ingrowth of ^{187}Os will likely contribute to the obliteration of these negative trends. This of course ultimately depends on the bulk $^{187}\text{Re}/^{188}\text{Os}$ of the BMS. For example, the negative trend exhibited among the BMS of the Sicilian peridotite GE12 (Sapienza et al., 2007) would likely be erased in 400 Myr while that defined by the BMS from the Montferrier peridotite Pg2 (Alard et al., 2011) would not be erased even after 4 Gyr.

So far, such inverse $^{187}\text{Os}/^{188}\text{Os}$ versus $^{187}\text{Re}/^{188}\text{Os}$ trends are restricted to BMS from non-cratonic and circum-cratonic mantle peridotites (i) from the French Massif Central volcanic province: Mtf37 and Pg2 from Montferrier (Pearson N.J. et al., 2002; Alard et al., 2002; 2011), MBS1 from Montboissier (Alard et al., 2002); MBr20 from Mont Briançon (Harvey et al., 2010); (ii) from the Cathaysia block in South East China: NTS2 from Niutoushan (Xu et al., 2008); KPH9816 and PH0201 from Penghu (Xu et al., 2008; Wang et al., 2009) and (iii) from the Hyblean Plateau, Sicily: GE12 (Sapienza et al., 2007). Among all these locations, the most comprehensive study has been undertaken on the Montferrier suite (Alard et al., 2011), as it integrates the whole-rock major elements, trace

elements, $^{187}\text{Os}/^{188}\text{Os}$ and HSE systematics with BMS petrography (abundances, textural relationships, mineralogy), HSE and $^{187}\text{Os}/^{188}\text{Os}$ systematics.

What stands out from the petrological description of all these specific mantle peridotite localities and from the detailed petrographical description of their BMS -when available- is the recurrent presence of fluids or hydrous minerals. For example, in the Mont Briançon suite (Harvey et al., 2010), peridotites from the Hyblean Plateau (Sapienza et al., 2007) and the Penghu Islands mantle xenoliths (Wang et al., 2009), the silicates enclosing BMS contain CO_2 -bearing fluid inclusions and possibly melt inclusions. Hydrous minerals, such as amphibole, phlogopite and apatite were additionally described as part of the peridotite paragenesis in the Penghu Island and Montferrier mantle xenoliths (Wang et al., 2009; Alard et al., 2011). In the Montferrier peridotite xenoliths Mtf37 and Pg2 (Alard et al., 2011), these features are associated with whole-rock LREE depletion ($\text{La}/\text{Sm}_{\text{PM}} < 1$, $\text{PM} = \text{primitive mantle normalized after McDonough and Sun, 1995}$) and the highest positive U anomalies ($\text{U}/\text{Th}_{\text{PM}} > 100$) of all Montferrier mantle xenoliths. Similar trace element features ($\text{La}/\text{Sm}_{\text{PM}} < 1$ and $\text{U}/\text{Th}_{\text{PM}} > 2-4$) are observed in Montboissier mantle xenolith MBS1 (Alard et al., 1996; Lorand and Alard, 2001) and in the Mont Briançon mantle xenolith MBr20 (Harvey et al., 2010). Such trace elements signatures (i.e., LREE depletion, positive U anomaly) were traditionally ascribed to oxidizing, carbonated and/or volatile-rich metasomatism (e.g. Yaxley et al., 1991). As observed in the Montferrier mantle xenolith suite, this metasomatic agent becomes progressively enriched in LREE+LILE and volatile (C-H-O-S+Cl) in the upper part of the lithosphere due to on-going reactions with the surrounding peridotite. This leads to significant BMS precipitation and subsequent whole-rock enrichment in S, Os, Pd and Re (concentrations $> \text{PUM}$ estimates of McDonough and Sun, 1995 and Becker et al., 2006) as documented by suprachondritic $\text{Os}_{\text{N}}/\text{Ir}_{\text{N}}$, $\text{Pd}_{\text{N}}/\text{Ir}_{\text{N}}$, $\text{Re}_{\text{N}}/\text{Os}_{\text{N}}$ and S/Se ratios in the most LREE-rich ($\text{La}/\text{Sm}_{\text{PM}} > 1$) Montferrier peridotites. Metasomatic BMS in such Montferrier peridotites exhibit suprachondritic $\text{Os}_{\text{N}}/\text{Ir}_{\text{N}}$, $\text{Re}_{\text{N}}/\text{Os}_{\text{N}}$ and $\text{Pd}_{\text{N}}/\text{Ir}_{\text{N}}$ ratios coupled with relatively low Os and Ir abundances (Type 4 BMS, see Figure 3). The preferential enrichment of Os over supports a

fluid, possibly oxidizing, as a metasomatic agent (McInnes et al., 1999; Lee, 2002; Lorand et al., 2004; Delpech et al., 2012). With a supercritical fluid as a metasomatic agent, BMS precipitation was proposed to occur via sulfidation reactions (Alard et al., 2011).

VI.3. Re-Os isotopic signatures of base metal sulfides and of their platinum group minerals inclusions

While millimeter-sized residual PGM (e.g., Os-rich alloys and Pt-Ir-Os alloys) found as placers derived from ophiolites, ultramafic massifs and greenstone belts have been the focus of LA-MC-ICPMS investigations over the last 15 years (e.g., Malitch and Merkle, 2004; Walker et al., 2005, Shi et al., 2007; Pearson et al., 2007; Nowell et al., 2008; Luguet et al., 2008; Coggon et al., 2011; 2012; González-Jiménez et al., 2012), the study of Wainwright et al. (2016) constitutes the only investigation of the $^{187}\text{Os}/^{188}\text{Os}$ signatures of micrometer to nanometer-sized PGM inclusions (i.e., Pt-Fe alloys) and their respective Ni-rich BMS (pentlandite) hosts in a mantle peridotite. The extreme rarity of such study is mostly due to the fact that PGM from mantle peridotites are easily overlooked due to (i) their extremely small size, (ii) their assumed small impact on the HSE and $^{187}\text{Os}/^{188}\text{Os}$ composition of the original BMS (in term of pre-exsolution HT component) and the whole-rock peridotite; and (iii) the fact that they necessitate a time-consuming chemistry and challenging mechanical FIB (focused ion beam) extraction from the BMS and thin section, before digestion and Os chemical separation.

The metasomatic Pt-Fe alloy inclusions identified by Wainwright et al. (2016) in a Bultfontein (Kaalpvaal craton) garnet harzburgite yield PUM-like to radiogenic $^{187}\text{Os}/^{188}\text{Os}$ composition (0.1294-0.1342) while their metasomatic BMS hosts are unradiogenic (0.1066-0.1084), even more unradiogenic than their whole-rock harzburgite (0.10895-0.10969). The striking difference in $^{187}\text{Os}/^{188}\text{Os}$ signatures between the Pt-Fe alloys and their BMS hosts reflects different Re/Os as demonstrated by the preliminary experimental investigations conducted in Wainwright et al., (2016) and confirmed by the

more comprehensive experimental study of Fonseca et al. (2017) (Figure 9). Metasomatic Pt-Fe alloys coexisting exclusively with sulfide melt and mss (experiments at $>950^{\circ}\text{C}$ in Fonseca et al., 2017) have $K_D^{\text{Re-Os}}$ ($D_{\text{Re}}^{\text{alloy/sulfide melt}}/D_{\text{Os}}^{\text{alloy/sulfide melt}}$) of 1.24-2.18 demonstrating that, upon alloy formation, the Pt-Fe alloy would have a much higher Re/Os ratio than those of the co-existing sulfide melt and mss. This, with time, will lead to the $^{187}\text{Os}/^{188}\text{Os}$ signatures of the alloys being more radiogenic compared to those of the BMS and/or sulfide melt. This partitioning behavior between Pt-Fe alloys and BMS perfectly explains the findings of Wainwright et al. (2016) (see Figure 9). However, the partitioning coefficients of Fonseca et al. (2017) are not directly applicable to the Pt-Fe alloy and pentlandite host from the Bultfontein peridotite as (i) the sulfide mineral and sulfide melt compositions are different between the natural sample and the experimental investigation and (ii) the temperature of exsolution of the Pt-Fe alloy from the Bultfontein BMS is much lower (likely $< 800^{\circ}\text{C}$) than those chosen for the experimental study ($1244\text{-}850^{\circ}\text{C}$).

The most significant implication of the Re/Os fractionation upon exsolution of PGM from metasomatic BMS is that the initial $^{187}\text{Os}/^{188}\text{Os}$ composition of both (if back-calculated following the T_{MA} model age principle) will date the time of the PGM exsolution (see Figure 9) but not the timing of metasomatism as would be generally considered for Re-Os isotopic dating of metasomatic BMS. How close this PGM exsolution age is to the age of the metasomatic overprinting cannot be realistically estimated on the basis of the stability fields of pentlandite and Pt-Fe alloys experimentally-determined at 1atm but requires a better understanding of the solidus temperatures of these phases at pressures relevant to cratonic peridotite mantle residence (4-6 GPa) (Wainwright et al., 2016).

VII. Re-Os isotopic signatures of base metal sulfides and of their whole-rock peridotites.

VII.1. Meaning of whole-rock Re-Os signatures and insights into the petrological history of mantle peridotites.

BMS Re-Os isotopic systematics are available, sometimes along with the whole-rock Re-Os isotopic systematics of their host mantle peridotites, from the whole spectrum of tectonic settings, in which mantle peridotites are found (e.g., tectonites: Brueckner et al., 2004; Marchesi et al., 2010; Warren and Shirey; 2012; non-cratonic xenoliths: Hart and Ravizza, 1996; Powell and O'Reilly, 2007; Harvey et al., 2011; González-Jiménez et al., 2014; circum-cratonic xenoliths: Xu et al., 2008; Kim et al., 2016; cratonic xenoliths: Griffin et al., 2004; Wainwright et al., 2015; van Acken et al., 2017, oceanic island xenoliths: Coltorti et al., 2010).

Typically, whole-rock mantle peridotite $^{187}\text{Os}/^{188}\text{Os}$ and $^{187}\text{Re}/^{188}\text{Os}$ compositions lie within the range defined by their BMS (see Figure 7A-B and Figure 8), demonstrating that the whole-rock Re-Os isotopic systematics represent an average of the different BMS populations (Griffin et al., 2004; Alard et al., 2005). There are a few exceptions where the whole-rock $^{187}\text{Os}/^{188}\text{Os}$ value is lower or higher than that of any of the BMS analyzed (e.g. MBr6 and MBr3 from Harvey et al., 2010) or where duplicated whole-rock peridotite analyses do not reproduce. These constitute evidences of the heterogeneous distribution of the HSE host phases and their nugget effect on the whole-rock Re-Os isotopic systematics or alternatively hint that some BMS or PGM types (i.e., different origins) significantly affecting the HSE budget were not analyzed during the in-situ Re-Os isotopic investigation, revealing an even more complex picture of the nature and number of Os-Re host minerals. Ultimately the fact that within a given mantle peridotite, BMS can have $^{187}\text{Os}/^{188}\text{Os}$ signatures less radiogenic than that of the whole-rock peridotite demonstrate that BMS may record model ages (T_{RD}) far older than their whole-rock peridotite, possibly by more than 3 Ga (see BMS 12a, peridotite JGR98/6: Griffin et al., 2004). This obviously challenges the “geological” meaning of the whole-rock Re-Os model ages, although investigations aiming to constrain the age of stabilization (melt extraction) should not select metasomatic BMS-rich peridotites as, for example, JGR98/6.

An positive relationship exists between the major element compositions of the peridotites (their “fertile/refractory” character) and the difference between the $^{187}\text{Os}/^{188}\text{Os}$ ratio of the whole-rock

peridotite and that of its most unradiogenic BMS (hereafter $\Delta^{187}\text{Os}/^{188}\text{Os}_{\text{WR-BMS}^*}$) (Figure 10) when the global dataset is considered as well as within some specific mantle peridotite localities (Massif Central and SE Australia: Pearson N.J. et al., 2002; Alard et al., 2002; Somerset, Bragagni et al., 2017). Generally, the $\Delta^{187}\text{Os}/^{188}\text{Os}_{\text{WR-BMS}^*}$ is the lowest for harzburgitic peridotites (i.e., 0.00038-0.010 with only two exceptions), which are predominantly from cratonic settings (Figure 10). In contrast, the most unradiogenic $^{187}\text{Os}/^{188}\text{Os}$ signatures of BMS from lherzolites, mainly erupted as non-cratonic xenoliths associated with continental rifts, diverge more significantly from their host peridotite (0.007 to 0.033). Whether we consider an PUM-like evolution or chondrite evolution through time for the terrestrial mantle, these deviations translate into T_{RD} modal ages differences of 0.05 to 1.43 Gyr for harzburgitic lithologies and 0.96 to 2.6 Gyr for lherzolitc lithologies. On the other hand, when the isotopic compositions of both the least radiogenic BMS and their host peridotite are both considered individually (Figure 11), then the least radiogenic BMS within lherzolites, have strikingly similar $^{187}\text{Os}/^{188}\text{Os}$ signatures (e.g., 0.1124-0.1151, peridotites Gam VL8, Gam VL11, Gam Tr6, MBr11, Mtf37, MBr20, Pearson N.J. et al., 2002; Alard et al., 2002; 2011; Harvey et al., 2011), independently of the fertility of their host peridotite (i.e., whole-rock Al_2O_3 content), whereas in contrast, the whole-rock lherzolite $^{187}\text{Os}/^{188}\text{Os}$ signatures evolve toward more radiogenic values with increasing fertility.

There are three major implications to these observations:

- 1- if the goal of whole-rock Re-Os isotopic investigations is to constrain the timing of melt extraction and therefore the age of stabilization of the lithospheric mantle, then the researcher should aim at dating the most refractory mantle peridotites, especially those virtually BMS-free (i.e. S-free/poor), devoid of metasomatic minerals (e.g. phlogopite, apatite, carbonates) and exhibiting whole-rock HSE patterns typical of partial melting residues ($\text{Pd}_\text{N}/\text{Ir}_\text{N} \ll 0.3$). This would generally correspond to spinel or spinel±garnet

harzburgites exhibiting relatively low pressure and temperature of equilibration. As such, Bragagni et al (2017) recorded the lowest $\Delta^{187}\text{Os}/^{188}\text{Os}_{\text{WR-BMS}^*}$ (0.0004) for the spinel-garnet harzburgite X07 ($\text{Al}_2\text{O}_3= 0.2$ wt. %; $\text{Pd}_\text{N}/\text{Ir}_\text{N}=0.21$: see Irvine et al., 2003). This corresponds to an age difference of only a 50 Myr between the oldest BMS and its whole-rock peridotite host. Among the different peridotite settings considered, harzburgitic lithologies are predominantly found within cratonic or circum-cratonic mantle xenoliths (e.g., Janney et al., 2010; Pearson and Wittig, 2014; Luguet et al., 2015), which are systematically dated to understand the early Earth evolution and the stabilization of the first continental masses.

- 2- Secondly, the lherzolites, which have been considered as fertile and primitive mantle peridotites for decades, have the largest $\Delta^{187}\text{Os}/^{188}\text{Os}_{\text{WR-BMS}^*}$ (Figure 10) but similarly unradiogenic $^{187}\text{Os}/^{188}\text{Os}$ compositions of their BMS (Figure 11) confirming that their whole-rock budget is very significantly affected by metasomatic HSE host phases. This supports the view that these rocks owe their fertility to melt-rock and/or fluid-rock interaction rather than representing any form of “primitive” unmelted mantle composition.
- 3- Consequently, lherzolites as well as BMS-rich harzburgites constitute the best targets for examining the post-melting petrological evolution of the Earth’s mantle. The petrological, mineralogical and geochemical investigations of lherzolites and BMS-rich harzburgites at the whole-rock scale in combination with the detailed petrographical and geochemical characterization of the Re-Os host phases would provide a comprehensive view of the timing and the nature of the metasomatic overprints that modify the composition of lithospheric mantle. This would in return help us better constrain the behavior of the HSE during specific types of metasomatism or refertilization, for example (i) those involving fluids from different compositions or (ii) metasomatism resulting from the percolation of

large volume of silicate melts. However, it is obvious that one should refrain from considering the whole-rock $^{187}\text{Os}/^{188}\text{Os}$ compositions of such metasomatic BMS-rich harzburgites and lherzolites as primitive, non-metasomatised signature and draw conclusions on timing of formation of early continental masses or the process responsible for the generation of the cratons and their thick mantle roots. This may lead to flawed interpretations such as the view that cratonic mantle root becomes younger with depth, whereas the varying whole-rock $^{187}\text{Os}/^{188}\text{Os}$ composition simply reflects rejuvenation and refertilization of the deepest parts of this lithospheric mantle by intensive metasomatism/refertilization.

If we now consider all the BMS analyzed for a given mantle peridotite and specifically the difference in $^{187}\text{Os}/^{188}\text{Os}$ composition between each BMS and its host peridotite (referred to as $\Delta^{187}\text{Os}/^{188}\text{Os}_{\text{WR-BMS}}$), the range of $\Delta^{187}\text{Os}/^{188}\text{Os}_{\text{WR-BMS}}$ is very large (Figure 12) in the most refractory harzburgites but becomes smaller, although still significantly variable, within the lherzolic lithologies. This confirms that the BMS occurring within mantle peridotites have different origins (residual versus metasomatic) and that they trace multiple metasomatic processes. This variability furthermore demonstrates that there is no mantle peridotite available at Earth's surface that is a pure residue of partial melting, devoid of any post-melting modification.

The decreasing scatter in the BMS $^{187}\text{Os}/^{188}\text{Os}$ compositions with increasing peridotite fertility (Figure 12) combined with the increasing $\Delta^{187}\text{Os}/^{188}\text{Os}_{\text{WR-BMS}}$ (Figure 10) clearly demonstrates a shift in the nature of the phases and/or BMS populations accounting for the whole-rock Os budget. For instance, in the harzburgites, Os-rich residual BMS or possibly Os-rich PGM (e.g., $(\text{Os},\text{Ru})\text{S}_2$ or Os-rich alloys) mainly control the whole-rock mass balance resulting in the smallest difference between the $^{187}\text{Os}/^{188}\text{Os}$ ratio of the most unradiogenic BMS and their corresponding whole-rock. In contrast,

the metasomatic BMS, independently of their origins (Types 2-3-4 BMS, see Part IV), dominate the whole-rock Os concentrations and $^{187}\text{Os}/^{188}\text{Os}$ ratios of the lherzolites, triggering a shift toward radiogenic values (See Figure 11) at the whole-rock scale and generating the largest difference between the Os isotope compositions of the most unradiogenic BMS and their corresponding lherzolite ($\Delta^{187}\text{Os}/^{188}\text{Os}_{\text{WR-BMS}^*}$) (see Figure 10). The corollaries to this are (i) that both residual and metasomatic BMS are present in harzburgites and the lherzolites and (ii) that the relative proportions of the residual versus metasomatic types get inverted from ultra-refractory harzburgites to fertile lherzolites due to increasing metasomatic overprinting.

VII.2. Using BMS Re-Os isotopic signatures to date lithospheric mantle formation and evolution

There is a general agreement that the first and likely most robust way to date a petrological event from the Re-Os isotopic signatures of BMS – as for whole-rock peridotites - would be to obtain a $^{187}\text{Os}/^{188}\text{Os}$ versus $^{187}\text{Re}/^{188}\text{Os}$ isochron. This has been demonstrated successfully from studies conducted on diamond-hosted BMS (e.g., Pearson et al., 1998; Aulbach et al., 2004; 2009a; Westerlund et al., 2006; Smit et al., 2010), as the BMS armored within their diamond hosts evolve in closed system since the time of their entrapment. As we discussed in Part VI.2., positive linear $^{187}\text{Os}/^{188}\text{Os}$ versus $^{187}\text{Re}/^{188}\text{Os}$ correlations do occur among BMS from a single mantle peridotite (e.g., Griffin et al., 2004; Brueckner et al., 2004; Harvey et al., 2006). However, only when the BMS petrography has been studied in great detail and the origin of the BMS (metasomatic versus residual) defining the $^{187}\text{Os}/^{188}\text{Os}$ versus $^{187}\text{Re}/^{188}\text{Os}$ trend has been constrained, can we make a clear judgement as to whether it represents an isochron (see Harvey et al., 2006) or a mixing line.

The typical situation when BMS from mantle peridotites are analyzed is, unfortunately, either the absence of isochron or if an “isochron-like” positive trend exists, the trend is defined by BMS from different origins, making it a mixing line of no age significance. Instead, the Re-Os isotopic signatures of BMS are typically converted into Re-Os model ages (see Part II), to try to constrain (i) the timing or

partial melting and stabilization of the lithospheric mantle, or (ii) the timing of metasomatism/refertilization events, which contributed to the petrological and chemical evolution of the lithospheric mantle (e.g., Pearson N.J. et al., 2002; Griffin et al., 2004; 2012; Powell et al., 2007; Sapienza et al., 2007; Gonzalez-Jimenez et al., 2014; Wainwright et al., 2015; Kim et al., 2016; Bragagni et al., 2017, van Acken et al., 2017).

Model ages for BMS are typically presented as probability density plots (see Griffin et al., 2004; Bragagni et al., 2017; van Acken et al., 2017) to highlight age clusters. In many ways, probability density plots, when improperly used, are no better than histograms in that they are subject to the vagueness of which “bandwidth” (broadly equivalent to the “bin width” in histograms) is chosen. The pros and cons of this approach in the context of Re-Os model ages have been discussed by Pearson et al. (2007) and Pearson and Wittig (2014). Appropriate approaches to estimating bandwidth should be explored because the selection of too small a bandwidth, or even the use of internal uncertainties on model ages that have not been fully propagated, will drastically over-emphasize individual ages by assigning too high a probability for single analyses. From the model age perspective, it is best to select a uniform, conservative bandwidth to avoid these problems.

Interestingly, when Re-Os isotopic analyses of the whole-rock host peridotite plus other peridotites from the same or nearby suite(s) are available, the BMS model ages appear to define somewhat clearer age clusters on probability density plots (Griffin et al., 2004; Bragagni et al., 2017; van Acken et al., 2017). Such observations are not unique to BMS from mantle peridotites. For example, Pearson et al. (2007) demonstrated that PGM from placers related to Phanerozoic ophiolites showed sharper clusters of model ages when compared to the Re-Os model ages of the ophiolitic peridotites they derived from. It is then clear that Re-Os isotopic signatures of BMS have the ability to provide a much higher resolution for petrological events, possibly also revealing a more complex

petrological history of the lithospheric mantle compared to that generally extrapolated from the whole-rock host peridotite $^{187}\text{Os}/^{188}\text{Os}$ signatures.

The clustering of BMS Re-Os model ages on probability density diagrams show prominent modes in the data that tend to overlap with age clusters from regional or local crustal material determined by Sm-Nd on whole-rocks or U-Pb on zircons. The correspondence in age clusters of crustal material and Re-Os host phases from mantle lithologies was also observed for zircons and Os-bearing PGM by Pearson et al. (2007) and Nowell et al. (2008). This overlap in age peaks hints at a mantle-crust genetic link that may be related to peaks in crust genesis (e.g., Parman et al., 2007) rather than crust preservation (e.g., Hawkesworth et al., 2017). This apparent synchronicity between crust and mantle ages is of global nature (Pearson et al., 2007; Dijkstra et al., 2016), coincident with the stabilization of lithospheric mantle roots and the subsequent large igneous events that modify the roots. The Re/Os ratios of the Os-rich PGM analyzed by Pearson et al. (2007) and Dijkstra et al. (2016) is typically extremely low meaning that the T_{RD} model age will closely approximate a melt-depletion event in ancient, unradiogenic samples. In contrast, when this approach is attempted en-masse using BMS (e.g., Griffin et al., 2004), a much greater spread in ages occurs possibly due to the inaccuracies induced in the laser ablation analysis of polished BMS, or possible analytical uncertainties related to the correction of Re on the Os mass spectra (Nowell et al., 2008).

Matching the BMS modes of Re-Os model ages with crustal ages should not be considered a rule of thumb. Decoupling between the formation age of lithospheric mantle and the overlying crust has been demonstrated from ultra-refractory spinel harzburgites (i.e., the most robust targets for whole-rock Re-Os approach) clearly associated with cratonic settings (Argyle: Luguet et al., 2009; Letlhakane: Luguet et al., 2015) and in much younger crustal terranes (Zealandia: McCoy-West et al., 2013; Liu et al., 2015). All these ultra-refractory peridotites yielded much older formation ages (up to 2.4 Byr) than their associated Proterozoic (e.g., Argyle and Letlhakane) or Phanerozoic (Zealandia) crust. This crust-mantle decoupling persists when the $^{187}\text{Os}/^{188}\text{Os}$ signatures of BMS from the same ultra-refractory

harzburgites (namely Letlhakane) were analyzed (Wainwright et al., 2015), with BMS confirming or even pushing the formation of the lithospheric mantle root further back in time by up to ~1 Byr (Wainwright et al., 2015).

VII.3. Large scale geodynamical implications for the terrestrial mantle evolution.

An interesting observation made from the overall $^{187}\text{Os}/^{188}\text{Os}$ database acquired so far on BMS (Figure 13) is that there is a clear difference in the range and distribution of the $^{187}\text{Os}/^{188}\text{Os}$ ratios of BMS from cratonic and circum-cratonic peridotites versus those from post-Archean terranes (non-cratonic and tectonites). Firstly, the BMS from cratonic and circum-cratonic peridotites extend to the most unradiogenic $^{187}\text{Os}/^{188}\text{Os}$ ratios (i.e. as low as 0.1016: Wainwright et al., 2015) while the BMS from tectonites and those from non-cratonic peridotite xenoliths have $^{187}\text{Os}/^{188}\text{Os}$ ratios only as low as ~ 0.114 (see Ronda: Marchesi et al., 2010). This confirms the contrast in their stabilization age, already clearly shown by the Re-Os isotope systematics of whole-rock peridotite data. The main contribution of the BMS is to push back in time the absolute ages. But ultimately the Re-Os isotopic system, used on both whole rock peridotites and BMS clearly shows the difference in formation ages between mantle lithosphere beneath cratonic regions and beneath Proterozoic-Phanerozoic terranes.

There is one exception to this general observation. The BMS from the peridotite xenoliths of the oceanic island of Cape Verde have $^{187}\text{Os}/^{188}\text{Os}$ ratios as low as 0.1013, similar to those of the cratonic and circum-cratonic BMS (Figure 13), suggesting the presence, under Cape Verde, of an Archean sub-continental lithospheric mantle fragment, that got stranded in the oceanic mantle during Atlantic opening (O'Reilly et al., 2009). Similarly, the existence of Mesoproterozoic and Paleoproterozoic Re-Os model in the ultra-refractory mantle lithosphere beneath Zealandia (McCoy-West et al., 2013; Liu et al., 2015), whose crust is no older than Cambrian in age and mostly of Jurassic age, were attributed to the recycling of Archean refractory mantle accreted beneath the Zealandia crust during Zealandia formation, and its subsequent mixing with modern convective mantle (Liu et al., 2015).

The preservation of ancient melting signatures for billions of years after the initial melt depletion event has been one of the striking revelations of the Re-Os isotope system. This is especially prominent for oceanic peridotites (abyssal and ophiolitic), which are emplaced within seafloor whose age varies from present-day to Mesozoic (e.g. Brandon et al., 2000; Alard et al., 2005; Schulte et al., 2009; Warren and Shirey, 2012; O'Driscoll et al., 2018). The survival of Proterozoic BMS±PGM in packages of mantle now resting within oceanic lithosphere that can have formed no earlier than the Mesozoic constitutes one of the clearest examples of the isotopic heterogeneity of the terrestrial mantle at the micrometer to nanometer-scale. Persistence of such ancient ages likely reflects the fact that portions of the oceanic mantle have melted extensively enough, billions of years prior to their encapsulation and stabilization in lithospheric plates, to exsolve Os-rich (i.e., wt.% Os) PGM such as laurite-erlichmanite or Os-Ru±Ir alloys (see Part IV.2). Because of their highly refractory and inert nature combined with their wt.% Os content and low Re/Os ratios (e.g., Meibom et al., 2004; Malitch and Merkle, 2004; Fonseca et al., 2017), these residual Os-rich PGM would not re-equilibrate and hence would preserve their $^{187}\text{Os}/^{188}\text{Os}$ signatures over billions of years, possibly surviving subsequent melting and metasomatic events. This view is specifically supported by the preservation of much older ages in Os-rich and Pt-rich PGM associated to ophiolitic massifs and which yield systematically much older ages than their host peridotites (e.g., Meibom et al., 2002; 2004; Pearson et al., 2007).

In some ways, it is surprising that the oldest ages within abyssal peridotites are found within BMS and not in Os-rich alloys, which have not been observed so far in these rocks (Alard et al., 2005; Harvey et al., 2006; Warren and Shirey, 2012). The absence of Os-rich alloys in these rocks is likely a result of the multi-stage petrogenetic history of the mantle peridotites. As soon as a mantle residue containing Os-rich PGMs experiences a metasomatic event that leads to the precipitation of base metal sulfides, it is very likely that the Os-rich PGM will redissolve within the sulfide matte (see Griffin et al., 2002; Delpech et al., 2012) due to the very high solubility of Os (Fonseca et al., 2011).

The variable Re-Os isotope systematics of abyssal peridotites at the whole-rock scale have been recently used to estimate a timescale of 1.2 Gyr for the homogenization of isotopic heterogeneities within the convective oceanic mantle (Chatterjee and Lassiter, 2016). However, because the BMS signatures in abyssal peridotites demonstrably control their whole-rock signatures, there is some doubt over this estimate. First, there is significantly more variation in both $^{187}\text{Os}/^{188}\text{Os}$ and $^{187}\text{Re}/^{188}\text{Os}$ among BMS compared to their corresponding whole rock abyssal peridotites and secondly, the 1.2 Gyr mixing timescale would not explain the survival of ca. 2 Ga old BMS (Alard et al., 2005; Harvey et al., 2006; Warren and Shirey, 2012), some clearly identified as residual BMS by Luguet et al. (2003, 2004) in abyssal and ophiolitic peridotites nor the survival of ancient (older than 2.45 Ga) S mass independent fractionation signature in a BMS grain from a 20 Myr lava of the Mangaia oceanic island locality (Cabral et al., 2013). This demonstrates that the prerequisite implied by the calculation of the timescales of isotopic homogenization, which assumes that $^{187}\text{Os}/^{188}\text{Os}$ signatures will re-equilibrate with time (1.2 Gyr), is not met by the oceanic peridotites as the $^{187}\text{Os}/^{188}\text{Os}$ signatures of their residual Os-rich PGM and BMS survive for > 2 billions of years.

Acknowledgements

We would like to thank Kate Kiseeva and Raúl Fonseca for inviting us to contribute to this special volume of American Mineralogist on "Planetary Processes as Revealed by Sulfides and Chalcophile Elements". Stephan Schuth is gratefully acknowledged for his comments on the original version of this manuscript. Sonja Aulbach and James Day are thanked for their thorough reviews and Kate Kiseeva, our guest editor, for her detailed comments, which all helped improve this manuscript.

References

- Abrajano, T., and Pasteris, J.D. (1989) Zambales ophiolite, Philippines II. Sulfide petrology of the critical zone of the Acoje massif. *Contribution to Mineralogy and Petrology*, 103, 64-77
- Ackerman, L., Walker, R.J., Puchtel, I.S., Pitcher, L., Jelínek, E., and Strnad, L. (2009) Effects of melt percolation on highly siderophile elements and Os isotopes in subcontinental lithospheric mantle: A study of the upper mantle profile beneath Central Europe. *Geochimica et Cosmochimica Acta*, 73, 2400-2414.
- Ackerman, L., Pitcher, L., Strnad, L., Puchtel, I.S., Jelínek, E., Walker, R.J., and Rohovec, J. (2013) Highly siderophile element geochemistry of peridotites and pyroxenites from Horní-Bory, Bohemian Massif: Implications for HSE behaviour in subduction-related upper mantle. *Geochimica et Cosmochimica Acta*, 100, 158-175.
- Alard, O., Dautria, J.-M., and Bodinier, J.-L. (1996) Nature and metasomatic processes of the lithospheric mantle on either part of Sillon Houiller (French Massif Central). *Comptes Rendus de l'Academie des Sciences, Serie Ila* 323, 763-770.
- Alard, O., Griffin, W.L., Lorand, J.-P., Jackson, S., and O'Reilly, S.Y. (2000) Non-chondritic distribution of highly siderophile elements in mantle sulfide. *Nature*, 407, 891-894.
- Alard, O., Griffin, W.L., Pearson, N.J., Lorand, J.-P., and O'Reilly, S.Y. (2002) New insights into the Re–Os systematics of subcontinental lithospheric mantle from in-situ analysis of sulfides. *Earth Planetary Science Letters*, 203, 651-663.
- Alard, O., Luguét, A., Pearson, N.J., Griffin, W.L., Lorand, J.-P., Gannoun, A., Burton, K., and O'Reilly, S.Y. (2005) In situ Os isotopes in abyssal peridotites bridge the isotopic gap between MORBs and their source mantle. *Nature*, 436, 1005-1008.
- Alard, O., Lorand, J.-P., Reisberg, L., Bodinier, J.-L., Dautria, J.M., and O'Reilly, S.Y. (2011) Volatile-rich metasomatism in Montferrier xenoliths (Southern France): Implications for the abundances of chalcophile and highly siderophile elements in the subcontinental mantle. *Journal of Petrology*, 52, 2009-2045.
- Andrews, D.R., and Brenan, J.M. (2002) The solubility of ruthenium in sulfide liquid: implications for platinum group mineral stability and sulfide melt-silicate melt partitioning. *Chemical Geology*, 192, 163-181.
- Aulbach, S., Griffin, W.L., Pearson, N.J., O'Reilly, S.Y., Kivi, K. (2004). Mantle formation and evolution, Slave Craton: constraints from HSE abundances and Re–Os isotope systematics of sulfide inclusions in mantle xenocrysts. *Chemical Geology* 208, 61-88.
- Aulbach, S., Stachel, T., Creaser, R.A., Heaman, L.M., Shirey, S.B., Muehlenbachs, K., Eichenberg, D., Harris, J.W. (2009a). Sulphide survival and diamond genesis during formation and evolution of Archaean subcontinental lithosphere: a comparison between the Slave and Kaapvaal cratons. *Lithos* 112, 747-757.
- Aulbach, S., Creaser, R.A., Pearson, N.J., Simonetti, S.S., Heaman, L.M., Griffin, W.L., Stachel, T. (2009b). Sulfide and whole rock Re–Os of eclogite and pyroxenite xenoliths from the Slave Craton, Canada. *Earth Planetary Science Letters*, 283, 48-58.
- Aulbach, S., Luchs, T., and Brey, G.P. (2014) Distribution and behaviour during metasomatism of PGE-Re and Os isotopes in off-craton mantle xenoliths from Namibia. *Lithos*, 184-187, 478-490.
- Aulbach, S., Mungall, J., and Pearson, D.G. (2016) Distribution and processing of highly siderophile elements in cratonic mantle lithosphere. *Reviews in Mineralogy and Geochemistry*, 81, 239-304.
- Aulbach, S., Creaser, R.A., Stachel, T., Heaman, L.M., Chinn, I.L., Kong, J. (2018) Diamond ages from Victor (Superior Craton): Intra-mantle cycling of volatiles (C, N, S) during supercontinent reorganization, *Earth Planetary Science Letters*, 490, 77-87.
- Ballhaus, C., Bockrath, C., Wohlgemuth-Ueberwasser, C., Laurenz, V., and Berndt, J. (2006) Fractionation of the noble metals by physical processes. *Contribution to Mineralogy and Petrology*, 152, 667-684
- Barnes, S.J., Naldrett, A.J., and Gorton, M.P. (1985) The origin of the fractionation of the platinum-

- group elements in terrestrial magma. *Chemical Geology*, 53, 303-323.
- Becker, H., Horan, M.F., Walker, R.J., Gao, S., Lorand, J.-P., and Rudnick, R.L. (2006) Highly siderophile element compositions of the earth's primitive mantle. *Geochimica et Cosmochimica Acta*, 70, 4528-4550.
- Becker, H., and Dale, C.W. (2016) Re-Pt-Os isotopic and highly siderophile element behavior in mantle tectonites. *Reviews in Mineralogy and Geochemistry*, 81, 369-440.
- Behncke, B. (2004) Late Pliocene volcanic island growth and flood basalt-like lava emplacement in the Hyblean Mountains (SE Sicily). *Journal of Geophysical Research*, 109, B09201.
- Bennett, V.C., Nutman, A.P. and McCulloch, M.T. (1993) Nd isotopic evidence for transient, highly depleted mantle reservoirs in the early history of the Earth. *Earth Planetary Science Letters*, 119, 299-317.
- Bennett, N.R., and Brenan, J.M. (2013) Controls on the solubility of rhenium in silicate melt: Implications for the osmium isotopic composition of Earth's mantle. *Earth Planetary Science Letters*, 361, 320-332.
- Bockrath, C., Ballhaus, C., and Holzheid, A. (2004) Fractionation of the Platinum-group elements during mantle melting. *Science*, 305, 1951-1953
- Bodinier, J.-L., and Godard, M. (2014) *Orogenic, Ophiolitic, and Abyssal Peridotites. Treatise on Geochemistry*, 2nd edition, Volume 2. Editor: Richard W. Carlson. Executive Editors: Heinrich D. Holland and Karl K. Turekian, p103-167
- Borisov, A., and Walker R (2000) Os solubility in silicate melts: New efforts and results. *American Mineralogist*, 85, 912-917.
- Bragagni, A., Luguët, A., Fonseca, R.O.C., Pearson, D.G., Lorand, J.-P., Nowell, G.M., and Kjarsgaard, B.A. (2017) The geological record of base metal sulfides in the cratonic mantle: A microscale $^{187}\text{Os}/^{188}\text{Os}$ study of peridotite xenoliths from Somerset Island, Rae Craton (Canada). *Geochimica et Cosmochimica Acta*, 216, 264-285
- Brandon, A.D., Snow, J.E., Walker, R.J., and Morgan, J.W. (2000) ^{190}Pt - ^{186}Os and ^{187}Re - ^{187}Os systematics of abyssal peridotites. *Earth Planetary Science Letters*, 177, 319-335.
- Brenan, J.M. (2008). Re-Os fractionation by sulfide melt-silicate melt partitioning: A new spin. *Chemical Geology*, 248, 140-165.
- Brenan, J.M., Bennett, N.R., Zajacz, Z. (2016). Experimental Results on Fractionation of the Highly Siderophile Elements (HSE) at Variable Pressures and Temperatures during Planetary and Magmatic Differentiation. *Reviews in Mineralogy and Geochemistry*, 81, 1-87.
- Brueckner, H.K., Roermund, H.L.M., and Pearson, N.J. (2004) An Archean (?) to Paleozoic Evolution for a Garnet Peridotite Lens with Sub-Baltic Shield Affinity within the Seve Nappe Complex of Jämtland, Sweden, Central Scandinavian Caledonides. *Journal of Petrology*, 45, 415-437.
- Burton, K.W., Schiano, P., Birck, J.-L., and Allègre, C.J. (1999) Osmium isotope disequilibrium between mantle minerals in a spinel-lherzolite. *Earth Planetary Science Letters*, 172, 311-322.
- Burton, K.W., Schiano, P., Birck, J.-L., Allègre, C.J., Rehkämper, M., Halliday, A.N., Dawson, J.B. (2000) The distribution and behaviour of rhenium and osmium amongst mantle minerals and the age of the lithospheric mantle beneath Tanzania. *Earth Planetary Science Letters*, 183, 93-106
- Burton, K.W., Gannoun, A., Birck, J.-L., Allègre, C.J., Schiano, P., Clochiatti, R., and Alard, O. (2002) The compatibility of rhenium and osmium in natural olivine and their behavior during mantle melting and basalt genesis. *Earth Planetary Science Letters*, 198, 63-76.
- Burton, K.W., Cenko-Tok, B., Mokadem, F., Harvey, J., Gannoun, A., Alard, O., and Parkinson, I.J. (2012) Unradiogenic lead in Earth's upper mantle. *Nature Geoscience*, 5, 570-573.
- Cabral, R.A., Jackson, M.G., Rose-Koga, E., Koga, K.T., Whitehouse, M.J., Antonelli, M.A., Farquhar, J., Day, J.M.D., and Hauri, E.H. (2013) Anomalous sulfur isotopes in plume lavas reveal deep mantle storage of Archaean crust. *Nature*, 496, 490-493.
- Carlson, R.W., (2005) Application of the Pt-Re-Os isotopic systems to mantle geochemistry and geochronology. *Lithos*, 82, 249-272.

- Chatterjee, R., and Lassiter, J.C. (2016) $^{186}\text{Os}/^{188}\text{Os}$ variations in upper mantle peridotites: Constraints on the Pt/Os ratio of primitive upper mantle, and implications for late veneer accretion and mantle mixing timescales. *Chemical Geology*, 442, 11-22.
- Chauvel, C., and Blichert-Toft, J. (2001) A hafnium isotope and trace element perspective on melting of the depleted mantle. *Earth Planetary Science Letters*, 190, 137–51.
- Chesley, J.T., Rudnick, R.L., and Lee, C.-T. (1999) Re-Os systematics of mantle xenoliths from the east African Rift: Age, structure and history of the Tanzanian Craton. *Geochimica et Cosmochimica Acta*, 63, 1203-1217.
- Coggon, J.A., Nowell, G.M., Pearson D.G., Oberthür, T., Lorand, J.-P., Melcher, F., and Parman, S.W. (2011) The ^{190}Pt – ^{186}Os decay system applied to dating platinum-group element mineralization of the Bushveld Complex, South Africa. *Chemical Geology*, 302-303, 48-60.
- Coggon, J.A., Nowell, G.M., Pearson, D.G., and Parman, S.W. (2012) Application of the ^{190}Pt – ^{186}Os isotope system to dating platinum mineralization and ophiolite formation: an example from the Meratus Mountains, Borneo. *Economic Geology*, 106, 93-117.
- Coggon, J., Luguët, A., Fonseca, R., Lorand, J.P., Heuser, A. and Appel, P. (2015) Understanding Re-Os systematics and model ages in metamorphosed Archean ultramafic rocks: A single mineral to whole-rock investigation. *Geochimica et Cosmochimica Acta*, 167, 205-240.
- Coltorti, M., Bonadiman, C., O'Reilly, S.Y., Griffin, S.Y., and Pearson, N.J. (2010) Buoyant ancient continental mantle embedded in oceanic lithosphere (Sal Island, Cape Verde Archipelago). *Lithos*, 120, 223-233.
- Craig, J.R., and Kullerud, G. (1969) Phase relations in the Cu–Fe–Ni–S system and their applications to magmatic ore deposits. *Economic Geology*, 4, 343-358.
- Dale, C.W., Gannoun, A., Burton, K.W., Argles, T.W., and Parkinson, I.J. (2007) Rhenium–osmium isotope and elemental behaviour during subduction of oceanic crust and the implications for mantle recycling. *Earth Planetary Science Letters*, 253, 211-225.
- Day, J.M.D. (2013) Hotspot volcanism and highly siderophile elements. *Chemical Geology*, 341, 50-74.
- Day, J.M.D., Brandon, A., and Walker, R.J. (2016) Highly siderophile elements in Earth, Mars, the Moon and asteroids. In *Reviews in Mineralogy and Geochemistry, Highly Siderophile and strongly chalcophile elements in high temperature geochemistry and cosmochemistry*, Day J, Harvey J (eds), Volume 81, 161-238.
- Day, J.M.D., Walker, R.J., and Warren, J.M. (2017) ^{186}Os – ^{187}Os and highly siderophile element abundance systematics of the mantle revealed by abyssal peridotites and Os-rich alloys. *Geochimica et Cosmochimica Acta*, 200, 232-254.
- DePaolo, D.J., (1981) Neodymium isotopes in the Colorado Front Range and crust-mantle evolution in the Proterozoic. *Nature*, 291, 193-196.
- Delpech, G., Lorand, J.-P., Grégoire, M., Cottin, J.-Y., and O'Reilly, S.Y. (2012) In-situ geochemistry of sulfides in highly metasomatized mantle xenoliths from Kerguelen, southern Indian Ocean. *Lithos*, 154, 296-314.
- Dijkstra, A, Dale, C.W., Oberthür, T., Nowell G.M. & Pearson, D.G. (2016). Osmium isotope compositions of detrital Os-rich alloys from the Rhine river provide evidence for a global Mesoproterozoic mantle depletion event. *Earth Planetary Science Letters*, 452, 115-122.
- Dromgoole, E.L., and Pasteris, J.D. (1987) Interpretation of the sulfide assemblages in a suite of xenoliths from Kilbourne Hole, New Mexico. *Geological Society of America, Special Paper* 215, 25-46
- Ertel, W., O'Neill, H.St.C., Sylvester, P.J., Dingwell, D.B., and Spettel, B. (2001) The solubility of rhenium in silicate melts: Implications for the geochemical properties of rhenium at high temperatures. *Geochimica et Cosmochimica Acta*, 65, 2161-2170.
- Escrig, S., Doucelance, R., Manuel, M., and Allègre, C.J. (2005). Os isotope systematics in Fogo Island: Evidence for lower continental crust fragments under the Cape Verde Southern Islands. *Chemical Geology*, 219, 93-113.

- Fischer-Gödde, M., Becker, H., and Wombacher, F. (2010) Rhodium, gold and other highly siderophile element abundances in chondritic meteorites. *Geochimica et Cosmochimica Acta*, 74, 356-379.
- Fischer-Gödde, M., Becker, H., and Wombacher, F. (2011) Rhodium, gold and other highly siderophile elements in orogenic peridotites and peridotite xenoliths. *Chemical Geology*, 280, 365-383.
- Fleet, M.E., Tronnes, R.G. and Stone, W.E. (1991) Partitioning of Platinum Group Elements in the Fe–O–S System to 11 GPa. *Journal of Geophysical Research Solid Earth* 96, 21949-21958.
- Fleet, M.E., and Pan, Y. (1994) Fractional crystallization of anhydrous sulfide liquid in the system Fe-Ni-Cu-S, with application to magmatic sulfide deposits. *Geochimica et Cosmochimica Acta*, 58, 3369-3377
- Fonseca, R.O.C., Mallman, G., O'Neill, H.St.C., and Campell, I.H. (2007) How chalcophile is rhenium? An experimental study of the solubility of Re in sulphide mattes. *Earth Planetary Science Letters*, 260, 537-548.
- Fonseca, R.O.C., Mallmann, G., O'Neill, H.St.C., Campbell, I.H., and Laurenz, V. (2011) Solubility of Os and Ir in sulfide melt: Implications for Re/Os fractionation during mantle melting. *Earth Planetary Science Letters*, 311, 339-350
- Fonseca, R.O.C., Brückel, K., Bragagni, A., Leitzke, F.P., Speelmanns, I., and Wainwright, A. (2017) Fractionation of rhenium from osmium during noble metal alloy formation in association with sulfides: Implications for the interpretation of model ages in alloy-bearing magmatic rocks. *Geochimica et Cosmochimica Acta*, 216, 184-200.
- Foustoukos, D.I., Bizimis, M., Frisby, C., and Shirey, S.B. (2015) Redox controls on Ni–Fe–PGE mineralization and Re/Os fractionation during serpentinization of abyssal peridotite. *Geochimica et Cosmochimica Acta*, 150, 11-25.
- Gannoun, A., Burton, K.W., Day, J.M.D., Harvey, J., Schiano, P., and Parkinson, I. (2016) Highly siderophile element and Os isotope systematics of volcanic rocks at divergent and convergent plate boundaries and in intraplate settings. *Reviews in Mineralogy and Geochemistry*, 81, 651-724.
- Gao, S., Rudnick, R.L., Carlson, R.W., McDonough, W.F., and Liu, Y.-S. (2002) Re-Os evidence for replacement of ancient mantle lithosphere beneath the North China Craton. *Earth Planetary Science Letters* 198, 307-322
- González-Jiménez, J.M., Griffin, W.L., Gervilla, F., Kerestedjian, T.N., O'Reilly, S.Y., Proenza, J.A., Pearson, N.J., and Sergeeva, I. (2012) Metamorphism disturbs the Re-Os signatures of platinum-group minerals in ophiolite chromitites. *Geology*, 40, 659-662.
- González-Jiménez, J.M., Villaseca, C., Griffin, W.L., Belousova, E., Konc, Z., Ancochea, E., O'Reilly, S.Y., Pearson, N.J., Garrido, C.J., and Gervilla, F. (2013a) The architecture of the European-Mediterranean lithosphere: A synthesis of the Re-Os evidence. *Geology*, 41, 547-550.
- González-Jiménez, J.M., Marchesi, C., Griffin, W.L., Gutiérrez-Narbona, R., Lorand, J.-P., O'Reilly, S.Y., Garrido, C.J., Gervilla, F., Pearson, N.J., and Hidas, K. (2013b) Transfer of Os isotopic signatures from peridotite to chromitite in the subcontinental mantle: insights from in situ analysis of platinum-group and base-metal minerals (Ojén peridotite massif, southern Spain). *Lithos*, 164-167, 74-85.
- González-Jiménez JM, Villaseca C, Griffin WL, O'Reilly SY, Belousova E, Ancochea E, Pearson NJ (2014) Significance of ancient sulfide PGE and Re–Os signatures in the mantle beneath Calatrava, Central Spain. *Contribution to Mineralogy and Petrology*, 168, 1047.
- Griffin, W.L., Spetzius, Z.V., Pearson, N.J., and O'Reilly, S.Y. (2002) In-Situ Re-Os analysis of sulfide inclusions in kimberlitic olivines: New constraints on depletion events in the Siberian lithospheric mantle. *Geochemistry Geophysics Geosystems* doi:10.1029/2001GC00287
- Griffin, W.L., O'Reilly, S.Y., Abe, N., Aulbach, S., Davies, R.M., Pearson, N.J., Doyle, B.J., and Kivi, K (2003) The origin and evolution of Archean lithospheric mantle. *Precambrian Research*, 127, 19-41

- Griffin, W.L., Graham, S., O'Reilly, S.Y., and Pearson, N.J. (2004) Lithosphere evolution beneath the Kaapvaal Craton: Re–Os systematics of sulfides in mantle-derived peridotites. *Chemical Geology*, 208, 195-215.
- Griffin, W.L., Nikolic, N., O'Reilly, S.Y., and Pearson, N.J. (2012) Coupling, decoupling and metasomatism: evolution of crust-mantle relationships beneath NW Spitsbergen. *Lithos*, 149, 115-135.
- Handler, M.R., and Bennett, V.C. (1999) Behavior of Platinum-group elements in the subcontinental mantle of eastern Australia during variable metasomatism and melt depletion. *Geochimica et Cosmochimica Acta*, 63, 3597-3618.
- Hart, S.R., and Ravizza, G. (1996) Os partitioning between phases in lherzolite and basalt. In: *Earth Processes: Reading the Isotopic Code* (eds. A. Basu and S. R. Hart). *Geophysical Monograph*, 95, 123-134.
- Harvey, J., Gannoun, A., Burton, K.W., Rogers, N.W., Alard, O., and Parkinson, I.J. (2006). Ancient melt extraction from the oceanic upper mantle revealed by Re–Os isotopes in abyssal peridotites from the Mid-Atlantic ridge. *Earth Planetary Science Letters*, 244, 606-621.
- Harvey, J., Gannoun, A., Burton, K.W., Rogers, N.W., Schiano, P., and Alard, O. (2010) Unravelling the effects of melt depletion and secondary infiltration on mantle Re–Os isotopes beneath the French Massif Central. *Geochimica et Cosmochimica Acta*, 74, 293-320.
- Harvey, J., Dale, C.W., Gannoun, A., and Burton, K.W. (2011) Osmium mass balance in peridotite and the effects of mantle-derived sulfides on basalt petrogenesis. *Geochimica et Cosmochimica Acta*, 75, 5574-5596.
- Hawkesworth, C., Cawood, P., Dhuime, B., and Kemp, T. (2017) Earth Continental Lithosphere through Time, *Annual Review of Earth and Planetary Sciences* 45, 169-198.
- Helmy, H., Ballhaus, C., Berndt, J., Bockrath, C., and Wohlgemuth-Ueberwasser, C. (2007) Formation of Pt, Pd and Ni tellurides: experiments in sulfide–telluride systems. *Contribution to Mineralogy and Petrology*, 153, 493-524.
- Horan, M.F., Walker, R.J., Morgan, J.W., Grossman, J.N., and Rubin, A.E. (2003) Highly Siderophile Elements in chondrites. *Chemical Geology*, 196, 5-20
- Irvine, G.J., Pearson, D.G., Kjarsgaard, B.A., Carlson, R.W., Kopylova, M.G., and Dreibus, G. (2003) A Re–Os isotope and PGE study of kimberlite-derived peridotite xenoliths from Somerset Island and a comparison to the Slave and Kaapvaal cratons. *Lithos*, 71, 461-488
- Jagoutz, E., Palme, H., Blum, H., Cendales, M., Dreibus, G., Spettel, B., Lorenz, V., and Wänke, H. (1979) The abundances of major, minor and trace elements in the Earth's mantle as derived from primitive ultramafic nodules. *Lunar and Planetary Science Conference*, 10th, Proceedings 2 (A80-23617 08-91), 2031-2050.
- Janney, P.E., Shirey, S.B., Carlson, R.W., Pearson, D.G., Bell, D.R., le Roex, A.P., Ishikawa, A. and Boyd, F.R. (2010). Composition, age and thermal characteristics of South African off-craton mantle lithosphere: evidence for a multistage history. *Journal of Petrology*, 51, 1849-1890.
- Keays, R.R., Sewell, D.K.B., and Mitchell, R.H., (1981) Platinum and Palladium minerals in upper mantle derived lherzolites. *Nature*, 294, 646-648.
- Kemppinen, L.I.M., Kohn, S.C., Parkinson, I.J., Bulanova, G.P., Howell, D.H., and Smith, C.B. (2018) Identification of molybdenite in diamond-hosted sulphide inclusions: Implications for Re–Os radiometric dating, *Earth Planetary Science Letters*, 495, 101-111.
- Kim, N.K., Choi, S.H., and Dale, C.W. (2016) Sulfide-scale insights into platinum-group element behavior during carbonate mantle metasomatism and evolution of Spitsbergen lithospheric mantle. *Lithos* 246-247, 182-196.
- Kullerud, G., Yund, R.A., and Moh, G.H. (1969) Phase relations in the Cu–Fe–S, Cu–Ni–S, and Fe–Ni–S systems. *Economic Geology*, 4, 323-343.
- Lainghas, F., Pearson, D.G., Phillips, D., Burgess, R., Harris J. W. (2009) Re–Os and $^{40}\text{Ar}/^{39}\text{Ar}$ isotope measurements of inclusions in diamonds from the Ural Mountains: constraints on diamond genesis and eruption ages. *Lithos*, 112S, 714–723

- Lee, C.T. (2002) Platinum-group element geochemistry of peridotite xenoliths from the Sierra Nevada and the Basin and Range, California. *Geochimica et Cosmochimica Acta*, 66, 3987-4005.
- Le Roux, V., Bodinier, J.-L., Tommasi, A., Alard, O., Dautria, J.-M., Vauchez, A., and Riches, A.J.V. (2007) The Lherz spinel lherzolite: Refertilized rather than pristine mantle. *Earth Planetary Science Letters*, 259, 599-612.
- Li, C., Barnes, S.J., Makovicky, E., Rose-Hansen, J., and Makovicky, M. (1996) Partitioning of nickel, copper, iridium, rhenium, platinum, and palladium between monosulfide solid solution and sulfide liquid: Effects of composition and temperature. *Geochimica et Cosmochimica Acta*, 60, 1231-1238
- Lissner, M., König, S., Luguët, A., le Roux, P.-J., Schuth, S., Heuser, A., and le Roex, A.P. (2014) Selenium and tellurium systematics in MORBs from the southern Mid-Atlantic Ridge (47–50°S). *Geochimica et Cosmochimica Acta*, 144, 379-402.
- Liu, J., Rudnick, R.L., Walker, R.J., Gao, S., Wu, F., and Piccoli, P.M. (2010) Processes controlling highly siderophile element fractionations in xenolithic peridotites and their influence on Os isotopes. *Earth Planetary Science Letters*, 154, 331-347.
- Liu J., Brin L.E., Pearson D.G., Bretschneider L., Luguët A., van Acken D., Kjarsgaard B.A., Riches A., Miskovic A. (2018) Diamondiferous Paleoproterozoic mantle roots beneath Arctic Canada: A study of mantle xenoliths from Parry Peninsula and Central Victoria Island, *Geochimica et Cosmochimica Acta*, 239, 284-311.
- Liu, J., Scott, J., Martin, C.E. & Pearson, D.G. (2015) The longevity of Archean mantle residues in the convecting upper mantle and their role in young continent formation. *Earth Planetary Science Letters*, 424, 109–118
- Liu, Y., and Brenan, J.M. (2015) Partitioning of platinum-group elements (PGE) and chalcogens (Se, Te, As, Sb, Bi) between monosulfide-solid solution (MSS), intermediate solid solution (ISS) and sulfide liquid at controlled fO_2 - fS_2 conditions. *Geochimica et Cosmochimica Acta*, 159, 139-161.
- Lorand, J.-P. (1987) Caractères minéralogiques et chimiques généraux des microphases du système Cu-Fe-Ni-S dans les roches du manteau supérieur : exemples d'hétérogénéités en domaine sub-continental. *Bulletin de la Société Géologique Française*, 8, 643-657.
- Lorand, J.-P. (1990) Are spinel lherzolite xenoliths representative of the sulfur content of the upper mantle? *Geochimica et Cosmochimica Acta*, 54, 1487-1493
- Lorand, J.-P. (1991) Sulfide petrology and sulphur geochemistry of orogenic lherzolites: a comparative study of the Pyrenean bodies (France) and the Lanzo massif (Italy). *Journal of Petrology, Lherzolites Special Issue*, 77-95
- Lorand, J.-P., Gros, M., and Pattou, L. (1999) Fractionation of platinum group element in the upper mantle: a detailed study in Pyrenean orogenic peridotites. *Journal of Petrology*, 40, 951-987.
- Lorand, J.-P., Alard, O. (2001) Platinum-group element abundances in the upper mantle: new constraints from in-situ and whole-rock analyses of Massif Central xenoliths (France). *Geochimica et Cosmochimica Acta*, 65, 2789-2806.
- Lorand, J.-P., Reisberg, L., and Bedini, L.M. (2003a) Platinum-group elements and melt percolation processes in Sidamo spinel peridotite xenoliths, Ethiopia, East African Rift. *Chemical Geology*, 196, 57-75.
- Lorand, J.-P., Alard, O., Luguët, A., and Keays, R.R., (2003b) Sulfur and selenium systematics of the sub-continental lithospheric mantle beneath the Massif Central (France). *Geochimica et Cosmochimica Acta*, 67, 4137-4151.
- Lorand, J.-P., Delpéch, G., Grégoire, M., Moine, B., O'Reilly, S.Y., and Cottin, J.-Y. (2004) Platinum-group elements and the multistage metasomatic history of Kerguelen lithospheric mantle, South Indian Ocean. *Chemical Geology*, 208, 195-215.
- Lorand, J.-P., and Grégoire, M. (2006) Petrogenesis of base-metal sulfide of some peridotites of the Kaapvaal craton (South Africa). *Contribution to Mineralogy and Petrology*, 151, 521-538.

- Lorand, J.-P., Luguët, A., Alard, O., Bezos, A., and Meisel, T. (2008) Distribution of platinum group elements in orogenic lherzolites: a case study in a Fontête Rouge lherzolite, (French Pyrenees). *Chemical Geology*, 248, 174-194.
- Lorand, J.-P., Alard, O., and Luguët, A. (2010) Platinum-group element micronuggets and refertilization process in Lherz orogenic peridotite (northeastern Pyrenees, France). *Earth Planetary Science Letters*, 289, 298-310.
- Lorand, J.-P., Luguët, A., and Alard, O. (2013) Platinum-group element systematics and petrogenetic processing of the continental upper mantle: A review. *Lithos*, 164-167, 2-21.
- Lorand, J.-P., and Luguët, A. (2016) Chalcophile/siderophile elements in mantle rocks: trace elements in trace minerals. *Reviews in Mineralogy and Geochemistry*, 81, 441-488.
- Luck J.-M. and Allègre, C.J. (1984) ^{187}Re - ^{187}Os investigation in sulfide from Cape Smith komatiite. *Earth Planetary Science Letters*, 68, 205-208.
- Luguët, A., and Lorand, J.P. (1998). Supergene weathering and sulphur contents of basalt-hosted mantle xenoliths: an appraisal from Montferrier lherzolites (Languedoc, France). *Comptes Rendus de l'Academie des Sciences, Paris, (Earth & Planetary Sciences)*, 327, 519-525.
- Luguët, A., Alard, O., Lorand, J.-P., Pearson, N.J., Ryan, C., and O'Reilly, S.Y. (2001) Laser-ablation microprobe (LAM)-ICPMS unravels the highly siderophile element geochemistry of the oceanic mantle. *Earth Planetary Science Letters*, 189, 285-294.
- Luguët, A., Lorand, J.-P., and Seyler, M. (2003) Sulfide petrology and highly siderophile element geochemistry of abyssal peridotites: A coupled study in samples from the Kane Fracture Zone (Mark area 45°W 23°20'N, atlantic ocean). *Geochimica et Cosmochimica Acta*, 67, 1553-1570.
- Luguët, A., Lorand, J.-P., Alard, O., and Cottin, J.Y. (2004) A multi-technique study of platinum group element systematic in some Ligurian ophiolitic peridotites. *Chemical Geology*, 208, 175-194.
- Luguët, A., Shirey, S.B., Lorand, J.P., Horan, M.F., and Carlson, R.W. (2007) Residual platinum-group minerals from highly depleted harzburgites of the Lherz massif (France) and their role in HSE fractionation of the mantle. *Geochimica et Cosmochimica Acta*, 71, 3082-3097.
- Luguët, A., Pearson, D.G., Nowell, G.M., Coggon, J.A., Dreher, S.T., Spetsius, Z.V., and Parman, S.W. (2008) Enriched Pt-Re-Os isotope systematics in plume lavas explained by metasomatic sulfides. *Science*, 319, 453-456.
- Luguët, A., Jaques, A.L., Pearson, D.G., Smith, C.B., Bulanova, G., Roffey, S., Rayner, M., and Lorand, J.P. (2009). An integrated petrological, geochemical and Re-Os isotope study of peridotite xenoliths from the Argyle lamproite, Western Australia and implications for cratonic diamond occurrence. *Lithos*, 112S, 1096-1108.
- Luguët, A., Behrens, M., Pearson, D.G., König, S., and Herwartz, D. (2015) Significance of the whole-rock Re-Os ages in cryptically and modally metasomatised cratonic peridotites. Constraints from the HSE-Se-Te systematics. *Geochimica et Cosmochimica Acta*, 164, 441-463.
- Luguët, A., and Reisberg, L. (2016) Highly Siderophile Element and ^{187}Os signatures in non-cratonic basalt-hosted peridotite xenoliths: Unravelling the origin and evolution of the Post-Archean Lithospheric Mantle. *Reviews in Mineralogy and Geochemistry*, 81, 305-367.
- Makovicky, E., (2002) Ternary and Quaternary Phase Systems with PGE, In: Cabri, L.J. (Ed.), *The Geology, Geochemistry, Mineralogy and Mineral Beneficiation of Platinum-Group Elements*. Canadian Institute of Mining, Metallurgy and Petroleum, Montreal, pp. 131-178.
- Malitch, K.N., and Merkle, R.K.W. (2004) Ru-Os-Ir-Pt and Pt-Fe alloys from the Evander Goldfield, Witwatersrand Basin, South Africa: Detrital Origin inferred from compositional and Osmium isotope data. *The Canadian Mineralogist*, 42, 631-650.
- Mallmann, G., and O'Neill, H.St.C. (2007) The effect of oxygen fugacity on the partitioning of Re between crystals and silicate melt during mantle melting. *Geochimica et Cosmochimica Acta*, 71, 2837-2857.
- Marchesi, C., Griffin, W.L., Garrido, C.J., Bodinier, J.-L., O'Reilly, S.Y., and Pearson, N.J. (2010) Persistence of mantle lithospheric Re-Os signature during asthenospherization of the

- subcontinental lithospheric mantle: insights from in situ isotopic analysis of sulfides from the Ronda peridotite (Southern Spain). *Contribution to Mineralogy and Petrology*, 159, 315-330.
- McCoy-West, A.J., Bennett, V.C., Puchtel, I.S., and Walker, R.J. (2013) Extreme persistence of cratonic lithosphere in the southwest Pacific: Paleoproterozoic Os isotopic signatures in Zealandia. *Geology*, 41, 231-234.
- McDonough, W., and Sun, S. (1995) The composition of the Earth. *Chemical Geology*, 120, 223-253.
- McInnes, B.I.A., McBride, J.S., Evans, N.J., Lambert, D.D., and Andrew, A.S. (1999) Osmium isotope constraints on metal recycling in subduction zones. *Science*, 286, 512-516.
- Meibom, A., Sleep, N.H., Page Chamberlain, C., Coleman, R.G., Frei, R., Hren M.T., and Wooden, J.L. (2002) Re–Os isotopic evidence for long-lived heterogeneity and equilibration processes in the Earth’s upper mantle. *Nature*, 419, 705-708.
- Meibom, A., Frei, R., and Sleep, N.H. (2004) Osmium isotopic compositions of Os-rich platinum group element alloys from the Klamath and Siskiyou Mountains. *Journal of Geophysical Research*, 109, B02203.
- Meisel, T., Walker, R.J., Irving, A.J., and Lorand, J.P. (2001) Osmium isotopic compositions of mantle xenoliths: a global perspective. *Geochimica et Cosmochimica Acta*, 65, 1311-1323.
- Meisel, T., and Moser, J. (2004) Reference materials for geochemical PGE analysis: new analytical data for Re, Rh, Pd, Os, Ir, Pt and Re by isotope dilution ICP-MS in 11 geological reference materials. *Chemical Geology*, 208, 319-338.
- Mitchell, R.H., and Keays, R.R. (1981) Abundance and distribution of gold, palladium and iridium in some spinel and garnet lherzolites: Implications for the nature and origin of precious metal-rich intergranular components in the upper mantle. *Geochimica et Cosmochimica Acta*, 45, 2425-2442.
- Morgan, J.W., Baedeker, P.A. (1983) Elemental composition of sulfide particles from an ultramafic xenolith and the siderophile element content of the upper mantle. *Lunar Planetary Science Conference*, 14, 513-514.
- Morgan, J.W. (1986) Ultramafic xenoliths: Clues to Earth’s late accretionary history. *Journal of Geophysical Research*, 91 (B12), 12375-12387.
- Mungall, J.E., and Brenan, J.M. (2014) Partitioning of Platinum Group Elements and Au between liquid and basalt and the origin of the crust-mantle fractionation of the chalcophile elements. *Geochimica et Cosmochimica Acta*, 125, 265-289.
- Nixon, P. H. (1987) *Mantle Xenoliths*. Wiley, Chichester.
- Nowell, G.M., Kempton, P.D. Noble, S.R., Fitton, J.G., Saunders, A.D., Mahoney, J.J., and Taylor, R.N. (1998) High precision Hf isotope measurements of MORB and OIB by thermal ionization mass spectrometry: insights into the depleted mantle, *Chemical Geology*, 149, 211-233.
- Nowell, G.M., Pearson, D.G., Parman, S.W., Luguet, A., and Hanski, E. (2008) Precise and accurate $^{186}\text{Os}/^{188}\text{Os}$ and $^{187}\text{Os}/^{188}\text{Os}$ measurements by Multi-Collector Plasma Ionisation Mass Spectrometry, part II: The application of laser ablation MC-ICPMS to single-grain Pt-Os and Re-Os geochronology in platinum group alloy grains. *Chemical Geology*, 248, 394-426.
- O’Driscoll, B., Day, J.M.D., Walker, R.J., Daly, J.S., McDonough, W.F., and Piccoli, P.M. (2012) Chemical heterogeneity in the upper mantle recorded by peridotites and chromitites from the Shetland Ophiolite Complex, Scotland. *Earth Planetary Science Letters*, 333-334, 226-237.
- O’Driscoll, B., Walker, R.J., Clay, P.L., Day, J.M.D., Ash, R.D., and Daly, J.S. (2018) Length-scales of chemical and isotopic heterogeneity in the mantle section of the Shetland Ophiolite Complex, Scotland. *Earth and Planetary Science Letters*, 488, 144-154.
- O’Reilly, S.Y., Zhang, M., Griffin, W.L., Begg, G., Hronsky, J. (2009) Ultradeep continental roots and their oceanic remnants: a solution to the geochemical “mantle reservoir” problem? *Lithos* 112S, 638-647.
- Parman, S.W. (2007) Helium isotopic evidence for episodic mantle melting and crustal growth. *Nature*, 446, 900-903.

- Patchett, P.J., and Tatsumoto, M. (1980) Hafnium isotope variations in oceanic basalts. *Geophysical Research Letters*, 7, 1077-1080.
- Pattou, L., Lorand, J.-P., and Gros, M. (1996) Non-chondritic platinum-group element ratios in the Earth's mantle. *Nature*, 379, 712-715.
- Pearson, D.G., Shirey, S.B., Carlson, R.W., Boyd, F.R., Pokhilenko, N.P., and Shimizu, N. (1995a) Re-Os, Sm-Nd, and Rb-Sr isotope evidence for the thick Archaean lithospheric mantle beneath the Siberian craton modified by multistage metasomatism. *Geochimica et Cosmochimica Acta*, 59, 959-977.
- Pearson, D.G., Carlson, R.W., Shirey, S.B., Boyd, F.R. and Nixon, P.H. (1995b) Stabilisation of Archean lithospheric mantle: A Re-Os isotope study of peridotite xenoliths from the Kaapvaal craton. *Earth Planetary Science Letters*, 134, 341-357.
- Pearson, D.G., Shirey, S.B., Harris, J.W., and Carlson, R.W. (1998) Sulfide inclusions in diamonds from the Koffiefontein kimberlite, S. Africa: Constraints on diamond ages and mantle Re-Os systematics. *Earth Planetary Science Letters*, 160, 311-362.
- Pearson, D.G., Shirey, S.B., Bulanova, G.P., Carlson, R.W., and Milledge, H.J. (1999) Single crystal Re-Os isotope study of sulfide inclusions from a zoned Siberian diamond. *Geochimica et Cosmochimica Acta*, 63, 703-712.
- Pearson, D.G., Irvine, G.J., Carlson, R.W., Kopylova, M.G., and Ionov, D.A. (2002) The development of lithospheric mantle keels beneath the earliest continents: time constraints using PGE and Re-Os isotope systematics. In: Fowler, C.M.R., Ebinger, C.B., and Hawkesworth, C.J. (eds) *The Early Earth: Physical, Chemical and Biological development*. Geology Society, London, Special Publications 199, 65-90.
- Pearson, D.G., Canil, D., and Shirey, S.B. (2003) Mantle samples included in volcanic rocks: xenoliths and diamonds. In Holland, H.D., and Turekian, K.K. (eds) *Treatise on geochemistry*: Elsevier Amsterdam 171-275.
- Pearson, D.G., Irvine, G.J., Ionov, D.A., Boyd, F.R., and Dreibus, D.E. (2004) Re-Os isotope systematics and platinum group element fractionation during mantle melt extraction: a study of massif and xenolith peridotite suites. *Chemical Geology*, 208, 29-59.
- Pearson, D.G., Parman, S.W., and Nowell, G.N. (2007) A link between large mantle melting events and continent growth seen in osmium isotopes. *Nature*, 449, 202-205
- Pearson, D.G., and Wittig, N. (2008) Formation of Archaean continental lithosphere and its diamonds: the root of the problem. *Journal of the Geological Society*, 165, 895-914.
- Pearson, D.G., and Wittig, N. (2014) The formation and evolution of the subcontinental mantle lithosphere - evidence from mantle xenoliths. *Treatise of Geochemistry, Volume 3: The Mantle and Core, Chapter 3.6*, 255-292.
- Pearson, N.J., Alard, O., Griffin, W.L., Jackson, S.E., and O'Reilly, S.Y. (2002) In situ measurement of Re-Os isotopes in mantle sulfides by laser ablation multicollector-inductively coupled plasma mass spectrometry: Analytical methods and preliminary results. *Geochimica et Cosmochimica Acta*, 66, 1037-1050.
- Peregoedova, A., and Ohnenstetter, M. (2002) Collectors of Pt, Pd and Rh in a S-poor Fe-Ni-Cu sulfide system at 760 C: experimental data and application to ore deposits. *The Canadian Mineralogist*, 40, 527-561.
- Pernet-Fisher, J.F., GH Howarth, G.H., Pearson, D.G., Woodland, S., Barry, P.H., Pokhilenko, N.P., Pokhilenko, L.N., Agashev, A.M., and Taylor, L.A. (2015) Plume impingement on the Siberian SCLM: Evidence from Re-Os isotope systematics. *Lithos* 218, 141-154
- Powell, W., and O'Reilly, S.Y. (2007) Metasomatism and sulfide mobility in lithospheric mantle beneath eastern Australia: implications for mantle Re-Os geochronology. *Lithos*, 94, 132-147.
- Richardson, S.H., Shirey, S.B., Harris, J.W., Carlson, R.W. (2001). Archean subduction recorded by Re-Os isotopes in eclogitic sulfide inclusions in Kimberley diamonds. *Earth Planetary Science Letters*, 191, 257-266.
- Roy-Barman, M., and Allègre, C.J. (1994) 187Os/186Os ratios of mid-ocean ridge basalts and abyssal peridotites. *Geochimica et Cosmochimica Acta*, 58, 5043-5054.

- Rudnick, R.L., and Walker, R.J. (2009) Interpreting ages from Re-Os isotopes in peridotites. *Lithos*, 112S, 1083-1095.
- Sapienza, G.T., Griffin, W.L., O'Reilly, S.Y., and Morten, L. (2007) Crustal zircons and mantle sulfides: Archean to Triassic events in the lithosphere beneath south-eastern Sicily. *Lithos*, 96, 503-523.
- Schulte, R., Schilling, M.E., Anma, R., Farquhar, J., Horan, M.F., Komiya, T., Philip, M., Piccoli, P.M., Pitcher, L., and Walker, R.J. (2009) Chemical and chronologic complexity in the convecting upper mantle: Evidence from the Taitao ophiolite, southern Chile. *Geochimica et Cosmochimica Acta*, 73, 5793-5819.
- Sharygin, V.V., Golovin, A.V., Pokhilenko, N.P., and Kamenetsky, V.S. (2007) Djerfisherite in the Udachnaya-East pipe kimberlites (Sakha-Yakutia, Russia): paragenesis, composition and origin. *European Journal of Mineralogy*, 19, 51-63.
- Shi, R., Alard, O., Zhi, X., O'Reilly, S.Y., Pearson, N.J., Griffin, W.L., Zhang, M., and Chen, X. (2007) Multiple events in the Neo-Tethyan Oceanic upper mantle: Evidence from Ru-Os-Ir alloys in the Luobusa and Dongqiao ophiolitic podiform chromitites, Tibet. *Earth Planetary Science Letters*, 261, 33-48.
- Shirey, S.B., and Walker, R.J. (1998) Re-Os isotopes in cosmochemistry and high-temperature geochemistry. *Annu. Review in Earth Planetary Science*, 26, 423-500.
- Simon, N.S.C., Neumann, E.-R., and Widom, E. (2008) Ultra-depleted domains in the oceanic mantle lithosphere: Evidence from major element and modal relationships in mantle xenoliths from ocean islands. *Journal of Petrology*, 49, 1223-1251.
- Smit, K.V., Shirey, S.B., Richardson, S.H., le Roex, A.P., and Gurney, J.J. (2010) Re-Os isotopic composition of peridotitic sulphide inclusions in diamonds from Ellendale, Australia: Age constraints on Kimberley cratonic lithosphere, *Geochimica et Cosmochimica Acta*, 74, 3292-3306.
- Smoliar, M., Walker, R.J., and Morgan, J.W. (1996) Re-Os Ages of Group IIA, IIIA, IVA, and IVB Iron Meteorites. *Science*, 271, 1099-1102.
- Szabó, C., and Bodnar, R.J. (1995) Chemistry and Origin of mantle sulfides in spinel peridotite xenoliths from alkaline basaltic lavas, Nögrád-Gömör volcanic field, northern Hungary and southern Slovakia, *Geochimica and Cosmochimica Acta*, 59, 3917-3927
- van Acken, D., Luguët, A., Pearson, D.G., Nowell, G.M., Fonseca, R.O.C., Nagel, T.J., and Schulz, T. (2017) Mesoarchean melting and Neoproterozoic to Paleoproterozoic metasomatism during the formation of the cratonic mantle keel beneath West Greenland. *Geochimica et Cosmochimica Acta*, 203, 37-53
- Wainwright, A.N., Luguët, A., Fonseca, R.O.C., and Pearson, D.G. (2015) Investigating metasomatic effects on the ^{187}Os isotopic signature: A case study on micrometric base metal sulfides in metasomatised peridotite from the Letlhakane kimberlite (Botswana). *Lithos*, 232, 35-48.
- Wainwright, A.N., Luguët, A., Schreiber, A., Fonseca, R.O.C., Nowell, G.M., Lorand, J.-P., and Janney, P.E. (2016) Nanoscale variations in ^{187}Os isotopic compositions and HSE systematics in a Bultfontein peridotite. *Earth Planetary Science Letters*, 447, 61-70.
- Walker, R.J., Carlson, R.W., Shirey, S.B., and Boyd, F.R. (1989) Os, Sr, Nd, and Pb isotope systematics of southern African peridotite xenoliths: implications for the chemical evolution of subcontinental mantle. *Geochimica et Cosmochimica Acta*, 53, 1583-1595.
- Walker, R.J., Brandon, A.D., Bird, J.M., Piccoli, P.M., McDonough, W.F., and Ash, R.D. (2005) ^{187}Os - ^{186}Os systematics of Os-Ir-Ru alloy grains from southwestern Oregon. *Earth Planetary Science Letters*, 230, 211-226
- Wang, K.-L., O'Reilly, S.Y., Griffin, W.L., Pearson, N.J., Matsumura, R., and Shinjo, R. (2005) Proterozoic mantle lithosphere beneath the East African Rift (Southern Ethiopia): In-situ Re-Os evidence. *Goldschmidt Conference abstract volume A284*
- Wang, K.-L., O'Reilly, S.Y., Griffin, W.L., and Pearson, (2006) In situ Os dating of peridotite xenoliths, Tariat, northern Mongolia, *Goldschmidt Conference abstract volume A687*

- Wang, K.-L., O'Reilly, S.Y., Griffin, W.F., Pearson, N.J., and Zhang, M. (2009) Sulfides in peridotite xenoliths from Penghu Islands, Taiwan: Melt percolation, PGE fractionation and the lithospheric evolution of the South China block. *Geochimica et Cosmochimica Acta*, 73, 4531-4557.
- Warren, J.M., and Shirey, S.B. (2012) Lead and osmium isotopic constraints on the oceanic mantle from single abyssal peridotite sulfides. *Earth Planetary Science Letters*, 359-360, 279-293.
- Westerlund, K.J., Shirey, S.B., Richardson, S.H., Carlson, R.W., Gurney, J.J., and Harris, J.W. (2006) A subduction wedge origin for Paleoproterozoic peridotitic diamonds and harzburgites from the Panda kimberlite, Slave craton: evidence from Re–Os isotope systematics. *Contribution to Mineralogy and Petrology*, 152, 275-294.
- Wiggers de Vries, D.F., Pearson, D.G., Bulanova, G.P., Smelov, A.P., Pavlushin, A.D. and Davies, G.R. (2013) Re–Os dating of sulphide inclusions zonally distributed in single Yakutian diamonds: Evidence for multiple episodes of Proterozoic formation and protracted timescales of diamond growth. *Geochimica et Cosmochimica Acta*, 120, 363-394.
- Wittig, N., Webb, M., Pearson, D.G., Dale, C.W., Ottley, C.J., Hutchinson, M., Jensen, S.M., and Luguet, A. (2010) Formation of the North Atlantic Craton: Timing and mechanisms constrained from Re–Os isotope and PGE data of peridotite xenoliths from S.W. Greenland. *Chemical Geology*, 276, 166-187.
- Wood, S.A. (1987) Thermodynamic calculations of the volatility of the platinum group elements: The PGE content of fluids at magmatic temperatures. *Geochimica et Cosmochimica Acta*, 51, 2041-3050.
- Xiong, Y., and Wood, S.A. (2000) Experimental quantification of hydrothermal solubility of platinum-group elements with special reference to porphyry copper environments. *Mineralogy and Petrology*, 68, 1-28.
- Xiong, Y., and Wood, S.A. (2002) Experimental determination of the hydrothermal solubility of ReS₂ and the Re–ReO₂ buffer assemblage and transport of rhenium under supercritical conditions. *Geochemical Transaction*, 3, 1-10.
- Xu, X.S., Griffin, W.L., O'Reilly, S.Y., Pearson, N.J., Geng, H.Y., and Zheng, J.P. (2008) Re–Os isotopes of sulfides in mantle xenoliths from eastern China: progressive modification of lithospheric mantle. *Lithos*, 102, 43-64.
- Yaxley, G.M., Crawford, A.J., and Green, D.H. (1991) Evidence for carbonatite metasomatism in spinel peridotite xenoliths from western Victoria, Australia. *Earth Planetary Science Letters*, 107, 305-317.

Figure Captions

Figure 1: $^{187}\text{Os}/^{188}\text{Os}$ isotopic evolution of Earth's mantle explaining the principles and potential pitfalls of Re-Os model ages.

A) Definition of the T_{MA} model age (mantle separation age: blue line) and the T_{RD} model age (rhenium depletion age: red line) for a mantle peridotite with a present day $^{187}\text{Os}/^{188}\text{Os}$ of 0.112. The expected difference of T_{MA} for lherzolite and harzburgite is illustrated. All these model ages are back-calculated to a primitive upper mantle (PUM)-like reservoir of reference (PUM from Meisel et al., 2001; Becker et al., 2006; Day et al., 2017).

B) Diagram illustrating the impact of the choice of the reference reservoir on the model age determination for T_{MA} (blue lines) and T_{RD} (red lines) for Archean and Proterozoic mantle samples. The reservoirs of reference are compositionally similar to the primitive upper mantle (PUM) (after Becker et al., 2006; Day et al., 2017) or CI-chondrites (CI, after Horan et al., 2003; Fischer-Gödde et al., 2010). For detailed explanations and parameters of calculations, see part II of the main text.

Figure 2: Composition (wt. %) of the typical BMS mineral assemblage in mantle peridotites (redrawn from Lorand and Luguet, 2016) in the Cu-Fe-S and Fe-Ni-S systems (integrated over the temperature range of 1192°C to ca. 100°C, see text). Aw: Awaruite, Bo: Bornite, Cb: Cubanite, Cc: Chalcocite, Cp: chalcopyrite, Cv: Covellite, Dg: Digenite, Hz: Haezlewoodite, Mi: Millerite, Mss: monosulfide solid solution, Mw: Mackinawite, Pn: Pentlandite, Po: Pyrrhotite, Py: Pyrite, Vi: violarite, Vs: Vaesite.

Figure 3: Petrographical features and geochemical signatures characterizing the different types of BMS±PGM of mantle peridotites. The HSE patterns of Type 3 BMS±PGM are not reported as they do not include Re. This summary should not be considered an absolute recipe, but instead reflects the current knowledge based on detailed studies from a few suites of mantle peridotites. It is likely that the characteristics of various BMS±PGM types may differ for each specific suite or a specific sample from a given suite, as each may have experienced a specific petrogenetic history (e.g., nature and extent of metasomatism, nature of protolith overprinted). CI-chondrites value for normalization of the HSE patterns from Horan et al. (2003) and Fischer-Gödde et al. (2010). Sulfide mineral abbreviations as in Figure 2.

Figure 4: Variations of the $\text{Re}_\text{N}/\text{Os}_\text{N}$ and $\text{Pd}_\text{N}/\text{Ir}_\text{N}$ in the different types of BMS±PGM recognized in mantle peridotites. Data from Alard et al., (2002; 2005; 2011). N=CI-chondrites normalized after Horan et al. (2003) and Fischer-Gödde et al. (2010).

Figure 5: Flow chart summarizing the methodological and analytical strategies used to determine the Re-Os isotopic composition of minerals and namely of the Re-Os main hosts (i.e., the base metal sulfides and platinum group minerals). The hatched lines associated with the “diamond-hosted sulfides” box refers to the original chemical procedure designed by Pearson et al. (1998) for Re-Os isotope analysis in single sulfide grain included in diamonds (see text for detailed explanations) and which was adapted to analysis of single BMS in mantle peridotites. Main advantages and disadvantages of each approach are listed. For detailed explanations, see text.

Figure 6: $^{187}\text{Os}/^{188}\text{Os}$ versus $^{187}\text{Re}/^{188}\text{Os}$ variations for constituent minerals of mantle peridotites from (A) Kilbourne Hole (USA: after Burton et al., 1999) and from (B) Mont Briançon, French Massif Central (after Harvey et al., 2011). Note that for the Mont Briançon minerals, the $^{187}\text{Re}/^{188}\text{Os}$ axis has a logarithmic scale. The “Bulk” enclosed or interstitial BMS from Burton et al. (1999) were analyzed as a fraction of separated BMS grains while the single BMS of Harvey et al (2011) indicate that one analysis represents one single BMS. PUM values from Meisel et al. (2001) and Becker et al. (2006).

Figure 7: $^{187}\text{Os}/^{188}\text{Os}$ versus $^{187}\text{Re}/^{188}\text{Os}$ variations within BMS of single peridotite. Both the BMS of (A) KN 3-4 abyssal peridotite (Alard et al., 2005) and (B) FRB 1510 cratonic peridotite (Griffin et al., 2004) define positive linear/non-linear (power) trends ($r^2=0.75$ and 0.85 respectively). No clear distinction in BMS type was reported by Griffin et al. (2004). PUM values from Meisel et al. (2001) and Becker et al. (2006).

Figure 8: $^{187}\text{Os}/^{188}\text{Os}$ versus $^{187}\text{Re}/^{188}\text{Os}$ variations within BMS of single peridotites. Interestingly, the BMS define negative trends (not necessarily linear) within the $^{187}\text{Os}/^{188}\text{Os}$ versus $^{187}\text{Re}/^{188}\text{Os}$ space (e.g., logarithmic regression with $r^2=0.97$ and 0.84 for Mbr20 and Pg2, power regression with $r^2=0.95$ for GP12, linear regression with $r^2=0.75$ for Mtf37). No clear distinction in term of the BMS origin was provided in the publications listed. Note that for the $^{187}\text{Re}/^{188}\text{Os}$ axis has a logarithmic scale. Data are from Sapienza et al. (2007); Xu et al. (2008); Alard et al. (2011) and Harvey et al. (2011). PUM values from Meisel et al. (2001) and Becker et al. (2006).

Figure 9: Schematic evolution of the $^{187}\text{Os}/^{188}\text{Os}$ signature of a metasomatic BMS and its PGM (Pt-Fe alloy) inclusions based on the experimental investigations on Re and Os partitioning between mss, HSE-rich alloys and sulfide liquids of Wainwright et al. (2016) and Fonseca et al. (2017). The blue triangles represent the $^{187}\text{Os}/^{188}\text{Os}$ composition of the Pt-Fe alloys, while the pink triangles represent the $^{187}\text{Os}/^{188}\text{Os}$ composition of their BMS host (data from Wainwright et al., 2016). The error bars on the alloy isotopic compositions are the measurement uncertainty (2σ), for the BMS the error bars are smaller than the symbol size. Note that the T_{MA} model age of the BMS would reflect the age of alloy exsolution rather than that of the BMS precipitation. See text for detailed discussion.

Figure 10: Difference in $^{187}\text{Os}/^{188}\text{Os}$ composition between a whole-rock peridotite and its most unradiogenic BMS ($\Delta^{187}\text{Os}/^{188}\text{Os}_{\text{SWR-BMS}} = ^{187}\text{Os}/^{188}\text{Os}_{\text{SWR}} - ^{187}\text{Os}/^{188}\text{Os}_{\text{BMS}}$) expressed as a function of the fertile/refractory character of the host peridotite (e.g., Al_2O_3 wt. %). A positive $\Delta^{187}\text{Os}/^{188}\text{Os}_{\text{SWR-BMS}}$ indicates that the whole-rock peridotite is more radiogenic (i.e., has a higher $^{187}\text{Os}/^{188}\text{Os}$ ratio) than its least radiogenic BMS.

Figure 11: Comparison of $^{187}\text{Os}/^{188}\text{Os}$ signatures of the most unradiogenic BMS and their corresponding whole-rock host peridotite as a function of the fertile/refractory character of the host peridotite (e.g., Al_2O_3 wt. %). In contrast to Figure 10, there are two data points per peridotite on this plot (the whole-rock $^{187}\text{Os}/^{188}\text{Os}$ composition and the $^{187}\text{Os}/^{188}\text{Os}$ composition of its most unradiogenic BMS). This representation is complementary to Figure 10 and illustrates the overall distribution and evolution of the $^{187}\text{Os}/^{188}\text{Os}$ signatures in the whole-rock peridotites and their most unradiogenic BMS. The color and shape of symbols; as well as the data sources are similar to Figure 10. PUM values from Meisel et al. (2001) and Becker et al. (2006).

Figure 12: Difference in $^{187}\text{Os}/^{188}\text{Os}$ composition between a whole-rock peridotite its various BMS grains ($\Delta^{187}\text{Os}/^{188}\text{Os}_{\text{SWR-BMS}} = ^{187}\text{Os}/^{188}\text{Os}_{\text{SWR}} - ^{187}\text{Os}/^{188}\text{Os}_{\text{BMS}}$) expressed as a function of the fertile/refractory character of the host peridotite (e.g., Al_2O_3 wt. %). As for Figure 10, a positive $\Delta^{187}\text{Os}/^{188}\text{Os}_{\text{SWR-BMS}}$ implies that the whole-rock peridotite is more radiogenic than its BMS involved in the comparison. Diagram B is a zoom-in of a portion of Diagram A. The color and shape of symbols; as well as the data sources are similar to Figure 10.

Figure 13: Distribution and variation of the $^{187}\text{Os}/^{188}\text{Os}$ signatures in BMS, PGM and host mantle peridotites. The x-axis has no unit and all BMS, alloys or whole-rocks aligned on one single vertical line correspond to all data obtained for an individual peridotite from a given locality in a specific tectonic setting. The arrows with values on the top of the diagram indicate the $^{187}\text{Os}/^{188}\text{Os}$ ratios of BMS from a given peridotite whose values are above the $^{187}\text{Os}/^{188}\text{Os}$ scale chosen here. It is important to note that a few studies provided the BMS $^{187}\text{Os}/^{188}\text{Os}$ composition but not the whole-

Figure 1

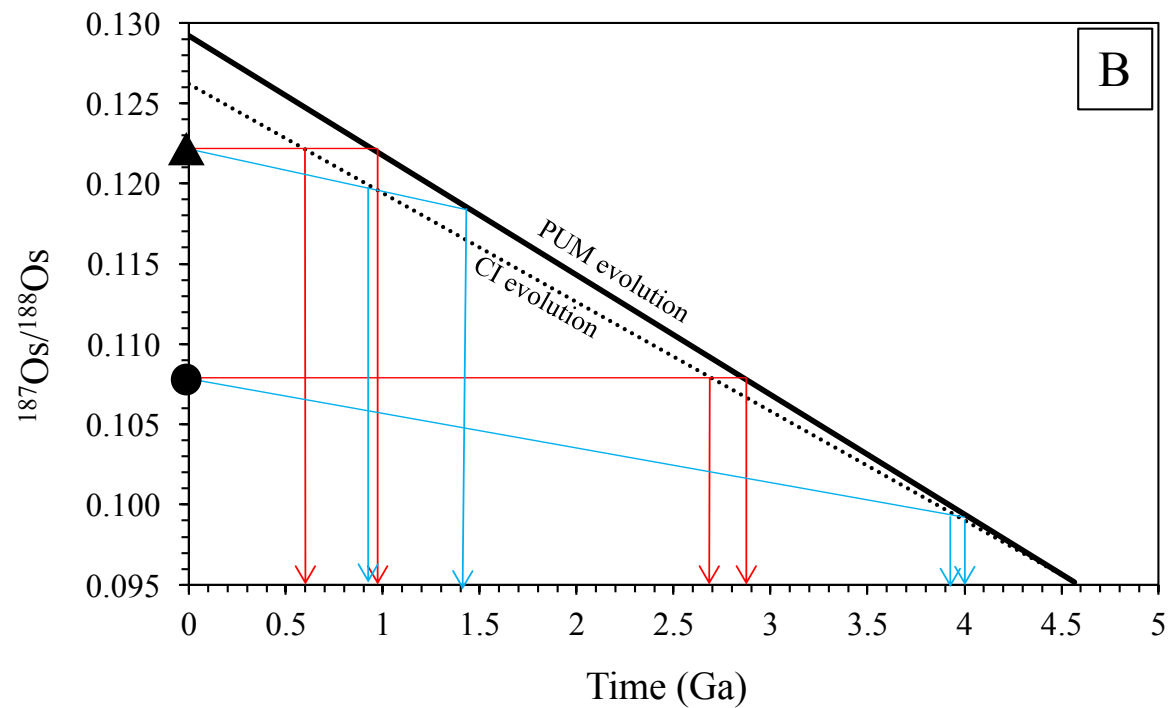
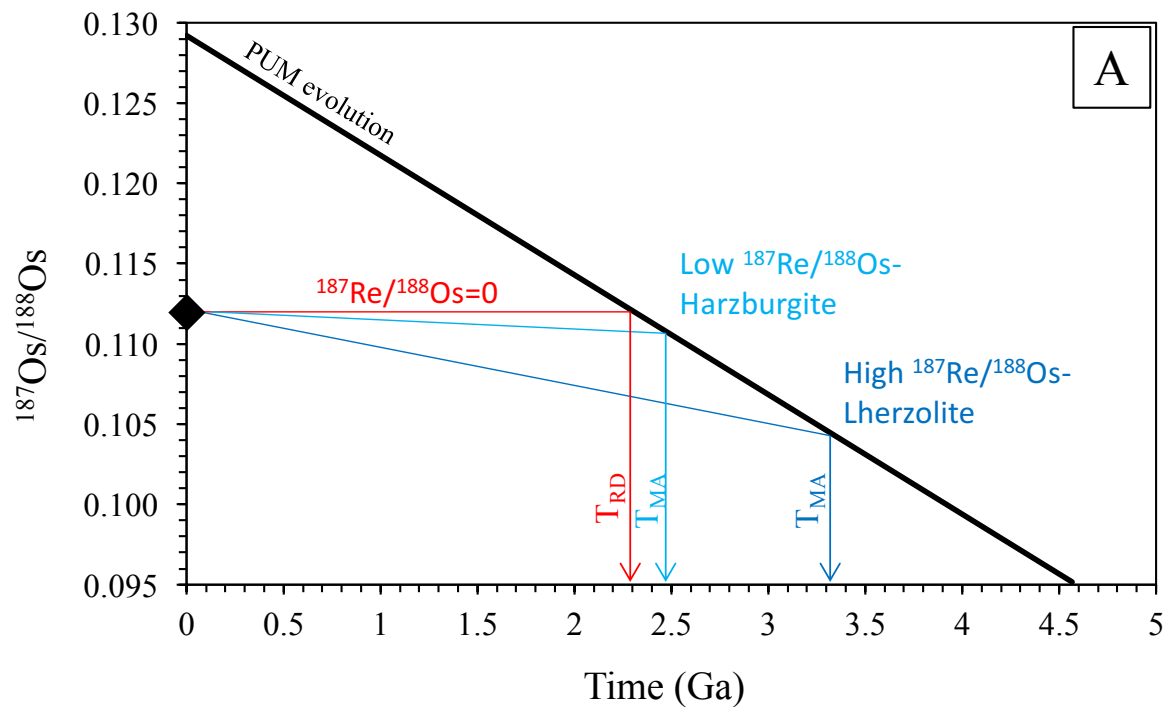
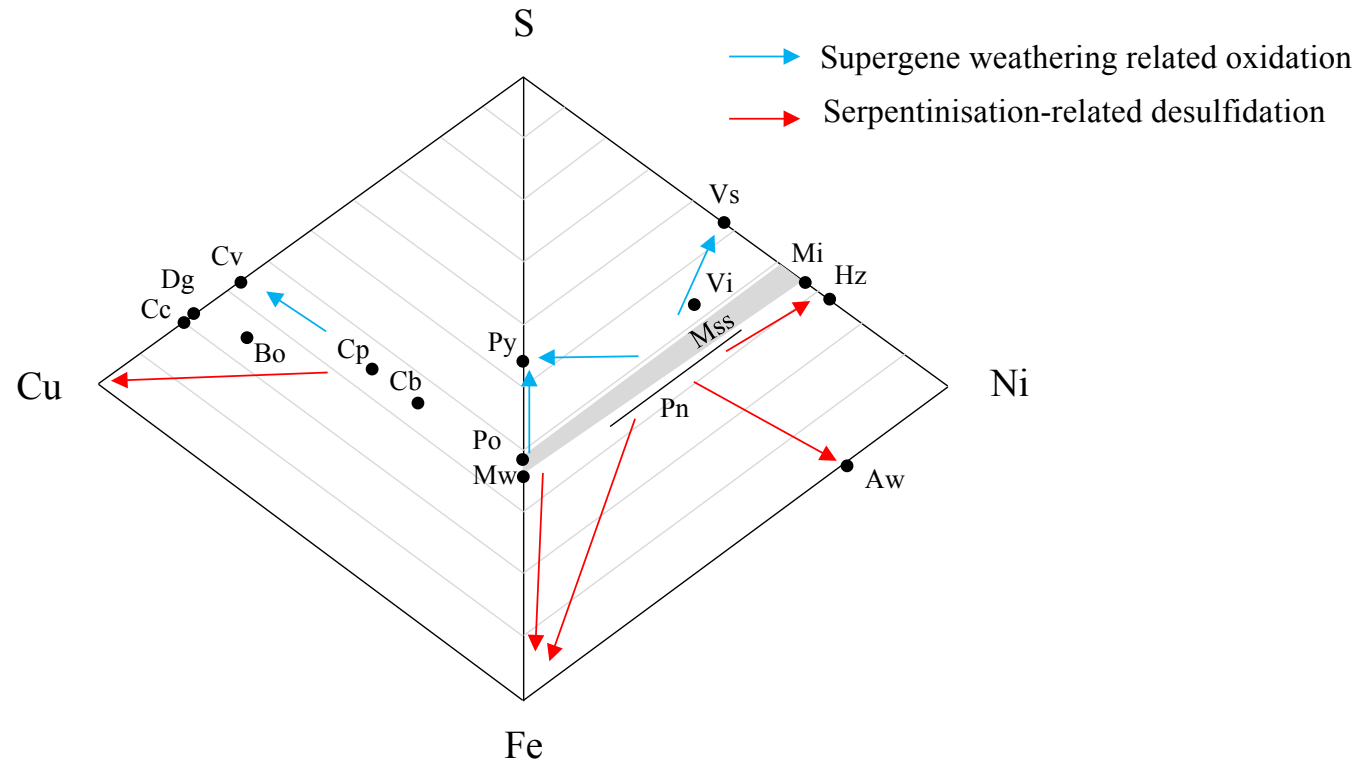


Figure 2 (Alternative)



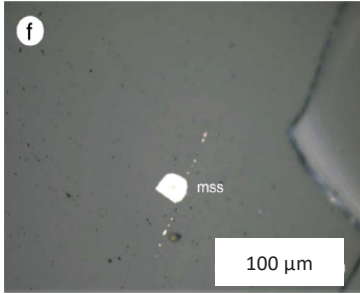
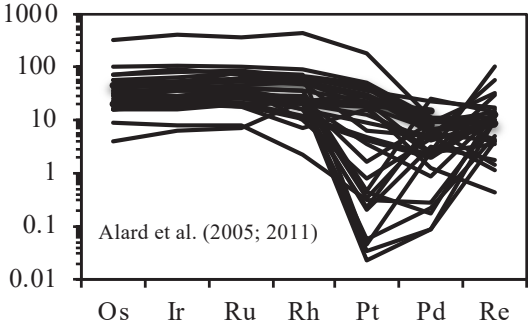
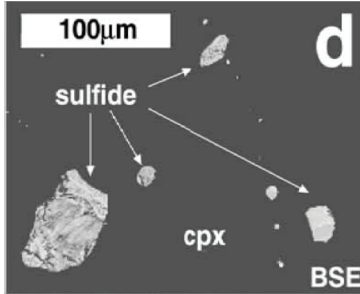
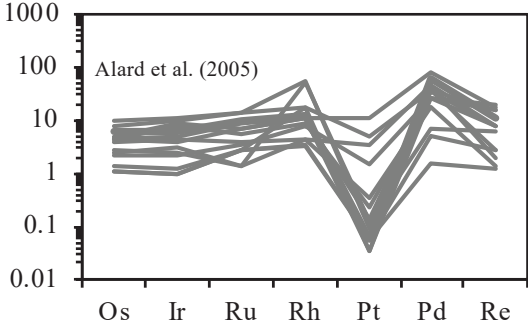
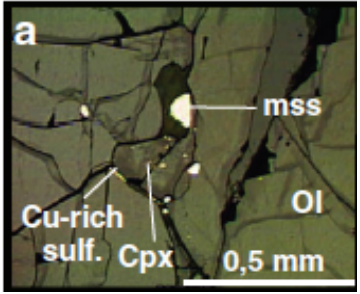
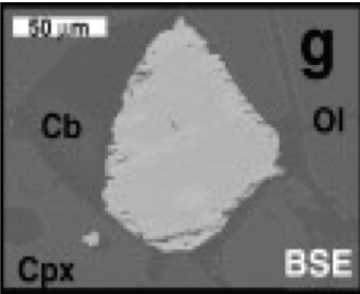
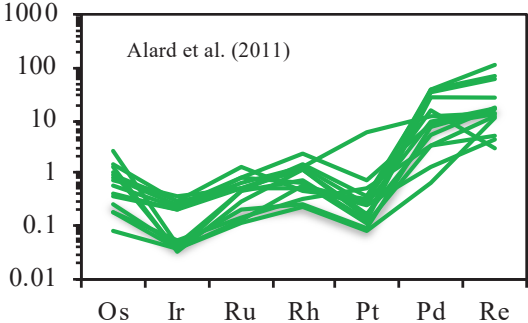
Type	Primary Mineralogy	Textural relationships	Origin	Microphotographs of Representative BMS	CI-Chondrites-normalised HSE patterns
Type 1	<p>BMS: Fe-Ni-rich S-rich assemblage Mss+Pn-Po±Cu-sulfides</p> <p>PGM: HT Os-Ru-Ir sulfides, Os-Ru-Ir alloys, Ir-Pt-Os alloys</p>	<p>Inclusions in Ol and Cpx (deformation features)</p>	<p>Residual to partial melting Result from fractional crystallisation of HT sulfide melt and complex sub-solidus reequilibration</p>	 <p>Liu et al. (2010)</p>	 <p>Alard et al. (2005; 2011)</p>
Type 2	<p>BMS: Ni-Cu-rich S-poor assemblage Mss+Pn-Po+Pn+Cu-sulfides</p> <p>Lower Mss/Po vs. Pn-Cp</p> <p>PGM: Pt-Pd tellurides, Pt-Pd bismuthides and Pt-Pd bismuto-tellurides</p>	<p>Inclusions within metasomatic silicates (Cpx), silicate and carbonate melt pockets.</p> <p>Intergranular blebs sometimes in close association to metasomatic Cpx</p>	<p>Metasomatic Result from fractional crystallisation of evolved (Ni-Cu-rich) sulfide melt and complex sub-solidus reequilibration (low melt-rock ratio)</p>	 <p>Alard et al. (2002)</p>	 <p>Alard et al. (2005)</p>
Type 3	<p>BMS: Fe-Ni-rich S-rich assemblage Mss+Pn-Po±Cu-sulfides</p>	<p>Inclusions within metasomatic silicates and glass pockets</p> <p>Intergranular components</p>	<p>Metasomatic Remobilisation of Type 1 BMS by pervasive melt percolation (high melt-rock ratio-> poikilitic-equigranular textures of peridotites)</p>	 <p>Delpech et al. (2012)</p>	
Type 4	<p>BMS: Fe-Ni-rich S-rich assemblage Mss+Pn-Po±Cu-sulfides</p> <p>PGM: Pt-Pd-Te-Bi arsenides</p>	<p>Intergranular associated with carbonates/dolomite</p> <p>High Dihedral angles</p>	<p>Metasomatic Sulfidation reaction of S-rich CO₂ vapor with silicates</p>	 <p>Delpech et al. (2012)</p>	 <p>Alard et al. (2011)</p>

Figure 4

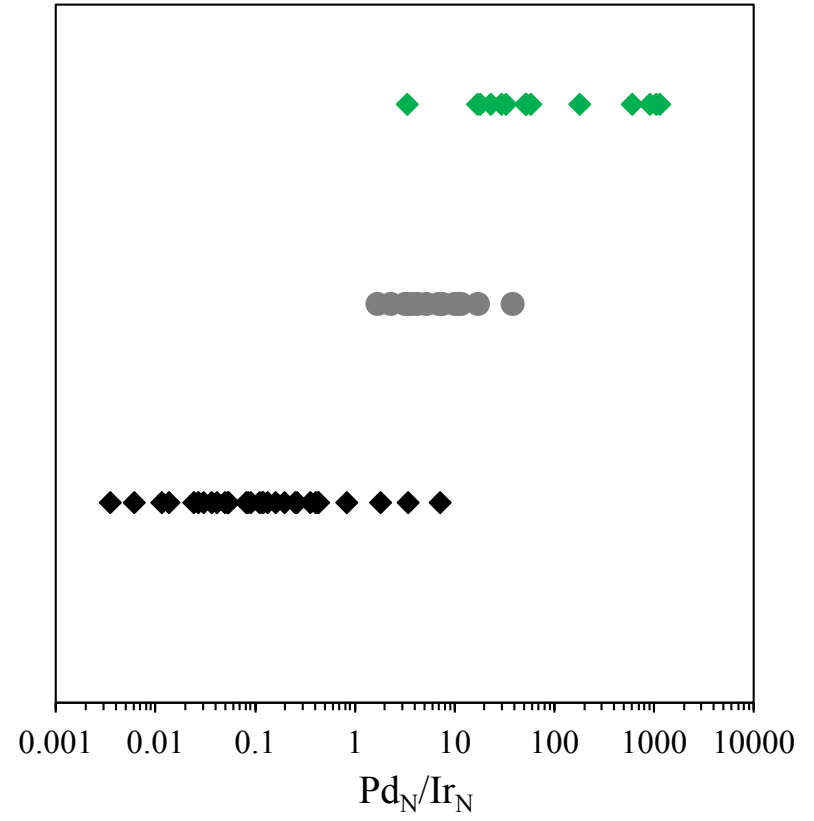
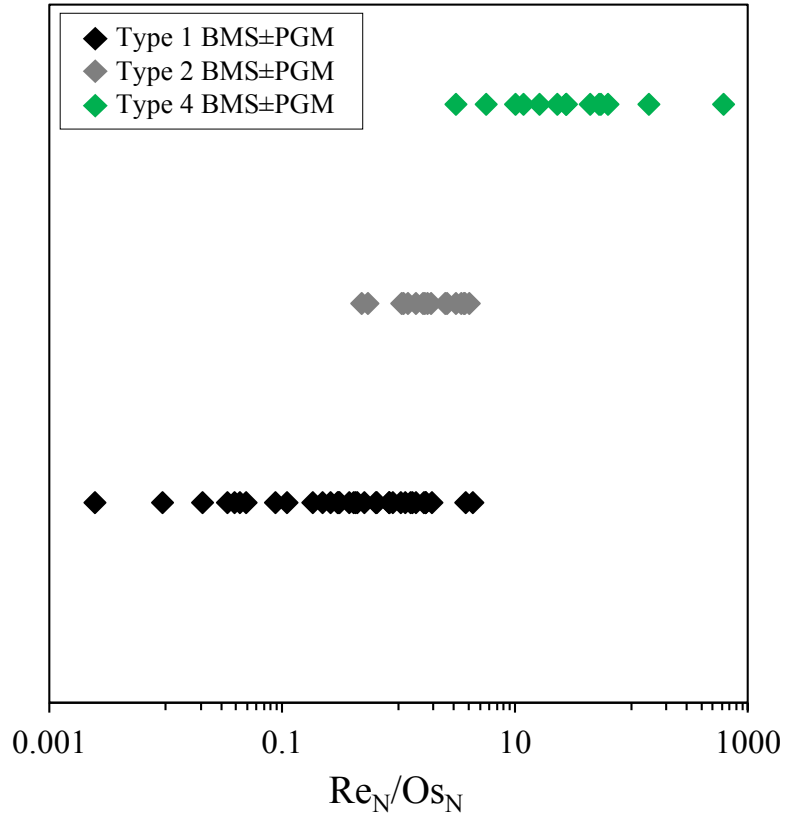
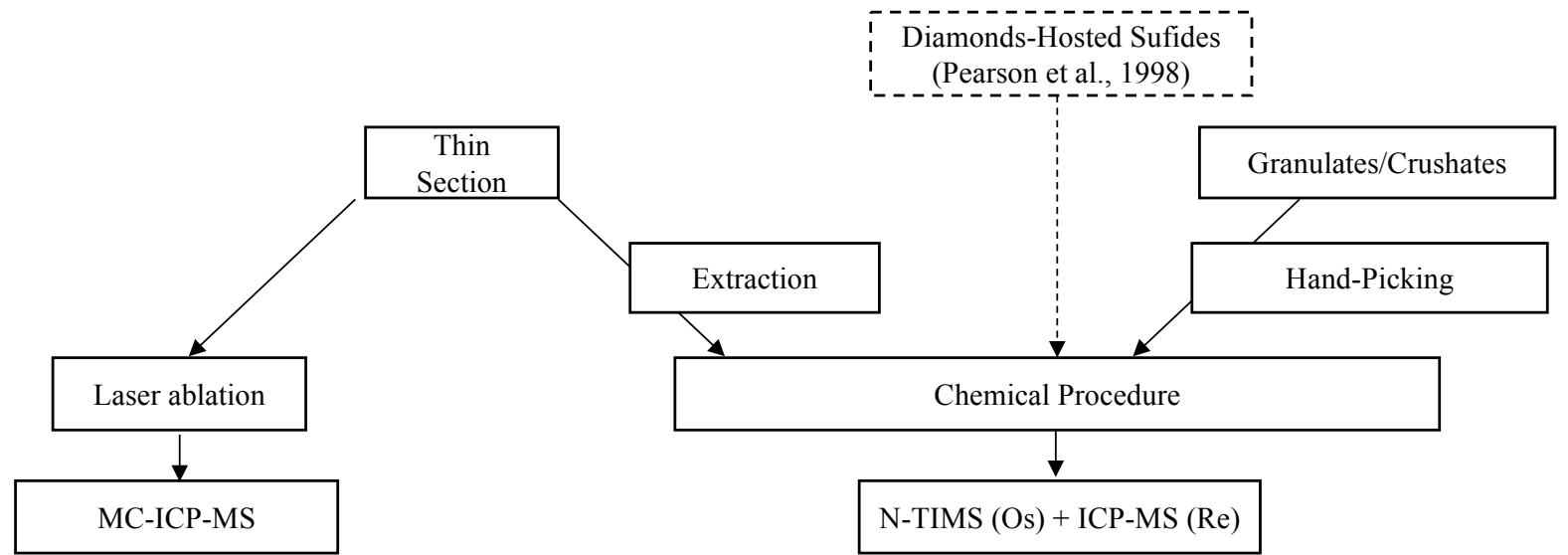


Figure 5



References	Pearson et al. (2002), Alard et al., (2002; 2005; 2011), Griffin et al. (2004, 2012); Brueckner et al. (2004); Powell and O'Reilly (2007); Sapienza et al. (2007); Xu et al. (2008); Wang et al. (2009); Marchesi et al. (2010), González-Jiménez et al. (2013a-b)	Warren and Shirey (2012); Wainwright et al. (2015; 2016); Bragagni et al., (2017), van Acken et al. (2017)	Pearson et al., (1998); Harvey et al., (2006; 2010; 2011); Kim et al. (2016)
Representative composition of Bulk BMS grains	No, only one portion of BMS exposed on the thin section is analyzed but could present the advantage of internal isochron as analyses with high-spatial resolution possible	No, whole BMS portion exposed on thin section analyzed (but not the whole BMS grain), still individual sulfide mineral analyses possible	Possibly Yes, but breaking of BMS during crushing may happen
Preservation of BMS petrographical information	Yes	Yes	Partial, only Fe/Ni/Cu composition potentially known
BMS grain size	>laser beam size, so generally BMS at least 60-80 μm long/wide	>10 μm (see Wainwright et al., 2016) No bias due to size of BMS (or alloys) potentially analyzed Allow to tackle BMS from ultra depleted cratonic peridotites (not possible via LA-MC-ICPMS)	Minimum size of BMS most likely intermediate between the other 2 approaches.
Separation ^{187}Re from ^{187}Os	Limited to BMS with $^{187}\text{Re}/^{188}\text{Os} < 0.5$ (Marchesi et al., 2010)	No limit	No limit
Simultaneous analyses	Semi-quantitative Os and Pt concentrations only– Other HSE from LA-ICPMS analyses on a different portion of the BMS	HSE (Os, Ir, Ru, Pt, Pd, Re) concentrations Pb isotopic compositions	HSE (Os, Ir, Ru, Pt, Pd, Re) concentrations Pb isotopic compositions
How easy and fast?	Fast, 10s-100s BMS analyzed in one session (day)	Extremely time consuming, painstaking work	Time consuming, painstaking work

Figure 6

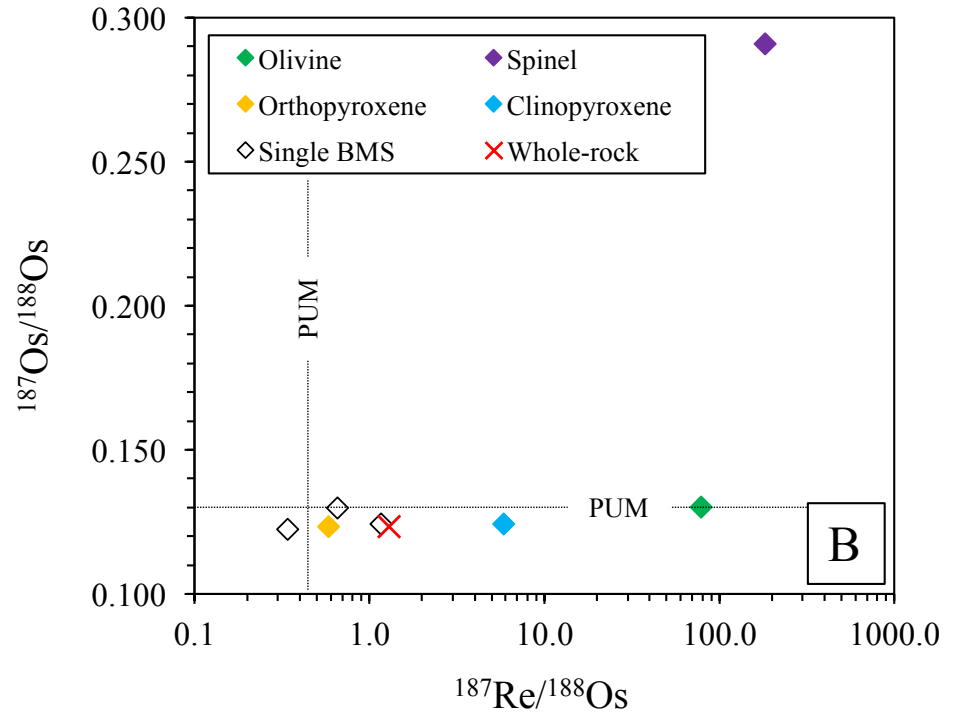
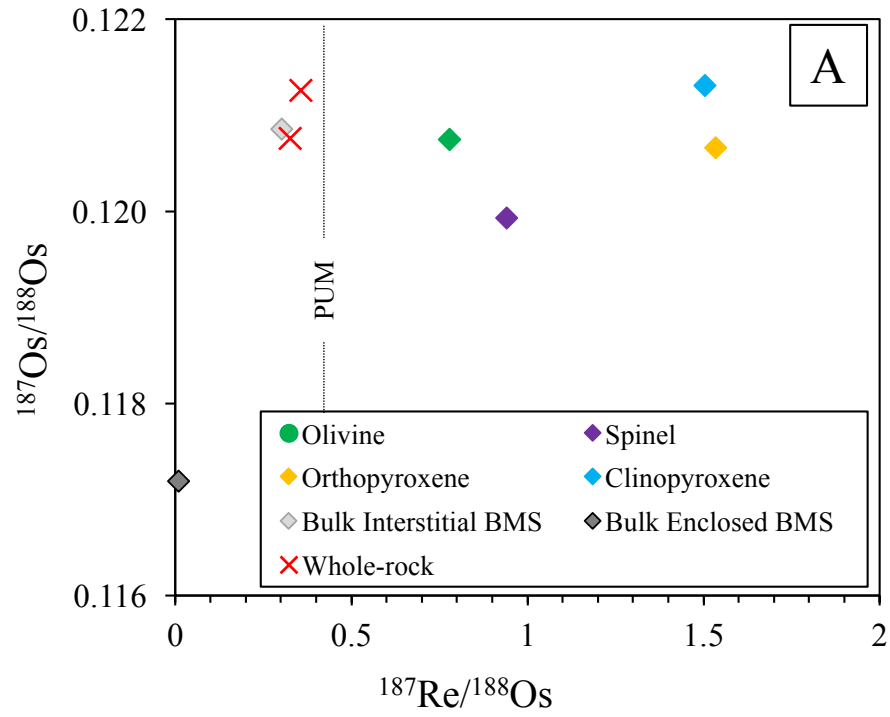


Figure 7

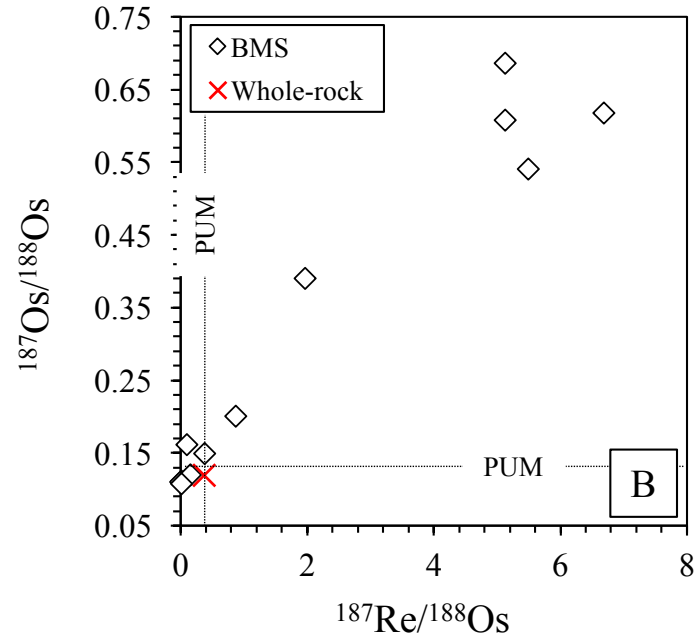
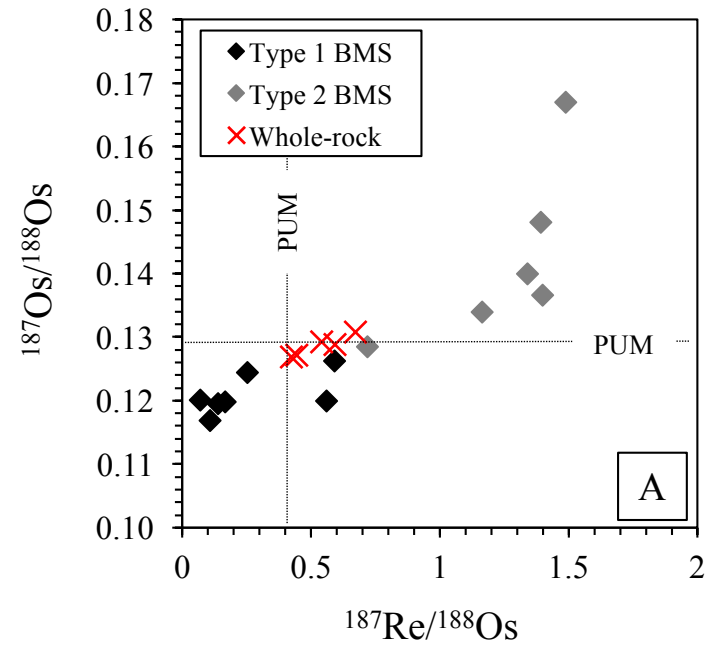
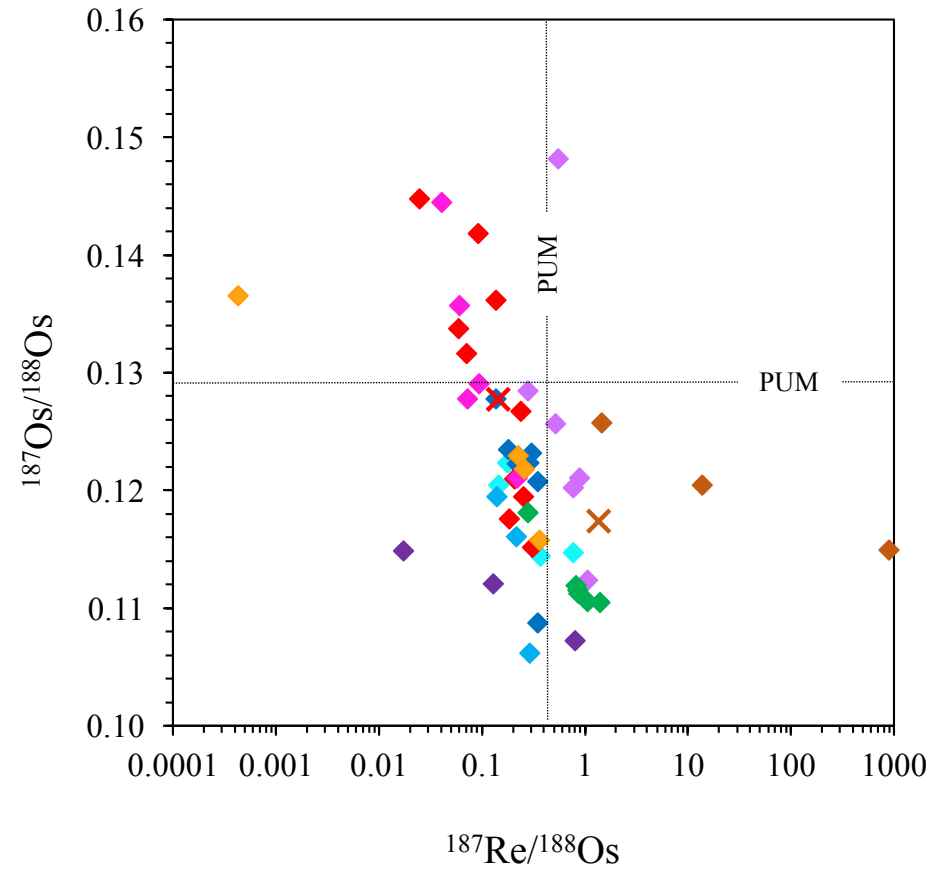


Figure 8



× Whole-rock peridotite		◆ BMS
<u>East China</u>	◆ Peridotite NTS2	◆ Peridotite KPH9816
◆ Peridotite YT09	◆ Peridotite KP0201	◆ Peridotite TC0247
<u>Massif Central</u>	◆ Peridotite MtF 37	◆ Peridotite Pg2
◆ Peridotite MBS1	◆ Peridotite MBr20	
<u>Sicily</u>	◆ Peridotite GE12	

Figure 9

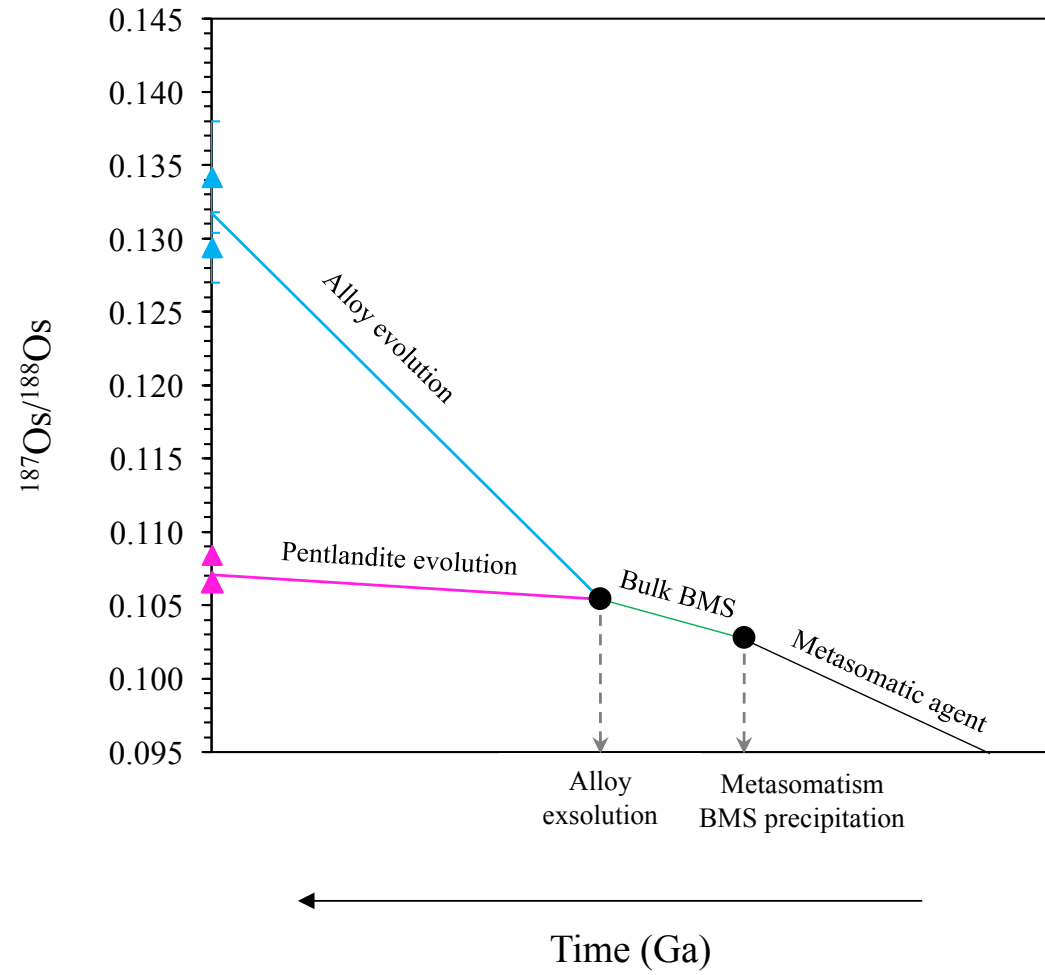


Figure 10

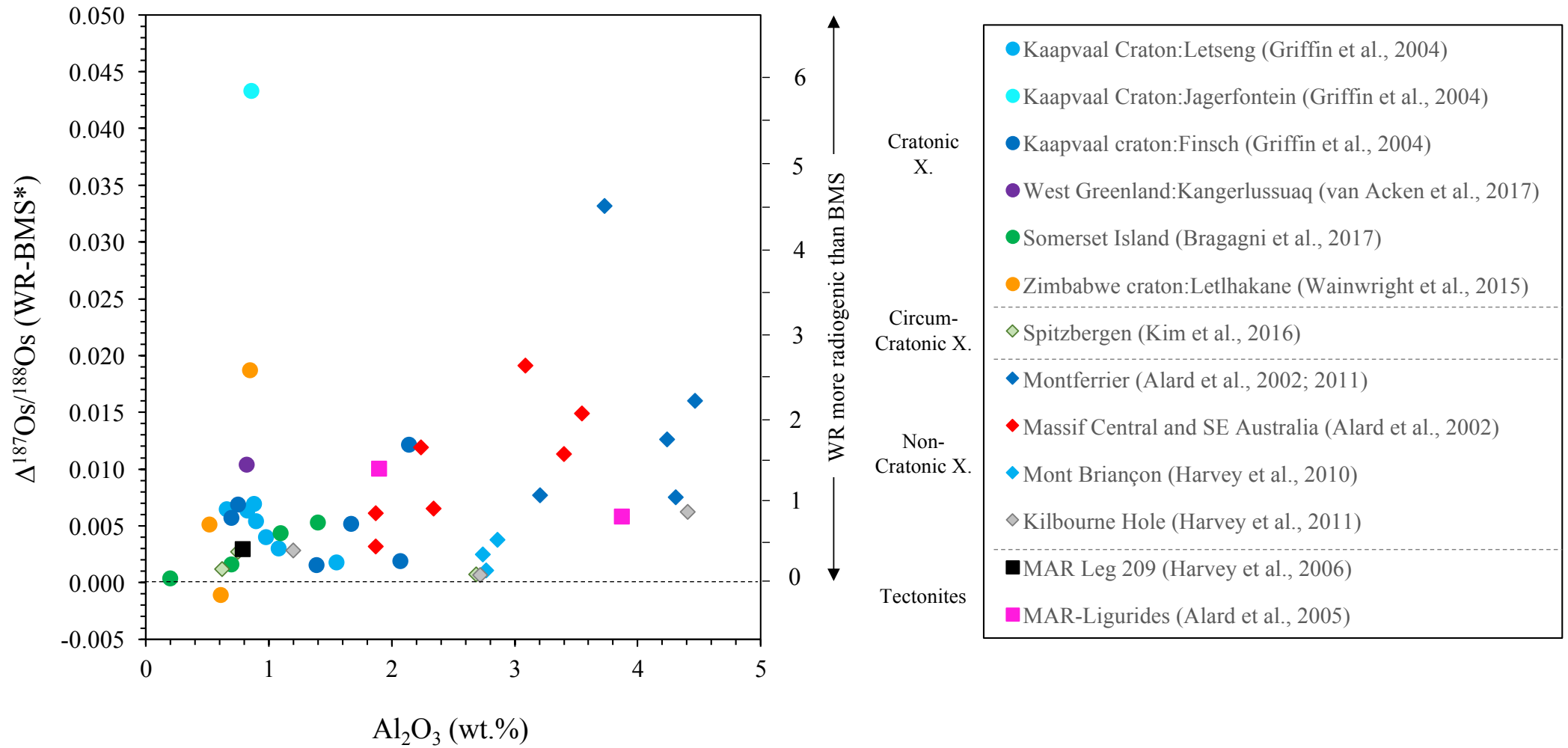


Figure 11

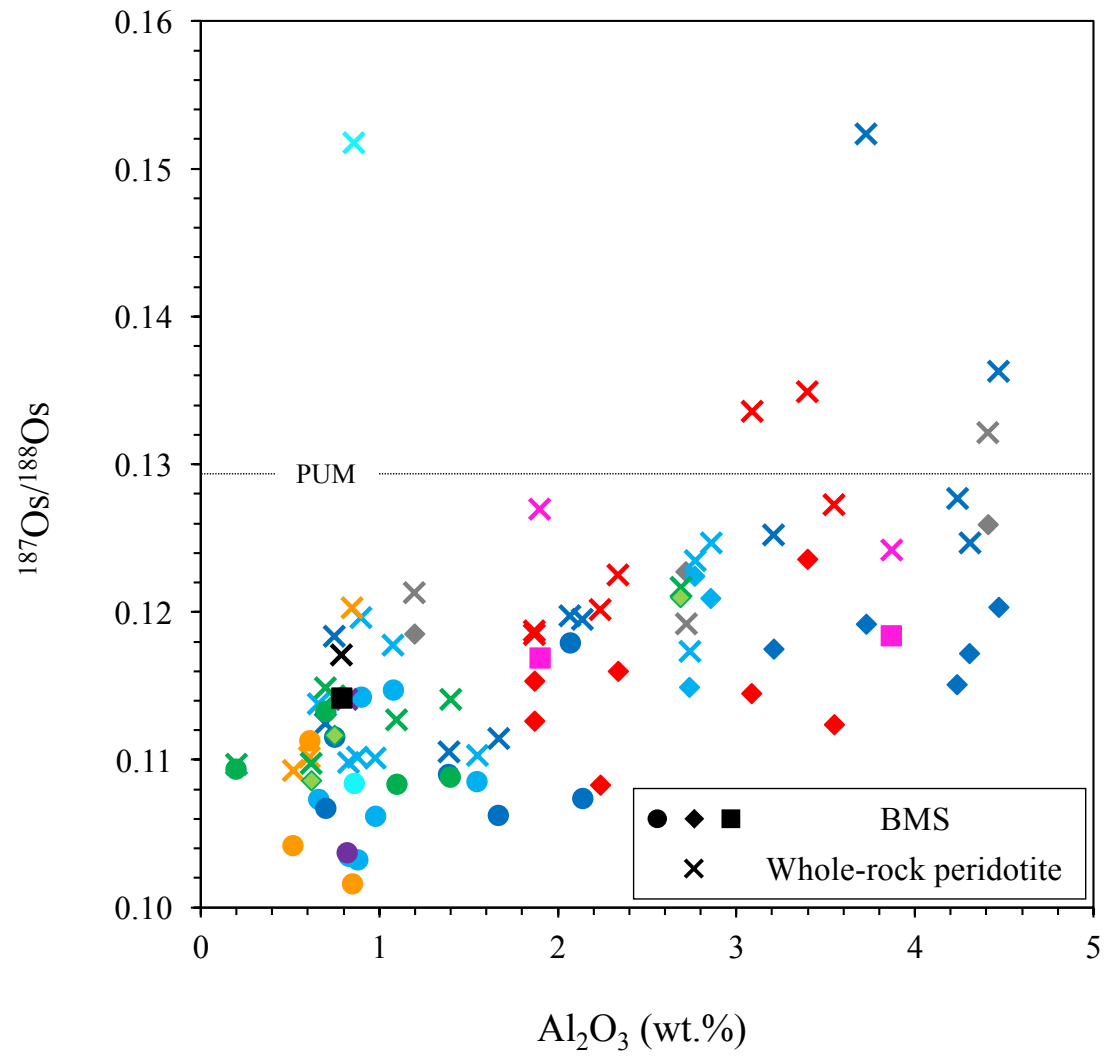


Figure 12

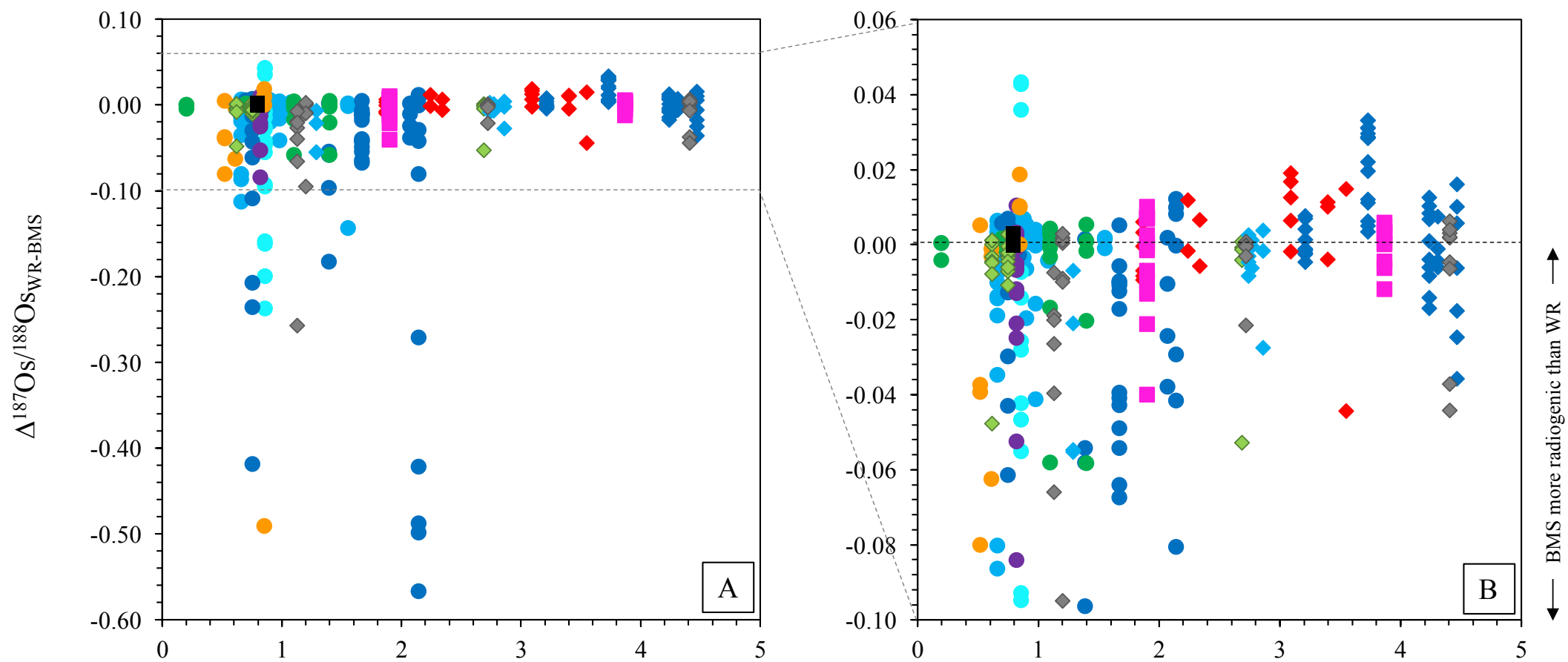


Figure 13

